Multimode Nonlinear Fibre Optics, a spatiotemporal avenue

Katarzyna Krupa, Alessandro Tonello, Alain Barthélémy, Tigran Mansuryan, Vincent Couderc, Guy Millot, Philippe Grelu, Daniele Modotto, Sergey Babin, Stefan Wabnitz

Multimode nonlinear fiber optics, a spatiotemporal avenue

Katarzyna Krupa,[1] Alessandro Tonello,[2] Alain Barthélémy,[2] Tigran Mansuryan,[2] Vincent Couderc,[2] Guy Millot,[1] Philippe Grelu,[1] Daniele Modotto,[3] Sergey A. Babin,[4,5] and Stefan Wabnitz[4,6,a)]

[1)] *Université Bourgogne Franche-Comté, ICB UMR CNRS 6303, 9 Avenue A. Savary, 21078 Dijon, France*

[2)] *Université de Limoges, XLIM, UMR CNRS 7252, 123 Avenue A. Thomas, 87060 Limoges, France*

[3)] *Dipartimento di Ingegneria dell'Informazione, Università di Brescia, via Branze 38, 25123, Brescia, Italy*

[4)] *Novosibirsk State University, Pirogova 1, Novosibirsk 630090, Russia*

[5)] *Institute of Automation and Electrometry SB RAS, 1 ac. Koptyug ave., Novosibirsk 630090, Russia*

[6)] *Dipartimento di Ingegneria dell'Informazione, Elettronica e Telecomunicazioni, Sapienza University of Rome, Via Eudossiana 18, 00184 Rome, Italy*

(Dated: 14 October 2019)

We provide a perspective overview of the emerging field of nonlinear optics in multimode optical fibers. These fibers enable new methods for the ultrafast light-activated control of temporal, spatial and spectral degrees of freedom of intense, pulsed beams of light, for a range of different technological applications.

[a)] stefan.wabnitz@uniroma1.it

I. INTRODUCTION

Nonlinear optical effects in multimode optical fibers (MMFs), such as the modal-phase matching of four-wave mixing (FWM) processes, have been known for a long time. However, the manipulation of the temporal and spectral properties of ultrashort pulses combined with the degrees of freedom provided by fiber multimodality is a research field which has only emerged in the past few years, as illustrated by the exponential growth of research interest (see Figure 1). In this review, we provide our perspectives on recent studies involving nonlinear optical pulse propagation in multimode optical fibers.

Over the past ten years, there has been a revival of interest in pulse propagation in multimode fibers, motivated by the exponential growth of traffic demand in optical networks on the one hand, and transmission capacity increase associated with the spatial dimension, or spatial division multiplexing (SDM), on the other hand. One of the main current limitations to the transmission capacity of both singlemode and multimode fiber optical communication links is provided by fiber nonlinearity[1]. Therefore, the study of nonlinear pulse propagation in MMFs and multicore fibers is of great practical relevance in the context of SDM.

However, this paper is devoted to discuss the perspectives of nonlinear optical MMFs beyond SDM communications. As a matter of fact, MMFs are being explored for different optical technologies, such as: a means to scale-up the power of fiber lasers and supercontinuum light sources, to perform high-resolution biomedical imaging, and to deliver powerful light beams for industrial processing. From a fundamental point of view, as illustrated by Figure 2, MMFs support a rich and complex mix of spatial and temporal nonlinear phenomena, so that they may serve as a testbed for the study of complex physical systems[2].

In Section II we provide a brief overview of the different models available to efficiently compute spatiotemporal beam propagation in nonlinear MMFs. In Section III we apply these models to discuss the intriguing phenomenon of multimode optical soliton (MMS) generation, where nonlinearity balances, at the same time, both chromatic and modal dispersion. Section IV is devoted, first, to a historical introduction of the early use of MMFs for extending the range of frequency conversion by nonlinear parametric wave mixing. Second, we describe the recent progress in nonlinear wave mixing research using modal and nonlinear phase matching in MMFs, alongside with relatively novel effects such as geometric parametric instabilities (GPIs). We also discuss in Section IV how the interplay of GPI,

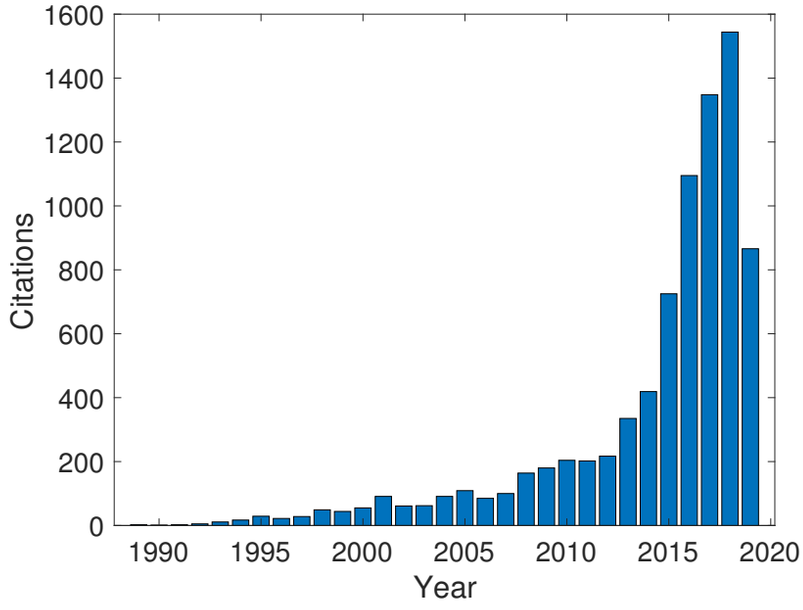

FIG. 1. Sum of times cited per year for source items indexed within Web of Science Core Collection, containing the words: *nonlinear multimode optical fiber* (as of July 7, 2019).

Raman scattering and MMS propagation lead to supercontinuum generation (SCG) in nonlinear MMFs. In the final part of Section IV, we present very recent experiments of second harmonic generation in optically poled MMFs.

A fascinating property of nonlinear MMFs, which has no counterpart in the world of singlemode optical fibers, is the possibility of reshaping, via the fiber nonlinearity, the transverse spatial beam pattern at the fiber output. In Section V we review different mechanisms for manipulating the transverse profile of multimode light beams by means of either nonlinear (dissipative) scattering (Brillouin, Raman) or (conservative) parametric interactions (Kerr effect). Very interestingly, all of these effects may lead to spatial beam cleaning, that is to the generation of high quality beams. Most remarkably, spatial beam cleaning occurs in spite of the multitude of randomly coupled fiber modes, which, in the absence of nonlinearities, lead to highly speckled or irregular intensity patterns at the MMF output. So, MMFs provide a fascinating example of a complex physical system exhibiting a nonlinear transition to *order out of chaos*.

One of the most promising fields of application of nonlinear MMFs is that of fiber lasers. Research in this field has been booming in recent years: as presented in Section VI, the non-

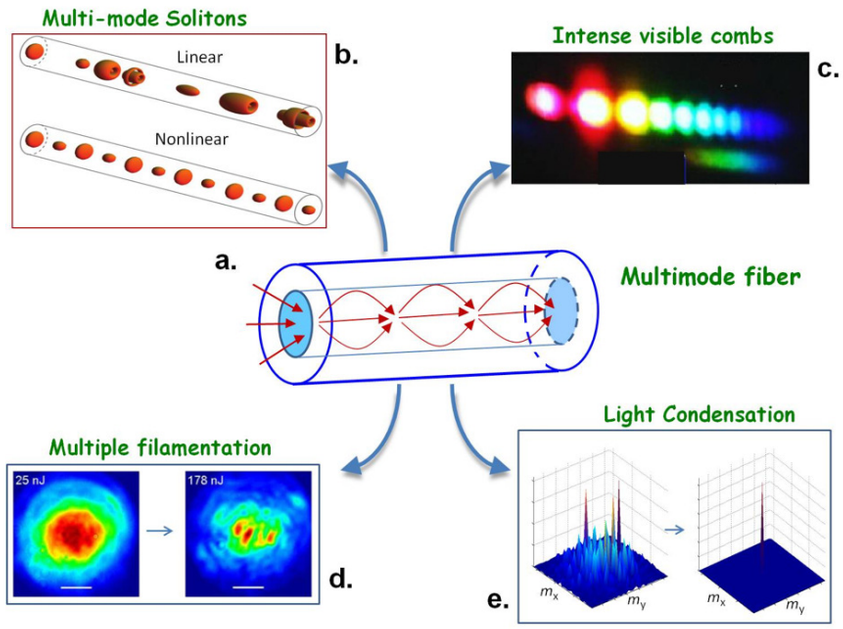

FIG. 2. Overview of nonlinear multimode optical fiber phenomena: multi-octave-spanning supercontinuum generation, spatial filamentation, multimode solitons, light condensation into the fundamental mode of the fiber [reproduced from ref.[2]].

linear transmission of a short span of graded-index (GRIN) MMF between singlemode fibers leads to an ultrafast saturable absorber mechanism with high damage threshold. Moreover, nonlinear multimode fiber lasers may permit both longitudinal and transverse, or total, mode-locking, as well as high energy and simultaneously beam quality multimode laser sources based on spatial beam cleaning.

The final Section VII concludes by pointing out what we believe are the main open problems in the rapidly advancing field of nonlinear MMF optics. Moreover, here we summarize our perspective views for future research and technology applications.

II. PROPAGATION MODELS AND NUMERICAL METHODS

Back in 1982, Crosignani et al. derived a general set of coupled-mode nonlinear Schrödinger equations (NLSEs), describing pulse propagation in multimode optical fibers in the presence of an intensity-dependent refractive index[3]. Their derivation was based on the coupled-mode theory, which is usually employed for describing the influence of weak fiber imperfections on linear wave propagation. Such approach takes into account the role of the

waveguide structure, in terms of both propagation constants and transverse spatial configurations of the linear eigenmodes. The resulting nonlinear coupled-mode equations may thus be applied to generic refractive-index distributions. The conditions for NLSE soliton propagation, and for the longitudinal self-confinement of a multimode pulse, were examined. In particular, if the different fiber modes are excited at different carrier frequencies, so that they all travel with the same linear group-velocity, then a multi-component envelope temporal soliton can be formed when the chromatic dispersion is anomalous for all modes. On the other hand, when all modes are excited at the same carrier frequency, nonlinearity may still lead to a trapping potential that prevents pulse spreading due to modal dispersion. The resulting condition for MMS formation was derived, which is a generalization of that derived by Hasegawa[4] and presented in Section III, since it allows the relative weights of the different modes to be taken into account, via their effective areas.

Manassah et al. studied the spatiotemporal evolution of a Gaussian (both in time and in the radial coordinate) pulsed beam in nonlinear GRIN MMFs[5]. They used an approximate, self-similar Gaussian trial solution, and showed that, also in the nonlinear regime, the parabolic index profile leads to a periodicity in the beam diameter, or self-imaging[6]. Waveguiding, self-focusing, and diffraction act together to determine the minimum magnitude of the beam-waist diameter.

Later on, Longhi and Janner analytically proved the existence of exact nonlinear and periodic propagation modes[7]. These nonlinear modes extend to the nonlinear regime the periodic self-imaging property of linear waves in a GRIN waveguide. They also studied, by a linear stability analysis and numerical simulations, the stability of these periodically focused modes, constructed as self-similar solutions of the fiber nonlinear eigenmodes. The self-similar solutions constructed from the fundamental nonlinear fiber mode were found to be linearly stable, whereas symmetry-breaking instabilities were found for nonlinear higher-order modes (HOMs).

In 2008, Poletti and Horak presented and discussed an extended (or generalized) version of the multimode NLSEs (or MM-GNLSEs) for MMFs, including polarization effects, high-order dispersion, Kerr and Raman nonlinearities, self-steepening effects, as well as wavelength-dependent mode coupling and nonlinear coefficients[8]. They also investigated the symmetry properties of the nonlinear coupling coefficients for the cases of step-index and circularly symmetric standard fibers, and for microstructure fibers with hexagonal sym-

metry. A numerical solution algorithm was presented, and its complexity was analyzed, showing that, although in principle it grows proportionally to the fourth power of the number of modes, M, it can be reduced to scale as $\simeq M^3$ by exploiting fiber symmetries and selection rules.

A later numerical study by the same authors considered supercontinuum generation by femtosecond pulses in MMFs. Quite interestingly, they showed that, due to pulse walk-off, a permanent intermodal power transfer between modes can be observed even in the absence of any phase matching[9]. The strength of intermodal effects is found to depend strongly on modal symmetries, which results in preferential coupling between LP_{0n} modes. Interestingly, simulations show that nonlinear intermodal power transfer is governed by two length scales. The first is the beat length $L_b = 2\pi/|\Delta\beta|$ (where $\Delta\beta$ is the linear propagation constant mismatch between the modes involved in the FWM process), leading to fast initial power oscillations, and the second is the modal walk-off length, leading to permanent power transfer among modes. To observe these effects, the nonlinear length of the pump pulses must be shorter than the walk-off length, i.e., high peak powers are required. It was determined that scaling a fixed fiber structure to larger core sizes allows for larger power throughput, but at the same time the longer beat and walk-off lengths lead to much stronger mode coupling, so that significant amounts of power can be transferred to HOMs.

In 2012, Mafi presented a detailed analysis of the modal properties, dispersive behavior, and nonlinear mode coupling in GRIN MMFs[10]. Starting from the general formulation of Poletti and Horak[8], and neglecting the presence of Raman and self-steepening effects, he derived a simplified set of coupled GNLSEs, that describe the propagation of radially symmetric, or zero angular momentum modes only. This hypothesis is accurate in sufficiently short lengths of GRIN MMFs, excited by radially symmetric laser beams, so that random coupling between nearly degenerate modes with different angular momentum can be safely neglected. An application of this formalism to the study of four-wave mixing in MMFs was discussed.

Later on, Pedersen et al. derived an improved version of the GNLSE, which takes into account the dispersion of the transverse field distributions. This approach leads to a version of the GNLSE including transverse field dispersion, which is able to reproduce experiments involving modal FWM in a high-order-mode (HOM) fiber, which supports the propagation of LP_{01} and LP_{02} modes with normal and anomalous dispersion when pumped at 1064 nm,

respectively[11].

Khakimov et al. introduced a method for numerically solving the MM-GNLSE[12]. An efficient approach to solve the scalar GNLSE for modelling supercontinuum generation in fibers involves transforming the equation into frequency domain, and integrating the resulting first-order ordinary differential equation by standard and stable procedures such as the fourth-order Runge-Kutta method. By the same approach, the MM-GNLSE can be reduced to a system of ordinary differential equations, thus facilitating the modeling of pulse propagation in MMFs. The solver was verified for the simplest multimode case in which only the two orthogonal polarization states in a non-birefringent microstructure optical fiber are involved.

So far, we discussed nonlinear beam propagation models for silica glass MMFs, whose nonlinear response originates from the electronic Kerr effect, alongside with nonlinear scattering from Raman or Brillouin effects. Appropriate modifications to the propagation equations should be made when the optical pulses are guided in MMFs containing different nonlinear materials. For example, gas-filled kagomé-style hollow-core photonic crystal fibers have emerged in recent years as highly versatile platform for ultrafast nonlinear optical experiments. They exhibit a broad transmission window, relatively low loss, and weak anomalous dispersion (which can balance that of a filling-gas). Most importantly, the anomalous dispersion can be tuned by changing the gas pressure, which permits the control of soliton dynamics and pulse compression down to few-cycles, as well as the generation of deep and vacuum ultraviolet light through dispersive-wave emission. In 2014, Tani et al. introduced a general full-field propagation equation for gas-filled waveguides, including both fundamental and HOMs, the full linear dispersion, the Kerr effects, and gas ionization effects[13]. The model was applied to study third-harmonic generation and soliton emission of resonant dispersive waves into HOMs, intermodal four-wave mixing (IFWM), and Kerr-driven transverse self-focusing and plasma-defocusing, which lead to beam filamentation based on a balance between modulation instabilities, plasma defocusing, and dispersive wave emission into HOMs.

For the advance of the theoretical modeling of nonlinear multimode fiber phenomena, it is important to develop efficient numerical methods for describing high-power ultrashort multimode pulses over a large spectral bandwith. The computational efficiency of MM-GNLSE solutions based on an expansion of the nonlinear polarization via nonlinear mode

overlap integrals have poor scaling with the number of modes. Moreover, it is necessary to take into account the mode profile variations with frequency. Laegsgaard introduced a new numerical propagation approach, based on the real-space Gaussian quadrature (GQ) integration of the nonlinear polarization[14]. The accuracy and computational efficiency of this method was compared with conventional approaches based on expansions using mode overlap integrals. Using the step-index MMF geometry as an example, it was shown that the GQ approach scales linearly or at most quadratically (as opposed with the third or fourth power) with the number of guided modes. Moreover, the method easily permits to take into account mode profile dispersion. The GQ method was shown to be superior to methods based on evaluating the nonlinear polarization by summing mode overlap integrals whenever more than six guided modes are involved, and when mode profile dispersion is important.

In 2018, Wright et al. introduced a parallel numerical solution method for the system of MM-GNLSEs[15]. This numerical solver is freely available for download from the internet, implemented in MATLAB, and includes a number of multimode fiber analysis tools. It features a significant parallel computing speed-up on modern graphical processing units, translating to orders-of-magnitude speed-up over the conventionally-used split-step Fourier method. The use of the method was demonstrated, and applied to several examples in both GRIN and step-index MMFs.

Looking forward, a further improvement to the accuracy and computational efficiency of ultrashort pulse propagation simulations in MMFs could involve the combining of a generalized (to an arbitrary fiber geometry) Laesgaard approach[14] with the parallel computation method by Wright et al.[15].

In general, all numerical methods for propagating the spatiotemporal optical field in MMFs that are based on modal expansions suffer from increasing complexity, hence computational inefficiency, as the number of modes involved is relatively large (typically, when more than 20 modes are involved). In situations where the propagation is highly multimode, it may be computationally much more efficient to use a direct numerical solution of the 3 + 1D NLSE. In the case of a GRIN MMF, the equation for the complex field envelope $A(x, y, t)$ $[\sqrt{W}/m]$ is the following one (such equation is also referred to as the Gross-Pitaevskii equation)[10,16–18]:

$$\frac{\partial A}{\partial z} - i\frac{1}{2k_0}\nabla_\perp^2 A + i\frac{\kappa''}{2}\frac{\partial^2 A}{\partial t^2} + i\frac{k_0\Delta}{R^2}r^2 A = i\gamma|A|^2 A, \tag{1}$$

where $k_0 = \omega n_{co}/c$, $\Delta = (n_{co}^2 - n_{cl}^2)/2n_{co}^2$ is the relative index difference, R is the fiber core radius, n_{co} is the maximum core refractive index, n_{cl} is the cladding refractive index, $\gamma = \omega_0 n_2/c$ is the fiber nonlinear coefficient, and z is the beam propagation coordinate. As we will discuss in Section IV and Section V, respectively, Eq. (1) can be successfully applied to model nonlinear beam shaping effects such as spatiotemporal parametric instabilities[19] and beam self-cleaning[20]. Eq. (1) can be solved by a standard split-step Fourier method with periodic boundary conditions in time t, while setting the field to zero at the boundaries of the spatial window. A typical integration step is 0.02 mm, with a 64x64 grid for a spatial window of 150 $\mu m \times 150$ μm[19].

III. MULTIMODE FIBER SOLITONS

A. Early theory

In order to properly appreciate the physics underlying nonlinear phenomena in MMFs, let us introduce the important concept of MMS. Optical solitons are well known to propagate in the anomalous group-velocity dispersion region of nonlinear singlemode fibers, and represent a balance between temporal broadening from material and waveguide contributions to chromatic dispersion, on the one hand, and temporal compression from the intensity-dependent frequency chirp, induced by self-phase modulation, on the other hand. Optical solitons play a key role in understanding purely one-dimensional pulse temporal dynamics in a variety of applications ranging from communications, supercontinuum generation, or mode-locked lasers.

Along the same lines, MMSs provide a natural platform to understand three-dimensional space-time dynamics of pulses in multimode nonlinear optical fibers. In essence, a MMS is a soliton with multiple components, self-consistently held together by fiber nonlinearity, so as to maintain its shape unchanged during propagation. In a MMF, because of modal dispersion, which is the dominant dispersive effect, one would expect that individual wave packet components traveling in different modes would propagate with their own group-velocities, thus leading to a temporal spreading of the input multimode optical pulse. However, thanks to nonlinear cross-phase modulation induced coupling among fiber modes, this may not always be the case.

As pointed out by Hasegawa[4], because of self and cross-phase modulation, in the anomalous dispersion regime a wave packet in a given mode, with index j, of the MMF experiences a force of attraction towards the center of mass of a pulse with power $P = \sum P_j$, resulting from the incoherent superposition of each wave packet with power P_j. This pulse acts as a potential, which may ultimately bind all individual wave packets together to form a MMS. The condition for trapping a wave packet in mode j can be written as[3,4,21]

$$\left(\frac{V_j - V_0}{V_j}\right)^2 \leq 2\frac{\partial V_j}{\partial \omega}\frac{\omega n_2 P}{n_0 A_j} \tag{2}$$

where V_j and V_0 are the group velocity of mode j with effective area A_j and the average group velocity of the modes, respectively, ω is the optical angular frequency, n_2 and n_0 are the nonlinear and the average linear refractive index. Note that, contrary to the case of single-mode fibers, the larger the group velocity dispersion of the mode, the lower the power required for trapping a pulse in that mode. In other words, MMS have their own identity: they do not simply result from the mutual trapping among individual solitons in each modal component, as one might expect for multi-component or vector solitons.

B. Early experiments

Now, these early theoretical studies of MMSs were carried out neglecting a fundamental property of MMFs: the presence of random linear mode coupling, that in long multimode fibers distributes the energy of a light pulse among a multitude of modes with random phases[22]. Very surprisingly, the first reported experimental investigation in 1988 of soliton propagation in MMFs by Grudinin et al.[23] has shown that femtosecond Raman solitons, generated in the anomalous dispersion regime of a GRIN MMF pumped by highly multimode 150 ps pulses from a Q-switched and mode-locked Nd:YAG laser, emerge with a clean beam size, close in size to that of the fundamental mode of the fiber. It was suggested that such Raman soliton beam cleaning is a manifestation of a universal property of nonlinear multimode systems[24]. Namely, that energy equipartition among all fiber modes, or thermalization, gives way to confinement into the first few low-order modes only. To date, the properties of that original fascinating discovery remain yet to be fully explained, although they appear to be a manifestation of Raman beam cleanup[25], an effect that will be discussed in details in Sections V-VI . First of all, it was observed that Raman solitons in a MMF

have a peak power (or energy) about 6 times larger than that of a singlemode fiber soliton with the same pulse duration. Second, the spatial field distribution of Raman solitons remains stable and quasi-singlemode as the pump power is increased above a threshold value, or when the GRIN fiber length increases from 10 m till 500 m. It was speculated that the observed energy flow towards low-order modes is due to some, yet unknown, nonlinear mode coupling process[23].

C. Recent experiments

1. Quasi-singlemode regime

In spite of the interest of Raman soliton beam cleaning and its unsolved origin, soliton propagation in MMS was left uninvestigated, largely because of the success of singlemode fiber based optical communications and devices in the 1990s. Over the past decade, the surge of data traffic over the internet driven by cloud computing and mobile applications has led researchers to the study of MMFs for their use in SDM long and ultra-long haul transmissions. In this context, in 2012 Mecozzi et al. have theoretically studied nonlinear propagation in long MMFs in the presence of random mode coupling[26,27]. They have shown that, in the presence of strong random mode coupling within quasi-degenerate groups of modes, one obtains a set of coupled NLSEs of the Manakov type, one for each group of modes, which are coupled via self-phase modulation and cross-phase modulation only. In other words, random mode coupling suppresses all four-wave mixing terms that lead to power exchange among the modes. This result is a generalization of the well-known Manakov equation, that describes polarization coupling in single-mode fibers in the presence of polarization mode dispersion. Interestingly, Mecozzi et al. predicted both analytically[26] (via a variational approach) and numerically[27] that a nonlinear compensation of the modal dispersion occurs, thus leading to stable MMS propagation.

The next year, Renninger and Wise carried out the first systematic experimental study of MMSs in GRIN MMFs[17]. In their experiments, 300 fs pulses at the carrier wavelength of 1550 nm with energies of up to a few nJ were injected into a multimode standard GRIN optical fiber with 62.5 μm core diameter. Since the MMF was excited by the output from a singlemode fiber, the input field diameter (11.5 μm) was smaller than the diameter of the

fundamental mode of the MMF ($\simeq 17.5\ \mu m$), which corresponds to exciting just three of its radially symmetric modes, with more than 90% of the energy coupled into the fundamental mode only. Numerical simulations demonstrated the stable trapping, in the temporal domain, of the pulse energy in these three modes. The HOMs exhibited a nonlinearity-induced blue shifting in the spectral domain. In other words, because of cross-phase modulation, HOMs shift their central frequency so that they slow down, and propagate with the same group velocity along with the fundamental mode. The situation is analogous to the case of birefringent optical fibers[28,29].

On the other hand, if instead of the multicomponent approach one uses the collective approach, based on the 3D+1 NLSE or the Gross-Pitaevskii equation, one can use the variational approach to find a stable spatiotemporal solution. One obtains that, under the conditions of the experiment in ref.[17], the MMS can be well approximated by a singlemode soliton solution of the NLSE, with an effective area equal to that of the fundamental mode of the GRIN MMF. The quasi-singlemode nature of the MMS was confirmed by measurements of the output pulse energy vs its duration, as well as of the Raman-induced soliton self-frequency shift (SSFS). A red-shift of the MMS frequency was observed, that could be accurately fitted by singlemode soliton perturbation theory, predicting a dependence of the wavelength shift which grows larger with the fourth power of pulse energy.

2. Fully multimode regime

A subsequent experiment aimed at studying the more general case where a proportionally much larger fraction of the MMS energy gets coupled into different HOMs at the input of a 62.5 μm core diameter GRIN fiber, so that MMS comprising up to 8-13 modes are formed, with an overall beam size up to $\simeq 3$ times the fundamental mode size. Such a situation can lead to a complex interplay of soliton fission and Raman scattering[30]. In the process of MMS undergoing SSFS, a transfer of energy from HOMs towards the fundamental mode may occur. In fact, the fundamental mode is slightly red-shifted from the HOMs as a result of the nonlinear trapping process that forms the MMS and it may receive energy from its HOM components via Raman gain. Moreover, the fundamental mode has also the strongest overlap with dispersive waves remaining around the pump wavelength, a process that is akin to Raman beam cleanup[25], so that an effective Raman soliton beam cleaning results.

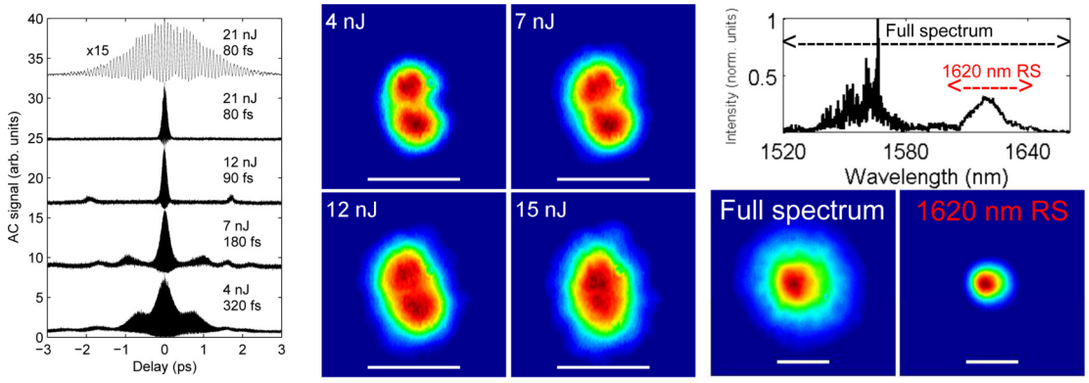

FIG. 3. Experimental study of MMS fission in GRIN MMF. Left: autocorrelation from 7 m of GRIN MMF for different input energies; Middle: output beam profiles corresponding to the cases in the left panel, showing that an initial beam composed by HOMs is progressively cleaned into LOMs as the pulse energy increases; Right: output spectrum along with total and filtered Raman soliton beam shape, showing that the Raman soliton is quasi-singlemode [Reprinted with permission from[30]. Copyright 2015 Optical Society of America]

For a MMS to form, since the relatively strong intermodal dispersion should be compensated for, the nonlinear phase shift corresponding to a MMS with a certain average (with respect to beam oscillations along the fiber due to self-imaging) spatial mode diameter should be at least equal or higher than that for a singlemode soliton (which is sufficient to balance chromatic dispersion only). In ref.[30], the slope of the dependence of the pulse energy versus the inverse of the pulse width (which measures the nonlinear phase shift) was measured for a variety of spatial beam widths, and found to be always significantly larger than that corresponding to pure singlemode solitons, in qualitative agreement with the early findings of Grudinin et al.[23]. Incidentally, the slope corresponding to the first experiments in ref.[17] was found to be very close to that of 1D solitons corresponding to propagation in the fundamental mode only. The experimental demonstration of an excess nonlinear phase shift by Wright et al.[30] can be seen as a consequence of Eq. (2), expressing the balance between self-phase modulation and modal walk-off which leads to MMS trapping. However, a direct experimental verification of the trapping condition for individual soliton components as expressed by Eq. (2) remains to be carried out.

For relatively large input pulse energies, so that multiple MMSs are generated, the initial pulse gets temporally compressed at first, and subsequently undergoes Raman-induced fis-

sion into multiple MMS and dispersive waves[30]. As shown in Figure 3, an initial beam mostly composed by HOMs is progressively cleaned into a bell-shaped beam composed by LOMs (lower-order modes) as the pulse energy grows larger. Moreover, filtering of the Raman shifted soliton shows that it emerges from the soliton fission essentially spatially bell-shaped as well, again in agreement with the original observations of Raman soliton beam cleaning by Grudinin et al.[23].

3. Few-mode fiber MMS

In a subsequent experiment, Zhu et al.[31] studied the intermediate (between quasi-singlemode and highly multimode) case of MMS dynamics in a so-called few-mode GRIN fiber, that supports propagation of LP_{01} and LP_{11} modes only (for a total of three spatial eigenmodes). This type of fiber is of interest for optical communication links using spatial-division-multiplexing[32]. Again, the Raman effect splits the input pulse into dispersive waves and a temporally compressed red-shifting MMS. The input pulse energy and its modal composition were varied, and the resulting SSFS was measured, and found to be in qualitative agreement with numerical simulations involving coupled mode GNLSEs. Moreover, experiments found that, for a given pulse width, MMSs have energies that can be larger than that of a singlemode soliton in each of the individual modes. This could be anticipated, given that nonlinearity should balance intermodal dispersion, which is generally larger than intramodal chromatic dispersion.

On the other hand, and quite surprisingly, experiments reported in Figure 4 have revealed that, as the MMS energy increases, the average spatial beam width also grows larger, and the Gaussian beam tends to evolve into a broader flat-top beam[31]. Thus, as the MMS energy increases, their temporal width decreases (as 1D NLSE solitons do), but their spatial width increases, unlike 3D+1 spatiotemporal solitons of bulk media under the action of chromatic dispersion and diffraction. This can be explained by the fact that higher pulse energies permit to bind a larger proportion of HOMs, with progressively larger mode areas.

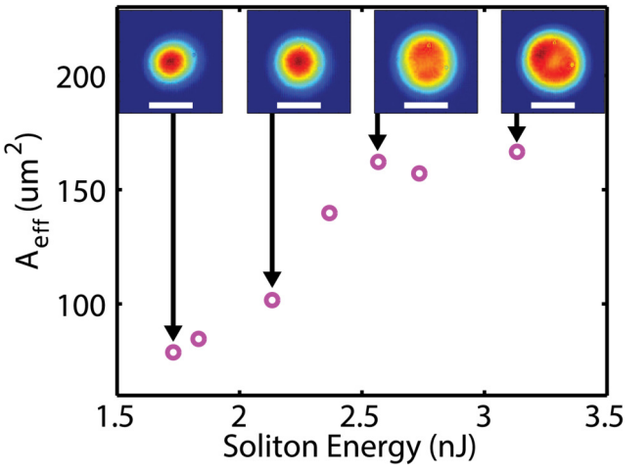

FIG. 4. Experimental dependence of MMS beam shape vs. pulse energy [Reprinted with permission from[31]. Copyright 2016 Optical Society of America]

4. Dispersive wave generation

Another fundamental mechanism, which is known to play a key role in SCG in singlemode fibers, is the process of dispersive wave emission from MMSs, that can be interpreted in analogy with Cherenkov radiation in electrodynamics[33]. Experiments by Wright et al. revealed the formation of broad multi-octave supercontinuum spectra, which are characterized by the presence of an ultra-wideband series of sharp spectral peaks extending from the visible into the mid-infrared regions[34]. As the physical origin of these spectral peaks was not yet clear, they were referred to as *mystery peaks*.

A subsequent study[35] revealed that the mechanism underlying the formation of a series of spectral peaks (see Figure 5) in the anomalous dispersion regime of the MMF is that of dispersive wave generation, resonantly phase-matched by the spatio-temporal intensity oscillations, due to self-imaging, of MMSs along the fiber. The mechanism is fully analogous to the multiple dispersive wave resonances of singlemode solitons, that occur in fiber lasers or in periodically amplified optical fiber links[36]. Figure 5 shows that the SCG featuring a series of unequally spaced dispersive wave peaks can be qualitatively well reproduced by using the generalized multimode coupled NLSEs[37]. As a matter of fact, the observed sideband peak positions can be well predicted by a simple reduction of the Gross-Pitaevskii equation (1) into a 1D NLSE with a periodically varying (because of MMS intensity oscillations due to self-imaging) nonlinear coefficient[35]. The resulting dynamics is essentially singlemode, and

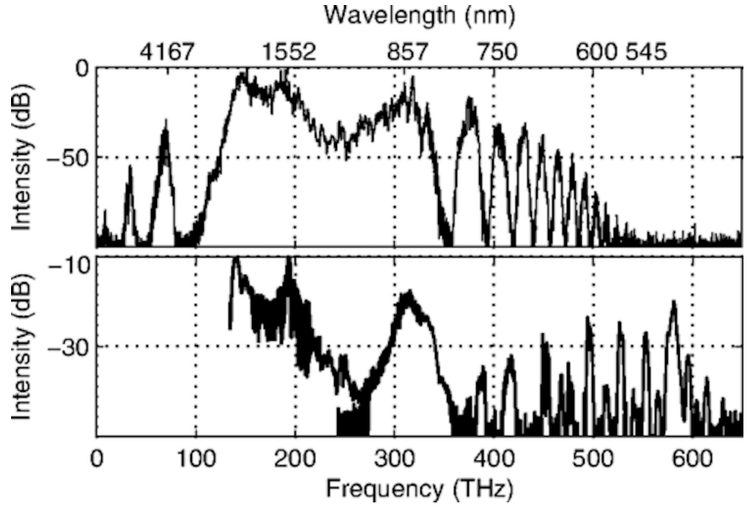

FIG. 5. Simulated (top) and experimental (bottom) supercontinuum generation in multimode GRIN fiber, showing a series of dispersive wave peaks [Reprinted with permission from[35]. Copyright 2015 by the American Physical Society]

the sideband frequencies are determined by the phase-matching condition between the wave numbers of the soliton, k_{sol}, and that of the dispersive wave, k_{dis}, that reads as

$$\begin{aligned} k_{sol} - k_{dis} &= 2m\pi/Z_c \\ &= \left(\frac{1}{2} + 4b_3^2 - 8b_3^4\right) + \left(\frac{\Omega^2}{2} + b_3\Omega^3\right) \end{aligned} \tag{3}$$

where Z_c is the self-imaging period, Ω is the frequency shift from the input pump pulse, and b_3 is associated with third-order dispersion[35].

D. Recent theory

1. Simplified 1D description

The simplified 1D NLSE description of nonlinear pulse propagation in a GRIN MMF permits a considerable improvement in computational efficiency[38]. The beam self-imaging dynamics taking into account the contribution of Kerr nonlinearity can be analytically described by means of the variational approach[39]. The variational analysis predicts that, even in the presence of Kerr nonlinearity, an input Gaussian beam in a GRIN MMF retains its

shape upon propagation, except for its amplitude and spatial width which evolve periodically along the fiber length z according to the function[39]

$$a(z) = a_0 \left[cos^2(\sqrt{G}z) + C sin^2(\sqrt{G}z) \right]^{1/2} \tag{4}$$

where a_0 is the input beam width, $G = 2n_0\Delta/R^2$, $C = (1-p)/(k_0^2 a_0^4 G)$, Δ is the index difference, and $p = P_0/P_c \leq 1$ is the input peak power normalized to the beam collapse power P_c. However, the analysis by Karlsson et al. neglected dispersion: their C parameter which describes the relative importance of diffraction and self-focusing, and characterizes the amplitude of the intensity oscillation, is time-dependent: different portions of a pulse experience different values of C. Therefore, strictly speaking one cannot use a single constant value of C in an equation that describes the propagation of ultrashort pulses. Nevertheless, the approximate periodic 1D NLSE reduction was shown to describe with good accuracy phase-matching conditions such as in Eq. (3). However, the 1D periodic NLSE reduction is based on the ansatz that the beam shape remains always a Gaussian upon propagation. Therefore, the range of validity of this simplified approach remains an open problem. This is because on the one hand, the 1D NLSE approach is only appropriate to quasi-singlemode MMS situations as in ref.[17], since it cannot describe, for example, intermodal energy conversions leading to beam shape dynamics, such as those described by Wright[30] and Zhu[31]. On the other hand, the presence of significant self-imaging beam oscillations means that the pulse is composed by a superposition of several modes, which is a contradictory requirement with the previous one. Incidentally, the reduced 1D approach is inherently unable to describe the well-known randomization of the transverse beam shape owing to random linear mode coupling, leading to output intensity speckles even for input axially symmetric beam, which is a well-known characteristic property of MMFs. It cannot describe beam self-cleaning either.

Later on, Ahsan and Agrawal[40] numerically studied the stability of MMSs in GRIN fibers by means of this reduced 1D NLSE approach. Since the self-imaging period is much shorter than the dispersion distance (as set by material chromatic dispersion), averaging over the fast oscillations of the soliton peak power leads to predicting the propagation of a guiding center[41], or path-average singlemode soliton in the GRIN MMF. Although their numerics showed a stability of fundamental MMSs as short as 100 fs over distances exceeding 1 km, the presence of Raman scattering, which is known to play a key role in leading to the fission

and modal energy redistribution for such short MMS[30,31], was neglected in those simulations. More recently, the case of an input Airy pulse in a GRIN MMF has also been investigated by the approximate 1D model, predicting the generation of breathing MMSs[42].

2. Multi-component NLS solitons

Having discussed the physical mechanism and the experimentally observed (so far, experiments have been limited to the case of GRIN MMFs) properties of *proper* MMSs (that is, as defined by Eq. (2), resulting from a balance between intermodal dispersion and fiber nonlinearity) in MMFs, it is worth mentioning that MMFs could also in principle support the propagation of individual, singlemode solitons in each modal component, where intramodal self-phase modulation and chromatic dispersion compensate each other. In the ideal case where pulses in all modes travel with the same speed, a multicomponent or vector soliton results, as analytically discussed by Crosignani et al.[3,21], and later numerically investigated by Buch and Agrawal[43]. However, numerics reveal that the propagation of multiple solitons may be subject to instabilities, owing to the non-integrability of the coupled NLSEs. In some cases, nonlinearity may counteract group-velocity walk-off and lead to soliton trapping: solitons in different modes shift their spectra in order to travel with the same speed in analogy with the case of two-mode, birefringent optical fibers[28,29].

In a subsequent study, the interactions of initially non time-overlapping solitons propagating in different modes of a few-mode GRIN MMF (supporting LP_{01} and LP_{11} modes only), and coupled via cross-phase modulation and four-wave mixing were numerically studied[44]. Because of the coherent nonlinear coupling, interaction forces were found to be phase-sensitive, similarly to singlemode soliton interactions. Here intermodal four-wave mixing leads to power transfer between the two mode components of a soliton, which however does not disrupt the bimodal nature of the solitons.

3. Raman solitons in step-index MMF

So far, MMSs in GRIN MMFs have been discussed. A recent numerical study investigated the Raman gain activated energy transfer between solitons with different carrier frequencies, propagating in different HOMs of a step-index MMF. For efficient Raman conversion, the

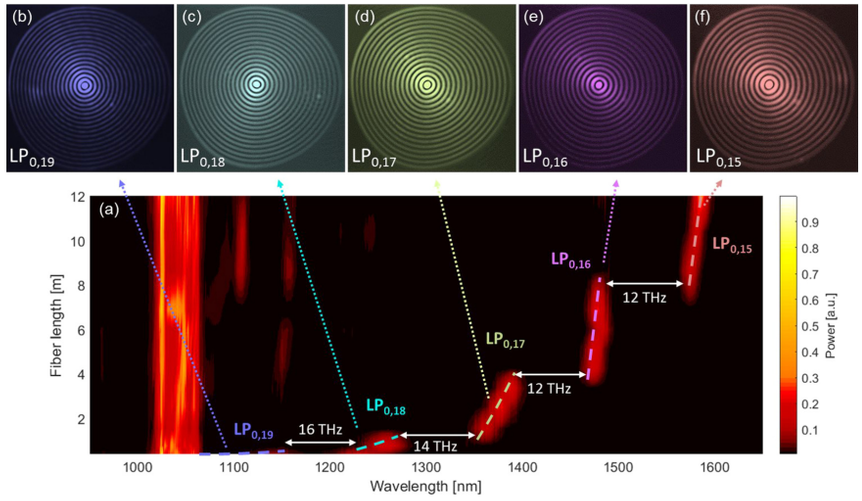

FIG. 6. (a) Spectra as a function of fiber length with input pulse at 1045 nm in the $LP_{0,19}$ mode. (b)-(f) Output mode images from different bandpass filters [Reprinted with permission from[46]. Copyright 2019 Optical Society of America]

carrier frequencies of the two pulses should be chosen in such a way that the group-velocity walk-off due to modal dispersion balances the walk-off due to chromatic dispersion. Interestingly, as a result of Raman gain, a soliton can build up from noise in a group-velocity matched, but red-shifted mode, over a distance that is shorter than the distance for significant SSFS (which would disrupt the group-velocity matching condition)[45].

This type of coherent frequency conversion between solitons in distinct spatial modes, whose modal and Raman shift group-velocity mismatches exactly compensate for each other, was recently experimentally demonstrated by Rishøj et al.[46] by using step-index silica MMFs with 0.34 numerical aperture (NA) and $87 - 97\mu m$ core diameters. As shown by Figure 6, pulses from a 1-μm fiber laser, injected into the $LP_{0,19}$ mode via a spatial light modulator, were frequency converted into MW-peak power, 75-fs pulses at the biologically crucial (because of increased attenuation length for in vivo deep tissue medical imaging) 1300-nm spectral range.

4. Spatiotemporal solitons

It is interesting to consider the possibility of generating spatio-temporal solitons in a MMF, as the power of the pulse approaches the critical value for self-focusing. In this

regime, self-similar optical wave collapse occurs when self-focusing due to the Kerr effect overcomes diffraction[47]. In spatio-temporal solitons (or light bullets), both chromatic dispersion and diffraction should be balanced by Kerr nonlinearity at the same time[48]. It is known that spatio-temporal solitons are unstable in more than one spatial dimensions in free space propagation: however, the linear index profile of the MMF, which acts as a guiding potential for light, may end up having a stabilizing action for the spatiotemporal solitons. To this end, the variational approach of Karlsson et al.[39] was extended by Yu et al.[18] and later by Raghavan and Agrawal[49], to include the temporal dimension via the contribution of chromatic dispersion. Variational solutions predict stable spatiotemporal solitons in the anomalous (normal) dispersion regime with a positive (negative) nonlinearity; however full simulations, aimed at demonstrating the validity of the predictions of the variational method, were only reported for a radially symmetric situation or a single transverse dimension, respectively. The dynamics of exact, spatiotemporal soliton solutions for pulse propagation in GRIN fibers was studied by analytical methods by Kong[50] and, more recently, by Shtyrina et al.[51]. The connections between classical and quantum nonlinear multidimensional wave propagation in MMFs may lead to interesting analogies such as the spatiotemporal soliton and bullet analogues of coherent and squeezed quantum states[52].

E. Hollow core and capillary MMSs

Another frontier for MMS and spatiotemporal soliton phenomena is provided by intense optical pulse propagation in multimode hollow-core, gas filled fibers and capillaries. At low powers, preferential guiding by the fundamental mode occurs because of its low loss. As the light intensity grows larger, ionization leads to plasma defocusing, which in turn excites HOMs. The resulting nonlinear mode coupling enables pulse compression, and sustains spatiotemporal localization and MMS propagation, at powers below the self-focusing threshold[53–55].

IV. FREQUENCY CONVERSION

A. Intermodal FWM

Back in 1974, Stolen, Bjorkholm and Ashkin used the modal dispersion in a small-core (10 μm core diameter), step-index MMF in order to compensate for material dispersion, and phase-match three-wave mixing (or degenerate FWM) processes[56]. In fact, in MMFs the propagation constant of HOMs is lower than that of lower-order modes. In their experiments, a frequency-doubled Nd:YAG pump laser was mixed with a tunable dye laser signal. For specific values of the relative frequency detuning between pump and signal, both coupled into the fundamental LP_{01} mode, an idler wave was generated at the fiber output, carried by different HOMs of the fiber. The shapes of the phase-matching curves and the shape of the idler HOMs were proposed as good potential indicators of fiber inhomogeneities along its length, as well as of the presence of a depressed index in the center of the core, and as a means to measure the strength of fiber nonlinearity.

In those early experiments, the effective coherence length was limited to 10 cm, owing to fiber imperfections such as variations of the core diameter. Later on, by using a single frequency-doubled Nd:YAG pump laser with no signal seed, Stolen demonstrated that selected mode combinations lead to FWM phase matching which is relatively insensitive to fiber perturbations (see Figure 7). This permits coherence lengths greater than 10 m, with parametric gains more than twice that of SRS gain[57]. As shown by calculating the sensitivity of the phase-matching condition to fluctuations of the core diameter, long coherence lengths and high conversion efficiencies are obtained with a mixed-mode pump, where the pump is split between two different transverse modes. Here the Stokes wave appears in one of these modes, while the anti-Stokes is in the other mode. To the contrary, in the previous experiments the two pump photons were coupled into the same transverse mode: the coherence length is approximately reduced by the ratio $\delta\nu/\nu$, where $\delta\nu$ is the sideband shift and ν is the pump wavelength[56].

In a subsequent paper, Stolen and Bjorkholm carried out an analytical study of parametric amplification in fibers based on coupled mode equations[58]. They demonstrated that parametric FWM gain decreases for fibers longer than a characteristic length, say, l_c. Beyond this length, SRS dominates over parametric scattering. A simple expression for the

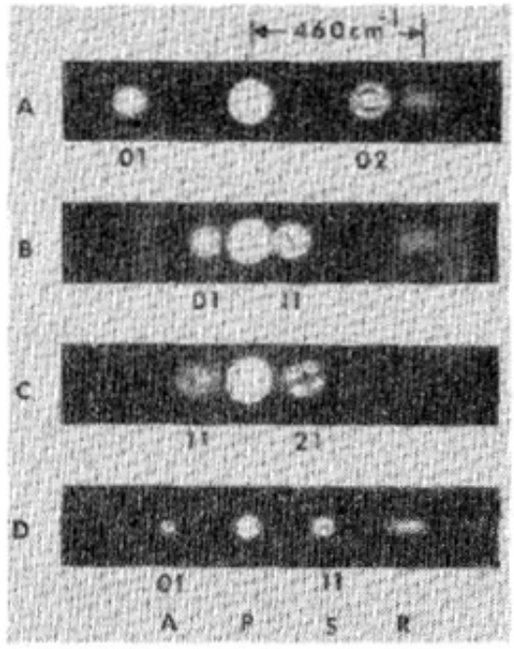

FIG. 7. Transverse patterns from different silica core optical fibers, where A, P, S, and R indicate anti-Stokes, pump, Stokes and Raman waves, respectively [Copyright 1975 IEEE. Reprinted, with permission, from[57]]

characteristic length l_c was obtained, involving only the initial pump linewidth $\delta\nu_p$ and the low-power parametric bandwidth. This bandwidth may be estimated from the pump wavelength and the frequency shift Ω between pump and sidebands. One obtains

$$l_c = \frac{2\pi}{\delta\nu_p}\frac{d\Omega}{d(\Delta k)}|_{\Delta k=0} \tag{5}$$

where, for the case of a mixed-mode pump, one has

$$\frac{d\Omega}{d(\Delta k)}|_{\Delta k=0} = (2\pi\lambda D(\lambda)\Omega_{pm})^{-1} \tag{6}$$

and Ω_{pm} is the phase-matched frequency shift, Δk is the FWM phase mismatch, and $D(\lambda)$ is the fiber chromatic dispersion.

In 1980, Hill et al. injected Q-switched and mode-locked pump pulses from a Nd:YAG laser into an external resonator, with a length matched to a multiple of the pump cavity length, in order to ensure the temporal overlap of pumping and recirculating pulses[59]. The external cavity included a Ge-doped, 62 μm core diameter GRIN MMF. In this situation, a

series of sidebands (including up to nine up-converted wavelengths, and unequally spaced in frequency) was generated in the fiber cavity, ranging from the visible (530 nm) up to the near-infrared (1630 nm). The phase-matching mechanism was identified as induced by transverse mode selection, since sidebands with higher frequencies were carried by progressively HOMs of the fiber. Brightest parametric oscillation was obtained when the mirror after the GRIN fiber reflected sidebands around either 790 nm or 1630 nm, respectively. In the presence of the parametric oscillation, SRS Stokes wave generation was suppressed. The apparent non-conservation of the photon energy in the sideband oscillation process led the authors to suggest that the wave-mixing process could involve phonon generation.

In a later experiment, Hill et al. analyzed in details the process of IFWM induced single-pass conversion of the 1064 nm radiation within a GRIN MMF with different core diameters. In this experiment, the mode patterns of the generated spectral components could be identified with great clarity[60]. It was also revealed that fiber birefringence played a key role in the phase-matching between the pump and the primary Stokes and anti-Stokes lines.

In the experiments by Stolen et al., the observed sideband frequency shifts were limited to 3-9 THz[56,57]. By using specialty fibers (e.g., Ge-doped with a large dip in the center of the core index profile, or square-well profile) which only support few modes in the visible, Lin and Bosch extended the IFWM frequency shift up in the range of 60 to over 120 THz, thus enabling frequency conversion down to near UV region of the spectrum[61].

By using a specially developed MM silica fiber with losses reduced down to the Rayleigh limit in the UV (i.e., 100 dB/km), in 1983 Pini et al. reported efficient frequency conversion by IFWM of the XeF excimer laser line (351.2 nm), leading to the observation of a Stokes peak at 355.5 nm with 1 kW peak power[62].

Over the next 17 years, there was little activity in studying parametric frequency conversion in MMFs. At the beginning of the present century, the development of microstructure and photonic crystal fibers, exhibiting a great degree of flexibility in the position of the zero dispersion wavelength owing to the significant contribution of waveguide dispersion, led to a surge of interest in SCG in optical fibers, as well as in the use of MMFs for nonlinear wave mixing. In one of those experiments, a highly multimode microstructure optical fiber, consisting of a silica core surrounded by a ring of large air holes, was used[63]. Owing to the large difference in effective index between the lowest-order guide modes, mode coupling

was prevented in that fiber, so that SCG could be achieved in the fundamental fiber mode only. However, the multimode nature of the fiber was exploited to effectively phase match harmonic generation and IFWM processes, leading to new wavelength components stably propagating into HOMs.

In 2009, Tu et al. generated large Stokes-shift ($\simeq 4700\ cm^{-1}$) IFWM by using a short (20 cm) piece of commercial large-mode-area photonic crystal fiber (PCF), which behaves as a two-mode fiber, pumped by amplified and chirped 210 fs pulses at $\simeq$ 800 nm from a Ti:sapphire regenerative amplifier[64]. In their experiments, IFWM in the single-mode configuration (i.e., two pump photons in the fundamental mode and Stokes/anti-Stokes photons carried by the HOM) was used, obtaining about 7% conversion efficiency from the pump into the 586 nm anti-Stokes wave. Pulse chirping was essential to obtain effective energy coupling into the fiber, and to generate IFWM, likely because of the large walk-off between pump and signal/idler pulses when transform limited 35 fs pulse were used. The advantage of using IFWM with respect to FWM in singlemode fibers is that frequency conversion can be achieved without generating a supercontinuum.

In 2012, Cheng et al. demonstrated high-efficiency IFWM in an all-fiber system, comprising a picosecond fiber laser at 1064 nm and a triple-clad HOM fiber, supporting the propagation of LP_{01} and LP_{02} modes[65]. A relatively stable single-mode IFWM configuration was used with the pump and the anti-Stokes in the LP_{01} mode (with large normal dispersion) and the Stokes LP_{02} mode (with large anomalous dispersion). The anti-Stokes wave at 941 nm is generated with 20% conversion efficiency for an input pulse energy of 20 nJ, and a peak power of 2 kW, which is orders of magnitude lower that the value required for spontaneous IFWM in a large-mode-area PCF[64]. The strong guidance of the anti-Stokes and Stokes waves in the HOM fiber also enhances system stability with respect to that using a PCF.

A HOM fiber exhibiting mode crossing (i.e., with two guided modes having the same propagation constant at the same wavelength) was used to demonstrate intermodal Cherenkov radiation generation[66]. A soliton propagating in the LP_{02} mode with anomalous dispersion, at the blue side of the mode-crossing wavelength, was shown to generate a redshifted, and phase-matched dispersive wave in the LP_{11} mode, which exhibits normal dispersion. Both modes are stably guided, and the strength of the conversion efficiency can be tuned by means of fiber bending, which is necessary for introducing symmetry breaking that leads to

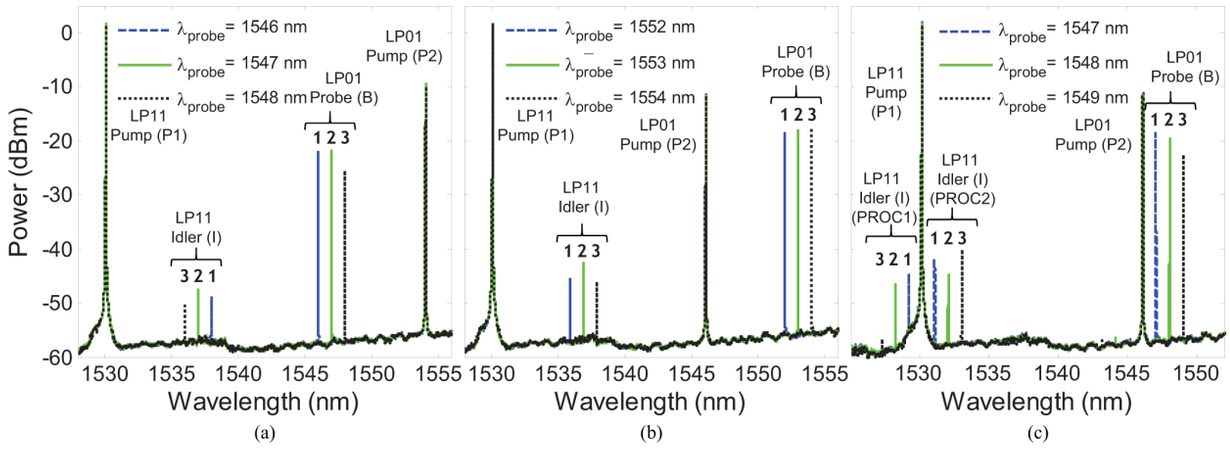

FIG. 8. Spectra of two IFWM processes named process 1 and process 2, seen separately in (a) and (b) and simultaneously in (c). [Copyright 2013 IEEE. Reprinted, with permission, from[67]]

a non-zero overlap integral between the two involved modes.

The research interest in SDM techniques has led to the development of few-mode fibers for optical communication transmissions. In this context, in 2013 Essiambre et al. experimentally demonstrated IFWM in a GRIN few-mode fiber supporting LP_{01} and $LP_{11a,b}$ modes (for a total of six modes when including polarization), as long as 5 km in length[67]. This is a breakthrough achievement with respect to early experiments, where the characteristic length for IFWM was limited to about ten meters[57,58]. Out of the three possible mixed-mode IFWM processes, only two of them were experimentally observed, leading to the generation of new frequencies with THz separations from the pump and probe waves (see Figure 8). The authors point out that for both of these processes, the phase matching condition means that the group velocities, evaluated at the average frequency of the two waves contained in each spatial mode, coincide. This condition is independent of the value of the propagation constant in each spatial mode, therefore the phase-matching condition is independent with respect to longitudinal fluctuations of the core diameter. Whereas, the phase matching condition for the process that was not observed depends on the difference between the propagation constants of the two modes, a quantity which is subject to fiber fluctuations. The difference between the two stable IFWM processes is that in one of them (process 1) the probe and signal waves have frequencies intermediate between those of the pump waves, whereas in the other process (process 2) the frequencies of pump waves alternate with the frequencies of probe and signal.

Later on, Friis et al. used a 1-km long two-mode GRIN fiber to demonstrate efficient different IFWM processes at telecommunication wavelengths[68]. Two pump photons were injected in LP_{01} and LP_{11} modes, together with a signal in the fundamental LP_{01} mode, which led to the generation of both phase conjugation (PC) and Bragg scattering (BS) idlers in the LP_{11} mode. The PC (BS) idler frequency is located in-between (outside) the frequencies of the two pumps, respectively. The phase matching efficiency and bandwidth of these processes were found to critically depend on the frequency separation among the pumps.

In the same context of km-long few-mode fibers developed for SDM applications, it is important to consider the impact on IFWM efficiency of fluctuations of the fiber birefringence and random linear mode coupling. Xiao et al. developed a theoretical treatment of IFWM in the presence of random fiber fluctuations, and evaluated the bandwidth of different IFWM processes, by including nonlinear contributions to the phase-matching condition[69]. In the absence of random mode coupling, the bandwidth of process 2 is found to be generally much larger than that of process 1. As expected, the numerical analysis shows that random mode coupling reduces the IFWM efficiency: this effect is particularly strong when also LP_{01} and $LP_{11a,b}$ modes are coupled, whereas even strong coupling between the $LP_{11a,b}$ modes does not significantly affect the IFWM efficiency.

The relatively large power fluctuations occurring in the IFWM process using km-long telecom few-mode fibers were experimentally demonstrated in 2017 by Esmaeelpour et al.[70]. These authors carried out measurements of the full bandwidth of IFWM efficiency in a 4.7-km three-spatial-mode fiber, by injecting two pumps in the same LP_{11} spatial mode, and a probe in the fundamental LP_{01} mode. Idler power fluctuations exhibit a strong dependence on the signal wavelength, that can be persistent in time, as well as a strong dependence on the polarization of the pumps (which can be reduced by pump polarization scrambling).

In 2015, Pourbeyram et al. carried out a detailed comparison between theory and experiments involving the generation of Stokes and anti-Stokes sidebands from vacuum noise via IFWM in a commercial telecom fiber (Corning SMF-28)[71]. The fiber supports the propagation of a few spatial modes when pumped by sub-nanosecond pulses from a green (532 nm) laser. Stokes and anti-Stokes beams are generated in the LP_{02} and LP_{01} modes, respectively, when the pump is coupled to the LP_{01} mode. The generated Stokes power was measured as a function of the pump power for 10 different fiber samples of same length, and the mea-

surements exhibit a significant scatter at the output of samples of nominally identical fibers, likely due to slightly different input alignment of the pump with each fiber. The predicted blue-shift of the Stokes peak with pump power was also observed.

In the same year, Pourbeyram and Mafi have theoretically studied the possibility to use IFWM in order to generate a third-harmonic beam, by coupling in a multimode fiber a fundamental beam and its second-harmonic[72].

When combined with new fiber designs and guiding concepts, IFWM is a flexible mean to achieve laser frequency conversion with large spectral shifts and to extend the spectral range of fiber laser sources. Petersen et al. carried out a comprehensive theoretical and experimental study of IFWM in large mode area, hybrid photonic crystal fibers, which combine photonic bandgap guidance with refractive index guidance[73]. The parametric gain of both intra and inter-modal FWM with both co- and orthogonally polarized pump, signal and idler fields was numerically evaluated, and validated by the experiments, where an IFWM conversion efficiency as high as 17% was achieved. The pump Ytterbium-doped 40 ps 1064 nm fiber laser was coupled to the fundamental mode of the PCF, and converted into a signal and idler emerging in the LP_{11} mode at 848 nm and 1425 nm, respectively.

By using a special PCF design with relatively large hole size (which reduces bending loss for the HOM) and long walk-off length between the fundamental and the HOM, Yuan et al. experimentally demonstrated comparatively enhanced IFWM by using 120 fs pump pulses from a Ti:sapphire laser at 800 nm[74], as in previous experiments by Tu et al.[64]. As a result of the longer interaction length, the maximum conversion efficiency into anti-Stokes (at 553 nm) and Stokes (ranging from 1445 nm till 1586 nm) waves reached 21% and 16%, respectively. The same group also used a birefringent PCF to experimentally demonstrate polarization-dependent IFWM[75]. The 800 nm femtosecond pump pulses were polarized along either the fast or the slow principal axis of the PCF. The resulting anti-Stokes and Stokes waves, generated in a HOM, were shown to exhibit pump polarization-dependent conversion efficiencies and wavelengths.

Subsequently, Yuan et al. could extend the range of IFWM generated wavelengths by using an air-silica, 22-cm long PCF with two zero dispersion wavelengths, and launching femtosecond pulses at 1550 nm into the deeply normal dispersion region of the fundamental mode of the fiber[76]. As a result, the pump was converted into an anti-Stokes wave around 1258 nm and a Stokes wave around 2018 nm, both carried by the second-order mode. The

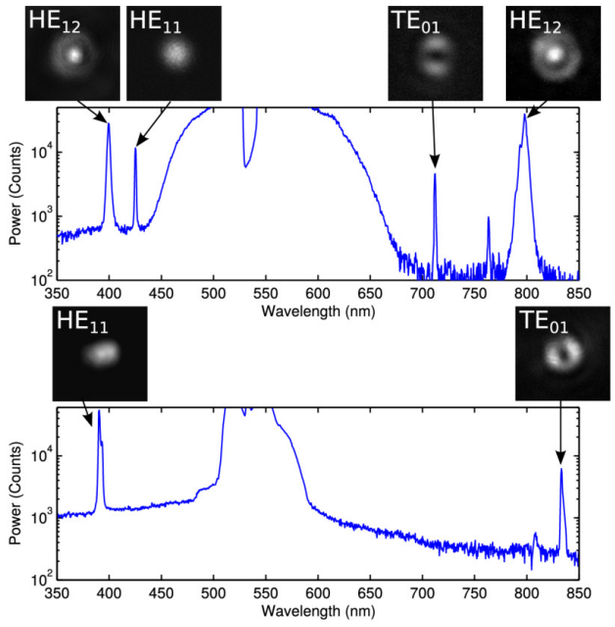

FIG. 9. Experimental spectra showing the generation of fundamental mode UV light by IFWM using a 532 mixed-mode pump [Reprinted with permission from[77]. Copyright 2015 Optical Society of America]

corresponding conversion efficiencies of generated anti-Stokes and Stokes waves was 8.5% and 6.8%, respectively. The PCF design led to a weak sensitivity of the conversion efficiency to fiber bending and mode walk-off.

By using a PCF, Sevigny et al. demonstrated the use of IFWM for the conversion of two mixed-mode pump photons at 532 nm into UV light at 390.5 nm in the fundamental mode (with the corresponding idler in a HOM), see Figure 9[77]. This scheme leads to a MMF-based source of high beam quality UV light, which is of great practical interest for many applications, ranging from industrial processes such high-resolution materials processing, to biomedical applications such as eye surgery. The use of a MMF for the generation of UV light with high beam quality circumvents the risks of material damage, because of their small core size, when using intra-modal FWM schemes with single-mode fibers.

A different strategy to demonstrate UV light generation, via cascaded IFWM in a solid core air-silica PCF was experimentally demonstrated by Yuan et al.[78]. Starting from femtosecond pump pulses at 800 nm injected in the fundamental mode of a multimode PCF, anti-Stokes waves in the second HOM were first generated via IFWM at 538.1 nm. This wave served as secondary pump for another IFWM process, leading to a second anti-Stokes

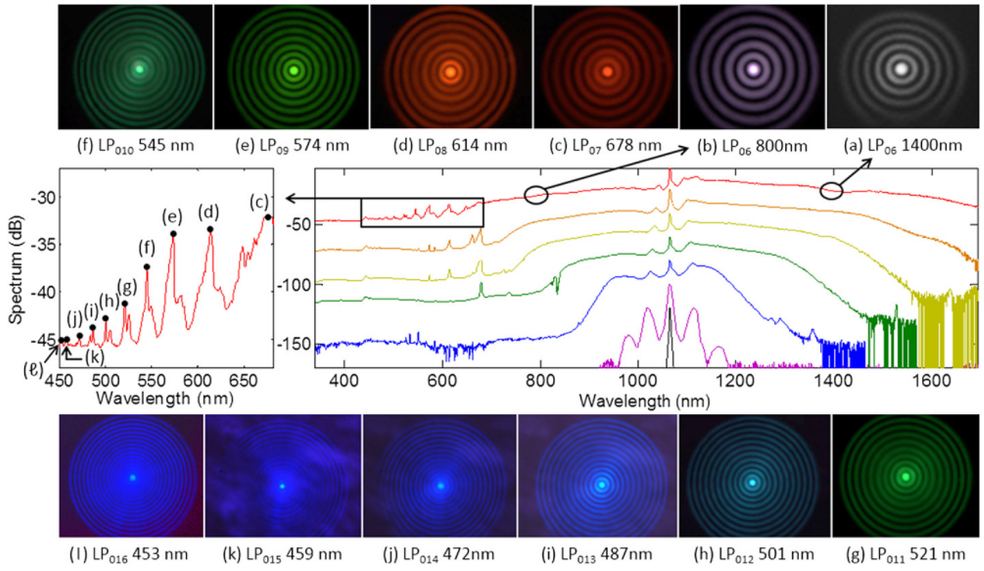

FIG. 10. Output spectra and mode images from intermodal FWM using Bessel-like beams in a step-index MMF [Reprinted with permission from[79]. Copyright 2015 Optical Society of America]

wave in the third HOM at the UV wavelength of 375.8 nm.

By exploiting the azimuthally symmetric, Bessel-like $LP_{0,n}$ modes of a step-index MMF, Demas et al. demonstrated over two octaves of coherent spectral translation by IFWM between subsets of 11 different fiber modes, i.e., $LP_{0,6} - LP_{0,16}$ modes (Figure 10 shows spectra and corresponding mode images of generated new frequency components)[79]. Nonlinear mode interactions are facilitated by the unique mode-coupling resistance of the used subset of azimuthally symmetric, zero orbital angular momentum fiber modes. Their stability allows overcoming previous limitations to the interaction length of IFWM processes, as imposed by random mode coupling, thus permitting long interaction lengths, large effective mode areas, and a highly multimode basis set for versatile frequency conversion.

Because of their relatively low modal dispersion, hence long interaction lengths of waves in different modes, GRIN optical fibers lead to highly efficient IFWM. Moreover, linearly polarized Laguerre-Gauss modes with the same mode number $g = 2p + m + 1$, where p and m are integers denoting radial and angular mode numbers, are nearly degenerate. Since the relative index difference Δ between core and cladding in GRIN fibers is typically less than 0.01, one obtains that different mode groups have equally spaced propagation constants. In fact, their propagation constant β_g can be written as

$$\beta_g = \frac{2\pi n_0}{\lambda} - \frac{\sqrt{2\Delta}}{R} g \tag{7}$$

This permitted Nazemosadat et al. to derive a simple analytical condition for IFWM phase-matching in GRIN fibers[80]. As a result, the frequency shift f from the pump of Stokes (signal) and anti-Stokes (idler) sidebands reads as

$$f^2 = \frac{\sqrt{2\Delta} G}{2\pi \lambda_p^2 n''(\lambda_p)} \frac{c^2}{R\lambda_p} \tag{8}$$

where $G = g_s + g_i - g_p^{(1)} - g_p^{(2)}$, and g_s, g_s, $g_p^{(1,2)}$, are the mode numbers of the signal, idler, and pump photons, respectively. This expression is very useful since it permits to predict the wavelengths of signal and idler by only using the mode group numbers of the different spatial modes involved in the FWM process, and the refractive index dispersion at the pump wavelength. The dependence of the phase-matching condition, and of the resulting wavelength shift of the newly generated frequencies, on a single integer G means that nearly identical signal and idler frequencies can be obtained for many different pump, signal, and idler spatial mode combinations .

By using IFWM in MMFs in a pump-seed configuration, one may obtain a whole new class of frequency agile, power scalable fiber-optic parametric amplifiers, for converting laser light from the NIR to the visible range of the spectrum via subsequent second-harmonic generation in a quadratic crystal. To this end, Demas et al. were able to inject, via spatial-light modulators, pump and signal beams in different HOMs of a specially designed step-index MMF[81]. This technique permits the range of available wavelengths to be extended into the NIR beyond the 10XX nm or 15XX nm ranges of fiber lasers based on rare-earth amplifiers, thus permitting access, via frequency doubling, the entire palette of visible wavelengths. Parametric sources using the LP_{07} and LP_{06} modes of different step-index MMFs led to output wavelengths of 880, 974, 1173, and 1347 nm, with peak powers of 10.0, 16.2, 14.7, and 6.4 kW respectively, and 300-ps pulse durations. .

In 2017, Dupiol et al. demonstrated far-detuned, noise-seeded frequency conversion in a few-mode, 22 μm diameter GRIN MMF pumped by a Q-switched picosecond laser at 1064 nm coupled into the fundamental LP_{01} mode, and propagating in the normal dispersion regime[82]. As shown in Figure 11, the parametrically generated sidebands span the visible down to 405 nm and in the near-infrared up to 1355 nm. By means of analytical

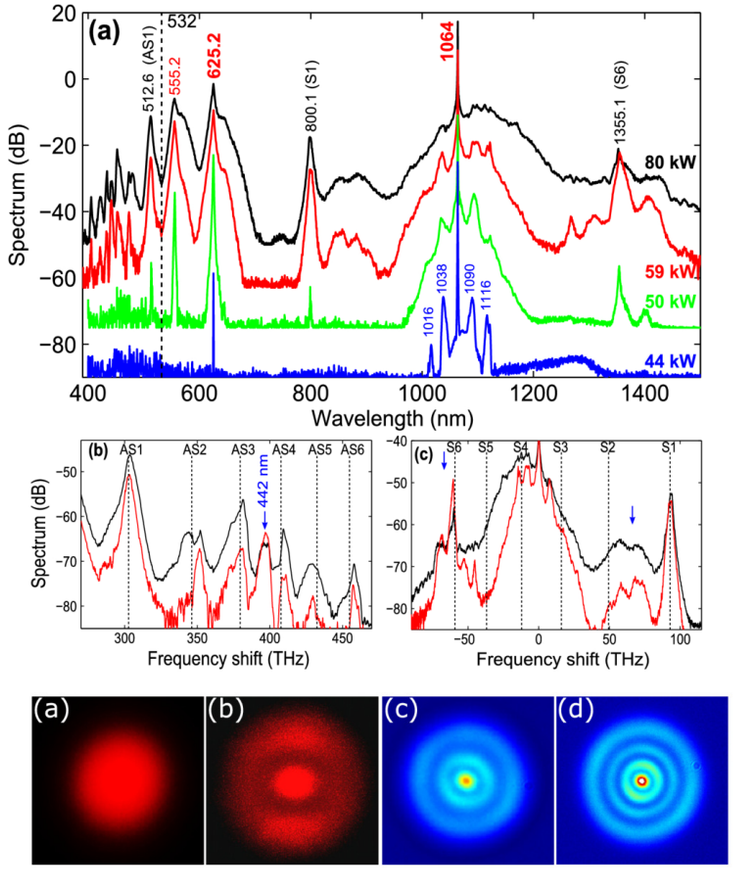

FIG. 11. Output spectra and mode images from cascaded intermodal FWM in GRIN MMF. The top panels show (a) the output spectra for different pump peak powers (44 kW (blue), 50 kW (green), 59 kW (red), and 80 kW (black)), and a zoom on (b) the visible and (c) infrared parts of the 59 and 80 kW spectra. Vertical dashed lines indicate the calculated IFWM frequencies for a secondary pump at 625.2 nm propagating in the LP_{06} mode; the bottom panels show output beam profiles recorded with a camera at (a), (b) 625 nm, (c) 473 nm, and (d) 433 nm [Reprinted with permission from[82]. Copyright 2017 Optical Society of America]

phase-matching considerations supported by a full numerical analysis, it was shown that the multiple sidebands are generated through a complex cascaded process involving intermodal four-wave mixing. In particular, the far-detuned sideband in the visible at 625.2 nm is the IFWM anti-Stokes wave. This wave is generated with high efficiency when the input pump coupling conditions are such that it is generated in the LP_{01} mode (corresponding to an anti-Stokes wave in the LP_{02} mode), so that it acts as a secondary pump for cascaded IFWM, leading to additional anti-Stokes spectral peaks in the visible between 400 and 500

nm (and a Stokes peak at 800 nm).

In a subsequent experiment, Bendahmane et al. experimentally and theoretically investigated in details the impact of seeding on IFWM in a 1 m long GRIN MMF, pumped at 1064 nm in the LP_{01} mode[83]. By using a GRIN fiber with a 100-μm core diameter and a tunable CW erbium-based laser as a seed, phase-matched IFWM led to a Stokes wave in the telecom C-band. It was observed, in addition to the primary IFWM sidebands at 808.5 nm and 1556.7 nm, the generation of several additional parametric sidebands both in the visible and in near-infrared regions of the spectrum. Again, the anti-Stokes sideband acted as a secondary pump for cascaded IFWM. Interestingly, it was demonstrated that both the second- and fourth-order dispersions must be included in the phase-matching conditions, in order to describe well the experimental measurements. The use of a seed significantly improved the frequency conversion efficiency, before it became limited by pump depletion effects. Temporal measurements performed with a fast photodiode revealed the generation of multiple pulse structures in the primary anti-Stokes sideband at 809 nm.

By pumping a standard SMF-28 fiber with a Q-switched, frequency-doubled Nd:YAG laser, Chatterjee and Vijaya experimentally demonstrated a so-called unconventional or nonphase-matched IFWM process, where, likely because of the presence of a LP_{02} mode component accompanying the main LP_{01} component in the pump mode, Stokes and anti-Stokes waves are both generated in the LP_{02} mode. Moreover, similarly to the previous experiments by Yuan et al., who used a solid-core air-silica PCF, by using the primary IFWM anti-Stokes wave at 447 nm as a secondary pump, UV peaks at 390.7 nm and 396.7 nm could be generated by using a standard telecom fiber[84].

The simultaneous presence of a phase-matched IFWM process alongside a nonphase-matched one, leading to the observation of Stokes and anti-Stokes waves both emerging in the LP_{02} mode of a standard SMF-28 telecom fiber was also reported by Pourbeyram and Mafi[85]. By means of a numerical study, they explained the emergence of the anti-Stokes wave in the LP_{02} mode as resulting from nonlinear mode coupling, owing to the light-induced grating generated, via the Kerr effect, by the beating of LP_{01} and LP_{02} mode components of the pump wave. In turn, nonlinear mode coupling between the corresponding LP_{01} and LP_{02} modes of the anti-Stokes wave leads to a saturation of the mode conversion induced by IFWM.

Although the availability of a discrete spatial dimension (i.e., the MMF modes) enhances

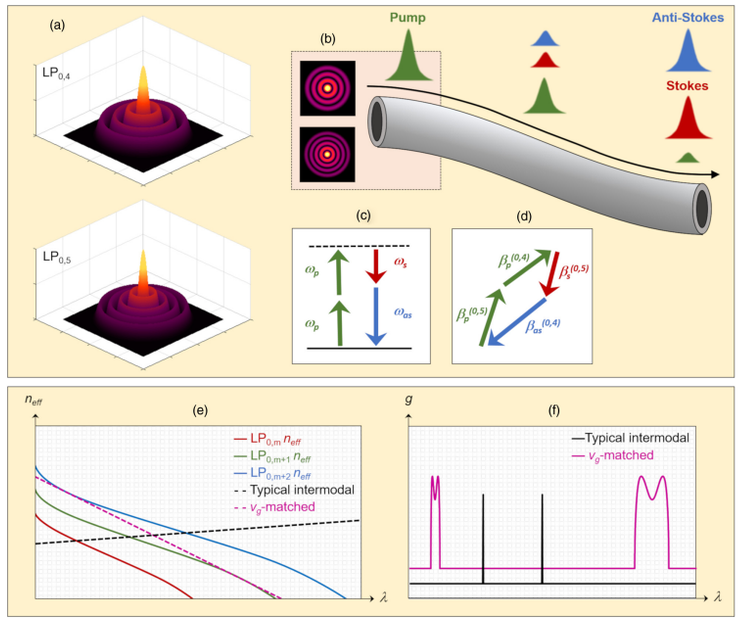

FIG. 12. (a) Intensity profiles of pump modes. (b) Schematic of IFWM of pump (green pulse) to anti-Stokes (blue pulse) and Stokes (red pulse) waves. Schematic representation of (c) energy conservation and (d) phase matching. (e) Phase matching in the effective refractive index picture: solutions exist where the straight, dashed lines intersect the effective index curves for different modes (solid lines). (f) Parametric gain for typical intermodal processes (black line) and a group-velocity-tailored process (purple line) [Reprinted with permission from[86]. Copyright 2019 Photonics Research]

the possibility of achieving phase-matched FWM interactions, the frequency bandwidth of IFWM processes is generally relatively narrow, unless simultaneous phase and group-velocity matching can be achieved by appropriate fiber engineering. To this purpose, Demas et al. have recently proposed and demonstrated a scheme for enhancing by more than an order of magnitude the phase-matching bandwidth of IFWM[86]. This was achieved by appropriate group-velocity-tailoring of the nonlinear mixing between HOMs in a MMF. Namely, by using a mixed mode pump configuration involving the LP_{04} and LP_{05} modes of a step-index MMF, broadband intermodal parametric frequency conversion was experimentally demonstrated (and whose bandwidth was equal to 63 nm at 1553 nm and to 17 nm at 791 nm) . Optimal parametric conversion bandwidth is achieved by adjusting the pump wavelength, until the anti-Stokes and Stokes wavelengths are such that the effective index curves of the respective interacting modes are tangential to the phase-matching line (see Figure 12). By subsequent

seeding of the IFWM process, a high-peak-power, wavelength-tunable all-fiber quasi-CW laser in the Ti:sapphire wavelength range was also demonstrated.

IFWM processes in MMFs can be exploited to generate photon pairs with a controlled degree of spectral correlation. Pourbeyram and Mafi have theoretically studied quantum correlations of generated signal and idler photons in a GRIN MMF, and demonstrated that their value can be preserved over a wide frequency range, while tuning the pump beam[87]. In other words, varying the pump wavelength will only vary the frequencies of Stokes and anti-Stokes waves, without affecting the purity of their photon state, which, on the other hand, depends on the sideband frequency separation from the pump. Moreover, it was predicted that it is possible to generate factorable two-photon states, which allow for heralding of pure-state single photons, without any necessity of narrowband spectral post filtering. Finally, by suitably adjusting the fiber length and/or the pump bandwidth, it is possible to simultaneously generate both correlated and uncorrelated photon pairs.

So far, IFWM has been intentionally exploited in MMFs for extending the spectral emission range of mode-locked lasers. On the other hand, when high-power CW fiber lasers based on large mode area or multimode fiber amplifiers are involved, IFWM is an unwanted effect that depletes the energy of the oscillator, hence it should be suppressed. By calculating the phase-matching frequency shift and coherence length of IFWM peaks, Yin et al. could determine the corresponding fiber mode combinations, so that the fiber laser parameters (core radius, numerical aperture) could be optimized in order to suppress IFWM emission[88]. Fiber coiling was also applied, to further suppress HOMs by reducing the bending radius of the fiber.

B. Intermodal MI

The concept of using group-velocity matching for enhancing the bandwidth of parametric frequency conversion in multimode fibers dates back to the pioneering 1997 work by Millot et al.[89]. By observing that the LP_{01} and LP_{11} modes of a bimodal step-index MMF have the same group-velocity at a particular wavelength (626.5 nm in their experiment), one obtains that propagation in a bimodal MMF is described by a set of two incoherently coupled NLSEs, where the cross-phase modulation (XPM) term is larger than self-phase modulation (SPM). This condition leads to the existence of XPM-induced intermodal modulation instability

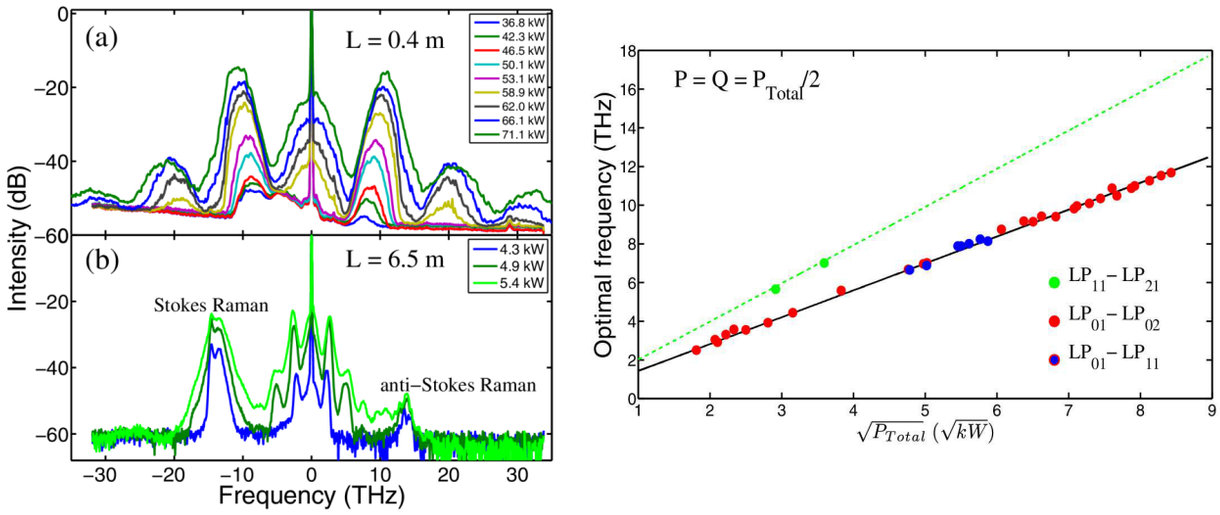

FIG. 13. Left panel: Experimental spectra recorded at different input total peak powers for excitation of LP_{01} and LP_{02} modes, and different fiber lengths; Right panel: Power dependence of the optimal IMI frequency. Experimental measurements (dots) are compared with theoretical results (lines) for different pairs of pump modes [Reprinted with permission from[91]. Copyright 2017 Optical Society of America]

(IMI), which is the only MI present when all modes propagate in the normal dispersion regime of the fiber. By tuning the pump laser wavelength, the group-velocity mismatch between the equally intense LP_{01} and LP_{11} modal components of the pump beam can be made to vanish. As a result, the condition of phase-matching for the spontaneously generated Stokes and anti-Stokes waves depends solely upon the total pump power. Therefore, a strong power dependence of the parametric gain (or IMI) spectra was observed: the peak sideband gain frequency varied by over 11% (from 0.65 to 1 THz) as the pump power increased from 100 to 400 W[89].

Later on in 2006, Tonello et al. carried out an experimental analysis of IMI in a birefringent holey fiber with elliptical core composed of a triple defect[90]. By shifting the pump wavelength from 532 to 625 nm, IMI sidebands shifted from 33 to 63 THz.

In 2017, Dupiol et al. have characterized the properties of IMI in a few-mode GRIN MMF[91]. At the pump wavelength of 1064 nm, the fiber supports the propagation of four modes, namely, the LP_{01}, LP_{11}, LP_{21} and LP_{02} modes. In the analysis and the experiments, the pump was divided in a pair of modes with different group number g, so that its propagation can be represented in terms of a pair of incoherently coupled NLSEs. The conditions

for the occurrence of IMI were determined, showing that, among the five pairs of modes, only three of them may be unstable. A strong power dependence of the IMI spectra was observed: as shown in Figure 13, the peak gain modulation frequency scales as the square root of the injected pump power.

The study of IMI has been theoretically extended by Guasoni[92] and by Li et al.[93] to the case of a step-index MMF which supports multiple modes. Whenever the pump power is equally divided in certain bimodal combinations, the peak sideband frequency scales as the square root of total power, and peak gain increases linearly with total power. Whereas for unequally excited pumps, there exists an optimal power ratio among different modes which leads to peak gain.

C. Geometric Parametric Instability

The spatiotemporal nature of optical beam propagation in highly-multimoded MMFs leads to a peculiar type of MI, which has no counterpart in singlemode or few-mode fibers. The periodic self-imaging of an intense CW beam in a GRIN MMF leads, via the intensity dependent contribution to the refractive index or Kerr effect, to a long-period refractive index grating. In the undepleted pump approximation, frequency-shifted sidebands experience propagation in a periodic fiber, which leads to quasi-phase-matching of FWM, or parametric instability, regardless of the sign of fiber dispersion[16].

This instability is analogous to Faraday instability in periodically modulated fluids: however, since it is generated by the geometric properties (i.e., the parabolic index profile) of a GRIN fiber, it has been called by Krupa et al. "geometric parametric instability" or GPI[19]. GPI is self-induced by the periodic focusing properties of the fiber, so that the space and time dynamics are intimately connected, and cannot be separated. As we have seen in Section III, the intensity and the width of an input Gaussian beam periodically oscillate along a GRIN MMF, as determined by Eq. (4). Note that if the input beam size is chosen such that $C = 1$, one obtains a self-trapped beam with no beam oscillations, hence the GPI gain vanishes. For example, with a pump at λ=800 nm, $R = 100\ \mu m$, and $\Delta = 0.005$, one obtains that $C = 1$ for $a_0 = 8.4\ \mu m$[16]. Otherwise, the frequency shift of GPI sidebands from the pump reads as

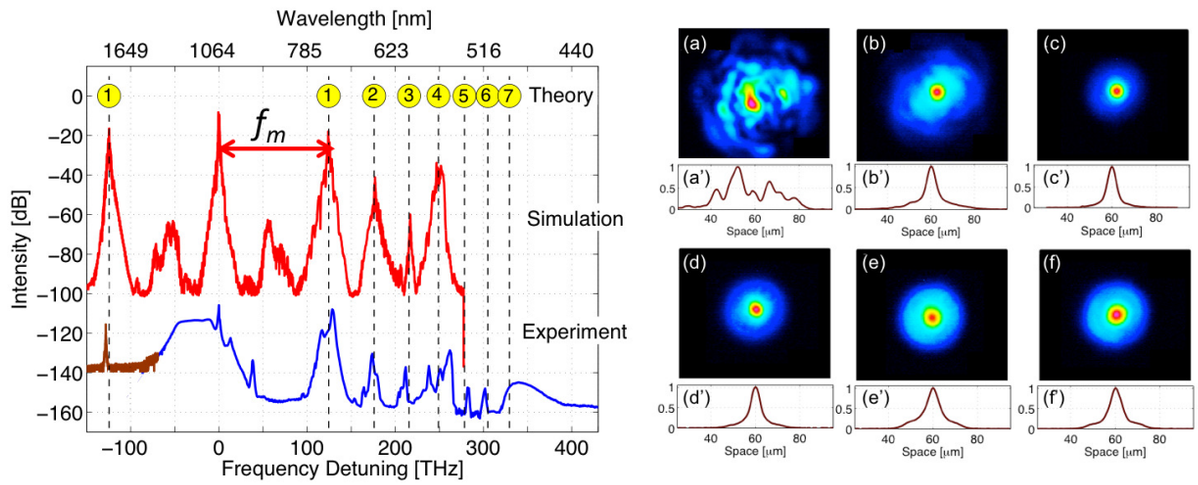

FIG. 14. Left panel: comparison of analytical, numerical and experimental GPI sidebands; Right panel: Experimental output spatial beam patterns and corresponding beam profiles (normalized intensity) versus x (y=0 section) at the pump wavelength for an input power (a, a') $P_{p-p} = 0.06$ kW and (b, b') $P_{p-p} = 50$ kW, as well as, at first four orders anti-Stokes sidebands at (c, c') 750 nm, (d, d') 650 nm, (e, e') 600 nm, (f, f') 550 nm, for $P_{p-p} = 50$ kW [Reprinted with permission from[19]. Copyright 2016 by the American Physical Society]

$$\Omega_N \simeq \pm \left(2N\sqrt{G}/|\beta_2|\right)^{1/2}, N = 0, 1, 2, ... \tag{9}$$

In 2016, Krupa et al. presented the first experimental demonstration of multiple GPI sideband generation in a standard GRIN MMF[19]. The input beam was launched in the fiber by means of an amplified microchip laser, emitting sub-ns pulses at 1064 nm. As shown by Figure 14, the experimentally observed frequency spacing among sidebands agrees well with both analytical predictions and numerical simulations. The first-order GPI peaks were located at the considerably large detuning of 123.5 THz from the pump. These experiments show that GPI may permit to convert a NIR laser directly into a broad spectral range, spanning visible and infrared wavelengths, by means of a single resonant parametric nonlinear effect which occurs in the normal dispersion regime. In addition, as shown by the right panel of Figure 14, the presence of a strong space-time coupling led to the surprising observation that, at high powers, the pump and all sidebands were carried by a well-defined and stable bell-shaped spatial profile.

The dependence of the GPI sideband frequency Ω_N on the fiber core radius R shown by Eq. (9) means that, as experimentally demonstrated by Sanjabi Eznaveh et al., their position can be varied by appropriate fiber design[94]. GPI sidebands were generated in three fiber samples with 50 μm, 60 μm, and 80 μm core diameter, respectively. Moreover, they demonstrated that, by cascading two 2.5 m long fibers of different core sizes (i.e., 50 μm and 80 μm) one may broaden the frequency band with respect to that produced by GPI in a single 5 m section with 50 μm core diameter. This is because the GPI sidebands are red-shifted as the core diameter gets larger. These results suggest that core scaling and fiber concatenation can provide an interesting method for designing optical sources with tailored output frequencies[94]. A natural extension of this approach is provided by using a GRIN MMF with a gradual tapering of its core diameter, as recently demonstrated by Eftekhar et al.[95].

A more accurate description of GPI sideband generation in GRIN MMF can be provided by including the power-dependence of the sideband positions, as well as higher-order dispersion. This approach leads to describing the periodic beam propagation subject to self-imaging and nonlinearity by means of a Hill's equation, whose stability can be studied by standard Floquet techniques. This theory predicts that unstable spectral domains associated with GPI can be significantly broadened at relatively high pump powers[96].

It is interesting to consider the emergence of parametric instabilities in the presence of a periodic variation of the linear fiber core diameter, combined with the intrinsic dynamic or light-induced grating due to self-imaging of the pump beam. Mas-Arabi et al. carried out such a theoretical and numerical study, showing that the additional degree of freedom represented by the core diameter modulation permits to modify the spatiotemporal dynamics of GPI[97]. This effect is more pronounced in the resonant case, namely, whenever the periodicity of the core diameter modulation is close to the self-imaging period, which leads to a Moiré-like pattern and additional spectral peaks.

In 2017, Teğin and Ortaç studied by both numerical simulations and experiments the propagation of 200 fs pulses at 800 nm from a Ti:sapphire laser in 2.6 m of a 50 μm core diameter GRIN MMF. For input pulse energies above 345 nJ, the generation of flat-top supercontinuum (as typical in the normal dispersion regime) was accompanied by the observation of Stokes and anti-Stokes sidebands, shifted by 91 THz from the pump. The generation of sidebands was ascribed to a spatiotemporal instability akin to GPI. In fact,

the input beam waist was estimated to be around 20 μm, which corresponds to the input excitation of a large number of HOMs, thus leading to collective beam oscillations or self-imaging. However, quite surprisingly, the experimental result could be reproduced by numerical simulations, where the pump was coupled to the first three radially symmetric modes only[98].

D. Supercontinuum Generation

The first report of SCG in MMFs dates back to the 1988 experiments by Grudinin et al.[23]: by pumping a GRIN fiber with 150 ps pulses at 1064 nm, a cascade of Raman Stokes lines was observed until crossing the zero-dispersion wavelength, so that femtosecond Raman solitons could be generated.

In a 2003 experiment, Mussot et al. demonstrated SCG spanning more than two octaves, by using a subnanosecond microchip laser pump at 532 nm and a conventional dispersion-shifted fiber[99]. Since the zero dispersion wavelength of this fiber at 1550 nm is far away from the pump wavelength, IFWM between the LP_{01} and LP_{11} modes (both excited by the input pump) was exploited as a starting process to seed SCG. Subsequently, a double cascade of SRS led to spectrum expansion towards the infrared, with a fundamental LP_{01}modal content for wavelengths above 650 nm, owing to the Raman beam cleanup effect. In the same year, Efimov et al. demonstrated the nonlinear generation of very high-order UV modes (with wavelengths as short as 260 nm), by pumping a coweb microstructure optical fiber with 100 fs Ti:sapphire pulses, by properly controlling the input launching conditions of the 800 nm pump[100]. For selective excitation of the HOMs, they used either offset pumping (i.e., the input beam was properly focused, possibly with an angle, on the input cross section of the fiber), or cleaving the fiber input by its exposure to a high input average power.

Later on in 2013, Pourbeyram et al. pumped with 8 ns pulses from a frequency-doubled Nd:YLF laser at 523 nm, a 1 km long, standard GRIN MMF: the generated Raman cascade reached up to 1100 nm[101]. Although the pump remains highly multimode, Raman peaks were generated in specific HOM of the fiber, a manifestation of Raman beam cleanup. Energy tunneling into the anomalous dispersion region leads to a Raman-shifting soliton reaching up to 1750 nm.

In 2015, Wright et al. studied SCG in a 1 m long GRIN MMF pumped by 500 fs pulses at

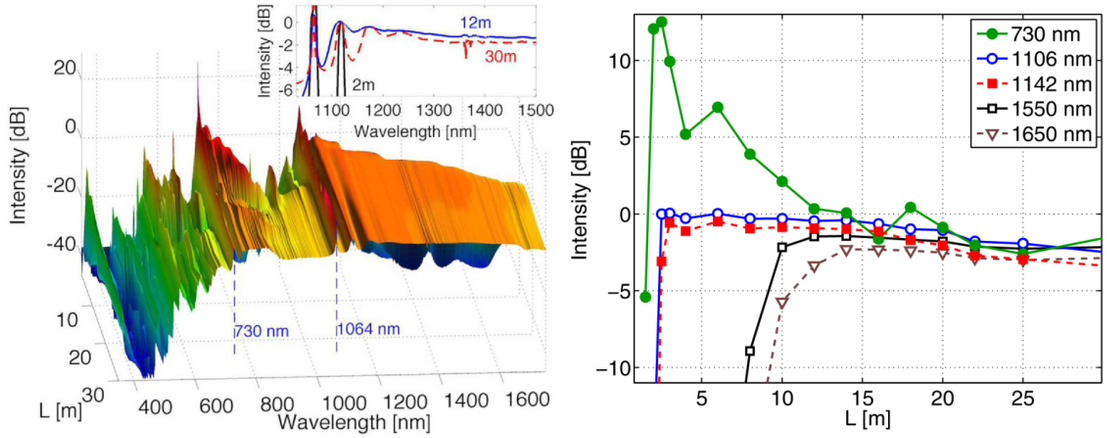

FIG. 15. Left panel: experimental results of the cut-back technique; right panel: evolution of the spectral intensity at selected spectral components from the left panel [Reprinted with permission from[104]. Copyright 2016 Optical Society of America]

1550 nm, propagating in the anomalous-dispersion regime[34]. By adjusting the spatial initial conditions, they showed that it was possible to generate Raman-shifted multimode soliton pulses tunable between 1550 and 2200 nm, as well as dispersive waves, intense visible combs, and a multi-octave-spanning supercontinuum. Later on, Eftekhar et al. demonstrated that, by adjusting the spatial input profile of the pump beam at 1550 nm, one may obtain a versatile tailoring of the spectral content of SCG in GRIN fibers[102]. By changing the modal composition of the input beam via off-axis excitation, or by using, e.g., a ring-shaped or two-spot input beam, one may alter the soliton fission process, as well as the SSFS and dispersive wave generation processes that seed the SCG.

Recent studies have investigated the details of SCG in GRIN MMFs, pumped with sub-ns pulses in the normal dispersion regime at 1064 nm. The combined action of GPI and SRS leads to efficient and spectrally flat SCG extending into the visible spectral range, as it has been independently reported by different groups[103,104]. The generated spectra span more than two octaves, and exhibit high-quality, bell shaped beams. These results lead to a new class of high brightness and power, compact multi-octave supercontinuum sources.

Lopez-Galmiche et al. used a 28.5 m long GRIN MMF, and demonstrated SCG spanning from below 450 nm and extending beyond 2400 nm[103]. By controlling the input launch conditions, they demonstrated versatile generation of visible spectral peaks in shorter fiber spans.

Krupa et al. characterized the development of SCG along the MMF by the cut-back method, which allows better characterization of the competition between GPI and SRS[104]. As can be seen in Figure 15, GPI and SRS provide the major contributions to the spectral broadening, but their effects occur over different length scales. In the very first meter of propagation, GPI generates the first-order anti-Stokes sideband at about 730 nm, which carries around 12% of the total input power. After 1.5 m of propagation, SRS causes a gradual spectral extension toward the IR: the resulting pump depletion inhibits GPI. For fiber lengths up to about 12 m, and for peak powers above 35 kW, SRS-induced SCG takes an unusual flat shape in the IR. A spectrally resolved temporal analysis of the supercontinuum emission revealed the presence of a deep temporal modulation within the flat portion of the NIR supercontinuum spectrum. The largest Raman frequency shift comes from the highest input peak power which, in turn, leads to the strongest pump pulse depletion at the MMF output. As a consequence, different power values across the temporal profile of the input pump pulse lead to different wavelength shifts.

SCG in a longitudinally tapered GRIN MMF was recently investigated by Eftekhar et al.[95]. When the input beam is coupled into the fiber side with the largest core diameter, the exponential decrease of the core diameter along the taper leads to accelerated self-imaging. This results in a progressive blue-shifting of GPI sidebands, and to stronger nonlinear intermodal interactions. When pumped in the anomalous dispersion region, accelerating self-imaging may lead to blue-shifted multimode solitons and dispersive wave combs. On the other hand, when the taper was pumped in the normal dispersion region, highly flat and uniform SCG was observed, extending over 2.5 octaves.

To fully exploit the scalability with respect to the average power of supercontinuum sources based on MMFs, it is important to use high-repetition rate pump sources. To this end, Teğin and Ortaç used a 2 MHz pump laser in order to demonstrate a 4 W average power supercontinuum source based on cascaded SRS in a GRIN MMF[105].

In all of previous experiments, GRIN MMFs were employed. In 2018, Perret et al. demonstrated broadband SCG from 560 nm up to 2350 nm, by coupling a Q-switched Nd:YAG pump into a step-index fiber supporting five modes[106]. In this fiber, SCG was activated by multiple cascaded IFWM and SRS.

E. Second harmonic generation

As is well known, the inversion symmetry of silica glass precludes silica fibers from having a macroscopic bulk quadratic nonlinear susceptibility. Nevertheless, a quadratic nonlinearity can be efficiently written in silica glass by either thermal or optical poling. The first process is based on exposing the fiber core, heated up at about 250 °C, to a strong static electric field which, by means of a charge transport process, and a consequent permanent static electric field, induces a quadratic nonlinearity. In the second process, an intense fundamental frequency (FF) pump generates a photo-induced charge distribution, giving rise to a permanent modulated $\chi^{(2)}$, whose period automatically satisfies the quasi-phase matching (QPM) between the FF and the second harmonic (SH) waves. Since the first experimental observations of SH generation in optically poled germanium-doped fibers[107,108], researchers have been investigating several mechanisms that could explain the onset of the quadratic nonlinearity[109]. The writing of the quadratic susceptibility is much faster if both the FF pump and its SH are injected into the fiber, and measurements have confirmed the presence of the static electric field due to the charge distribution inside the poled fibers. Those experimental data strongly support the hypothesis that a multiphoton ionization process[110,111] leads to a periodic static electric field which, through the glass cubic nonlinearity, gives rise to an effective $\chi^{(2)}$[109].

In a GRIN fiber, because of self-imaging, the pump intensity oscillates along the fiber, and so does the $\chi^{(2)}$ amplitude. In conclusion, the photo-induced $\chi^{(2)}$ of a GRIN MMF has a double periodicity, that of QPM (about 48 μm) and that of self-imaging (about 1 mm).

The spectral and spatial properties of SH generation in an all-optically poled GRIN fiber were recently studied by Ceoldo et al.[112]. In contrast with poled singlemode fibers, because of the additional slow modulation of $\chi^{(2)}$ induced by pump self-imaging, the FF generates a series of sharp sidebands around its SH (see the left panel in Figure 16).

In addition, similar to the case of GPI induced sidebands, the mutual interaction between the FF and its SH strongly affects the spatial distribution of guided light for both colors at the fiber output. As can be seen in the right panel in Figure 16, when increasing the pump power, both FF and SH output beams evolve from disordered multimode speckles into two bell-shaped beams. While the mechanism for pump beam reshaping can be ascribed to that of Kerr beam self-cleaning, as discussed in the next section, the fact that the SH beam

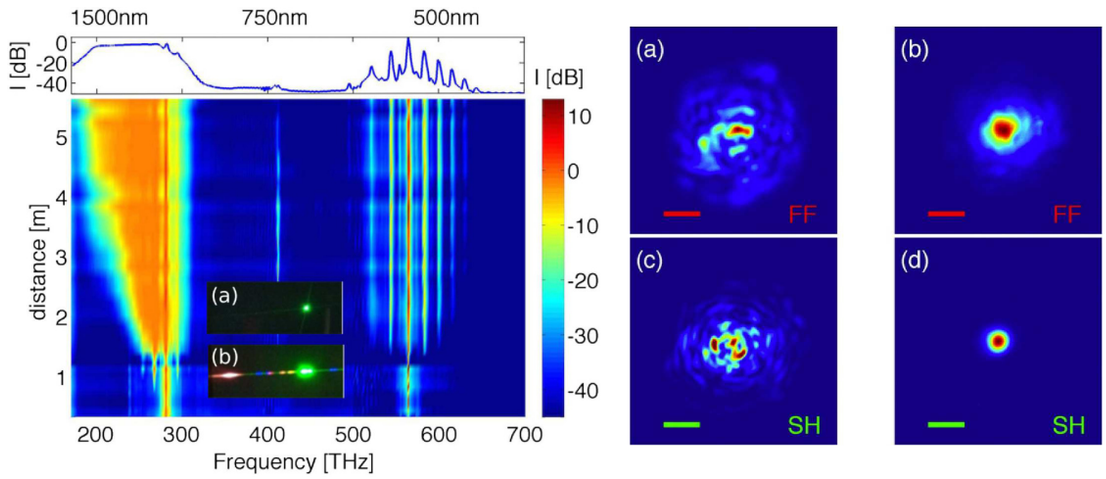

FIG. 16. Left panel: Experimental spectra measured along the poled MM-GRIN fiber by the cut-back method; insets show a photo of the output beam (a) without and (b) with GPI; Right panel: Measured FF and SH beam shapes at the output of a 2 m long poled fiber, for (a, c) low (0.94 kW) and (b, d) high (39 kW) pump powers [Reprinted with permission from[112]. Copyright 2017 Optical Society of America]

also acquires a bell shape was unexpected. In fact, propagation at the SH is much more multimodal than at the FF; moreover, the SH power is only about 1% of the FF power, thus it is well below the self-cleaning threshold. Therefore, SH beam cleaning is a cascade process: the presence of a self-cleaned pump leads to maximum overlap with the fundamental mode at the SH wavelength, which thus experiences the highest gain.

Subsequently, Eftekhar et al. showed that germanium-doped GRIN MMFs can exhibit relatively high conversion efficiencies (up to 6.5%) for SH generation when excited by a FF at 1064 nm[113]. In their experiments, SH generation was found to be accompanied by an effective downconversion, whose phase-matching mechanism remains unexplained. SH generation experiments in a step-index MMF showed that in this case the green light was much weaker (by almost 2 orders of magnitude) than that observed in a GRIN MMF. The reason for that was ascribed to the facilitating presence of GPI as a seeding process in a GRIN MMF. However, the measurements by Ceoldo et al. (see the insets of the left panel in Figure 16) have shown that GPI, although its presence enhances the SH brightness, is not a required process in order to obtain SH generation in a GRIN MMF[112]. Therefore it is possible that pump beam self-cleaning (which is not observed in step-index MMFs) is rather

the enabling mechanism for efficient SH generation in GRIN MMFs.

F. Wavefront shaping control

Wavefront shaping is a technology that enables the control of light propagation through linear media, and permits focusing of an image through scattering objects. In 2018, Tzang et al. demonstrated that a wavefront shaping approach can also be used for controlling nonlinear frequency conversion processes (such as IFWM and SRS) in MMFs[114]. By using a spatial light modulator at the fiber input, real-time spectral feedback and a genetic algorithm optimization, the multimode SRS cascade and its interplay with IFWM could be tailored via a flexible implicit control on the superposition of modes coupled into the fiber. It has thus been demonstrated that wavefront shaping permits a versatile manipulation of the spectrum generated by MMFs, including shifts, suppression, and enhancement of Stokes and anti-Stokes peaks.

V. SPATIAL BEAM SHAPING

Along the propagation in MMFs, random linear mode coupling, caused by mechanical perturbations and technological imperfections, leads to spreading of an input spatially Gaussian light beam among a large number of guided transverse modes. The unavoidable consequence is the emergence, at the fiber output, of a speckled beam pattern that is not ideally suited for beam delivery. The poor spatial beam quality, together with the spatiotemporal complexity of beam propagation in MMFs, have rapidly redirected the interest for both fundamental and applied research towards singlemode fibers (SMFs) since the early days of their advent, leaving MMFs substantially unexplored. As a matter of fact, SMFs can deliver output beams whose high spatial quality is close to that of a Gaussian beam: this fact is due to the single-mode nature of the propagation, which affects only temporal domain.

However, as pointed out in the introductory part, in the last several years we have observed a strong resurgent interest for the research on MMFs. Moreover, recent works demonstrated how specific signal-processing algorithms could be used to manage the output beam pattern of MMFs by controlling the corresponding input field[115–117]. In the nonlinear

regime, instead, light propagating in MMFs unveils striking effects, as the spatial beam reshaping arising from collective beam dynamics (e.g., from self-imaging). Several works have already demonstrated how the self-organization of spatiotemporal content of multimode light beams is possible by exploiting the fiber nonlinearities, rather than relying only on complex devices for input/output mode composition control.

A. Beam cleanup through dissipative and other nonlinear process

A spontaneous recovery of spatial beam quality, called spatial beam cleanup, was observed in GRIN MMFs pumped by nanosecond pulses through nonlinear dissipative processes such as stimulated Raman scattering (SRS) or stimulated Brillouin scattering (SBS), where the Stokes waves evolve into one of the lowest-order fiber modes, including, in particular, the fundamental mode, while the pump remains in the initially excited multimode structure. In addition to the single-pass configuration[118–120], Raman-induced and Brillouin-induced beam cleanups were also obtained in cavities[120]. Demonstration of Raman fiber lasers pumped by multimode pump lasers able to generate Stokes beams with good beam quality was then possible[121,122], as will be discussed later in Section VI-C1. Beam cleanups, based on these two dissipative processes, have been further used for highly efficient beam combination in optical fibers[123–125], and multimode fiber communication links[126].

An explanation for why the SRS and SBS beam cleanups require the use of GRIN MMFs, and do not occur in step-index fibers was provided by Terry et al.[25] and Lombard et al.[120], respectively: they demonstrated that, in both dissipative effects, mode-dependent gain favors the Stokes carried by the lower-order modes, thanks to their higher overlap with the pump modes of the fiber. The dominant mode of the Stokes beam can thus propagate in various lower-order fiber modes by adjusting the launching conditions of the pump beam[25,120,127]. Step-index MMF was found instead to be an excellent waveguide for the observation of the phase conjugation phenomenon, because of the mode overlap factor which is similar for all modes of this fiber[120,128]. A different explanation of the SBS beam cleanup in MM fibers is based on the seeding process, in which the Stokes beam is expected to preserve the same modes of the seed beam, which are externally excited. SBS beam cleanup should then occur if only a seed beam with a low-order mode, especially a fundamental mode, has been selectively excited[127–129]. Such a seeding process was further exploited to preserve a

single-mode beam quality and a narrow spectral bandwidth of the master oscillator[127].

More recently, in 2015, Wright et al. reported supercontinuum generation of femtosecond light pulses in the anomalous dispersion regime of GRIN MMFs, suggesting the potential role of self-focusing and multiple filamentation, as well as soliton fission and Raman self-frequency shift of multimode solitons in the observed beam cleanup, controlled by the input launching conditions[34]. The possibility to obtain beam cleanup through multimode soliton interactions has also been pointed out by Buch and Agrawal[43]. More detailed description of multimode solitons has been presented in the previous section III. Lushnikov and Vladimirova proposed instead the use of the self-focusing effect to combine multiple laser beams into a single one: It is known that if one increases the power above the critical level, the nonlinear self-focusing can overcome the diffraction at any size of the beam and the beam may collapse into a filament[130].

B. Kerr beam self-cleaning

1. Kerr beam self-cleaning in lossless multimode fibers

In a more recent experiment by Krupa et al., it was demonstrated that the pure intensity-dependent contribution to the refractive index, or Kerr effect, in MMFs also has the capacity to form a highly stable, spatially compressed beam with a diameter close to that of the fundamental fiber mode[19,20]. The same input conditions led to an irregular multimode pattern at the fiber output in the linear regime. This observation showed that, unexpectedly, above a certain power threshold, light itself can trigger a self-organization process within MMFs, through a complex nonlinear mode mixing. Initial experimental demonstrations of spatial beam self-cleaning were performed by using sub-nanosecond pulses in normally dispersive standard commercially available GRIN MMFs[19,20,103,104,131]. An example of the obtained results is presented in Figure 17, where we can see how a speckled beam at the output of the fiber at low power, can evolve into a robust bell-shaped output transverse profile surrounded by a weak and broad speckled background, when the input pump power grows larger[20].

Note that the Kerr beam self-cleaning is fundamentally different from the aforementioned cleanup effect induced via SRS or SBS, where only red-shifted wavelengths have been carried

by the fundamental fiber mode; the Kerr beam self-cleaning appears at the pump itself, without any significant spectral broadening, frequency conversion, and dissipative processes. This effect is also different from the catastrophic self-focusing[47], which requires instead peak power levels of the order of several MWs, that is orders of magnitude larger than the ones used in self-cleaning experiments. The improvement of Kerr-induced output beam quality is testified by the important decrease upon input power of the M^2 beam parameter, as illustrated in Figure 18[20]. Importantly, this spatial self-organization phenomenon has been found to be robust against fiber bending and squeezing, as well as moderate variations in input launching conditions, leading to different energy distributions among the guided modes.

In this context, Laegsgaard has demonstrated numerically by means of a statistical study that indeed the reduction of spatial input fluctuations during beam propagation in GRIN MMFs may occur due to a purely Kerr-induced transfer of disorder from the spatial to the temporal/spectral domain, in accordance with fundamental considerations on entropy conservation[132]. The effect has been found to be only weakly dependent on the absolute magnitude of spectral broadening. However, according to the model spatial beam cleaning should disappear for a perfectly continuous wave (CW) beam, that is, when only one frequency component is considered in the nonlinear propagation. The reduction of spatial fluctuations was numerically observed for a spectral broadening of less than 100 pm when using 1-ns input pulse[132].

In Kerr self-cleaning experiments, spectral broadening above the onset of beam fluctuation reductions was barely noticeable and below 50 pm[20]. As it will be described later in this section, Kerr beam cleaning is accompanied by clearly measurable changes in the temporal pulse profile, leading to complex pulse break-up and pulse compression, already at power levels below the onset of spatial beam reshaping[133].

Asawa and Taylor have instead studied theoretically and experimentally the influence of bending perturbations on CW light propagation in GRIN MMFs[134]. They found that when the fundamental mode is excited, light is converted into a set of lowest-order modes, remaining trapped in that set even for small bend diameters. Whereas, light launched into the lowest-order modes remains in low-order modes, and it is not converted into cladding modes, even for relatively small-diameter ($\simeq$ 1 cm) bends. Only recently, Boonzajer Flaes et al. revisited the influence of bending deformations on multimode light transport[135]. They

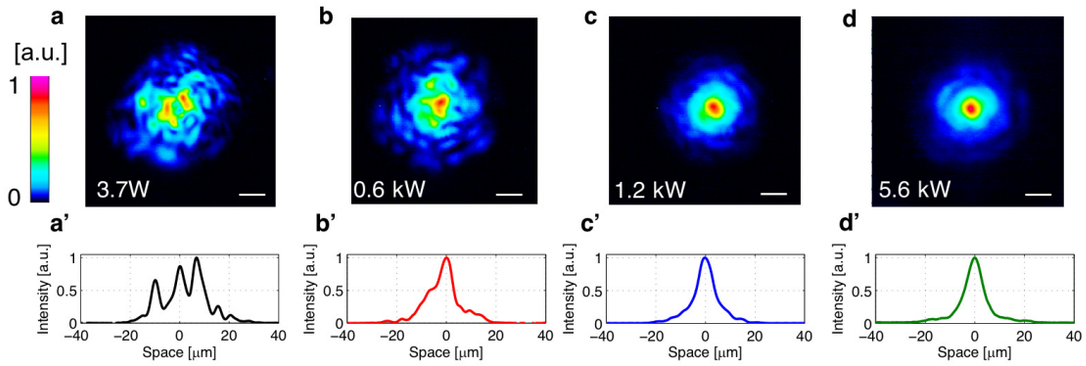

FIG. 17. Kerr beam self-cleaning in 12-m long GRIN MMF with sub-nanosecond pulses. (a-d) Near-field output images at 1064 nm versus output peak power. Scale bars, 10 μm. (a'-d') Corresponding beam profiles versus x (y=0 section). [reproduced from ref.[20]]

have shown that MMFs with a perfectly parabolic refractive index profile are very resilient to bending deformations, conserving the structure of propagation-invariant modes. They experimentally verified their theory by using a large core graded-index rod with a very precise refractive index pattern. As far as commercially available GRIN MMFs are concerned, they found instead that the tested fibers suffer from strong deviations from the ideal parabolic index profile, which precluded a direct experimental verification of the bending resilience. However, they demonstrated that even with the manufacturing imperfections, the imaging performance of GRIN MMFs is indeed significantly less influenced by bending deformations than step-index MMFs, under the same conditions.

Dealing with relatively long pulses propagating in the anomalous dispersion regime, Leventoux et al. have recently investigated Kerr beam self-cleaning by using 160 ps duration, highly chirped (6 nm bandwidth at -3dB) optical pulses at telecom wavelengths from a fiber laser operating at 1562 nm, injected into a GRIN MMF[136]. The laser beam was coupled into a 12 m long piece of GRIN MMF by means of a short section of standard SMF, which leads to optimized free-space coupling efficiency (up to 80%) into the MMF. These input conditions lead to more than 99% of the input pulse energy coupled into the first three radial symmetry modes only. This greatly facilitates the output beam cleaning process, and permits a more than one decade reduction (from 1 kW to 100 W) of the power threshold for beam self-cleaning, with respect to previous experiments in the normal dispersion regime, where a substantial amount of HOMs was excited at the fiber input. Moreover, nearly com-

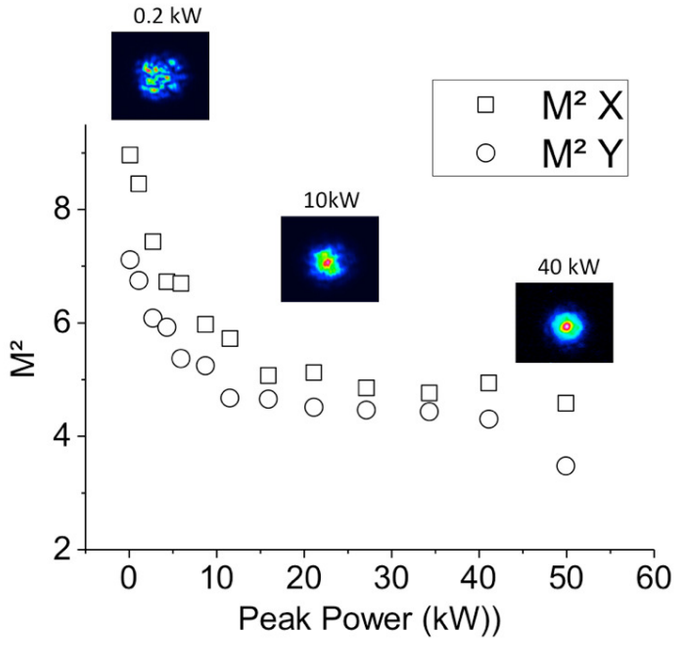

FIG. 18. M^2 measurements at the output beam of a 3-m long GRIN MMF and for the X and Y axis. Insets: Three corresponding near-field patterns. [reproduced from ref.[20]]

plete intensity correlation with the fundamental mode was achieved at the fiber output, in contrast with experiments in the normal GVD regime, where a large residual high-order mode background was generally observed around the self-cleaned beam. Self-cleaned beams were shown to remain spatio-temporally stable for more than a decade of variation of the input peak pulse power.

Dupiol et al. have experimentally studied spatial beam cleaning effects with a specially designed multimode photonic crystal fiber (MM PCF), based on a hexagonal pure silica core surrounded by three layers of air holes as optical cladding, whose diameters gradually increase when moving away from the fiber axis[137]. Such structure leads to a gradual decrease of the azimuthal average refractive index, and thus may be considered to be roughly the equivalent of a standard fiber with an index profile intermediate between that of a step-index and that of a GRIN fiber. The obtained results revealed the presence of a competition between Kerr and Raman beam self-cleaning. Namely, unlike standard GRIN MMFs, Kerr-induced beam reshaping and compression were only observed for a certain range of input powers, being next gradually spoiled by effective Raman conversion, which led to both

depletion and degradation of pump beam quality. Moreover, the authors observed that the interplay of modal four-wave-mixing and Raman scattering in the infrared domain can lead to the generation of a multimode supercontinuum ranging from 500 nm up to 1800 nm, with all induced sidebands carried by higher order modes.

The possibility to control spatiotemporal nonlinear beam shaping in MMFs by tailoring of the refractive index profile of the fiber was addressed in ref.[138] by using a standard GRIN MMF featuring a local depression (or dip) in the parabolic index profile. A central index dip may appear during the high temperature collapse of the preform tube. This effect is usually unwanted, and it can be circumvented by increasing the concentration of the more volatile dopant. However, as showed in ref.[138], the refractive index dip can also provide an interesting possibility for spatiotemporal multimode beam shaping. A small deviation from the parabolic index profile of a GRIN MMF breaks the dynamic grating periodicity resulting from self-imaging of the pump beam: this fact has a strong impact on spatial and spectral properties of parametric sideband generation. Kerr beam self-cleaning towards a bell-shaped spatial pattern could still be clearly observed (when considering that the dip is only a minor modification to the index profile of the fiber), but at several times higher threshold power than with an ideal parabolic profile. The dip also dramatically changes the spatial content of spectral sidebands due to the modifications of the mode propagation constants, which disrupts their regular spacing, and hence the collective beam oscillations. As a result, the sideband generation mechanism is no longer GPI, leading to bell-shaped beams all over the spectral range, but IFWM with sidebands carried by higher-order transverse modes (see also section IV). Breaking of oscillation synchronism has also strongly reduced the efficiency of frequency generation.

It is worth stressing that the core refractive index profile of the MMF plays a significant role in the self-cleaning process, by means of intermodal dispersion and by the creation of a periodic self-imaging process. If the main experiments on spatial Kerr self-cleaning have been made in pure GRIN fibers, we carried out several investigations of beam cleaning in nonparabolic MMFs. In these experiments, a progressive decrease of the self-cleaning efficiency was observed, alongside with an increase of the peak power threshold when the refractive index profile get closer to a step-index profile (see Figure 19).

Beyond the shape of the fiber core, the maximum refractive index difference between the core and the cladding appears also as a key issue, because of its direct impact on the

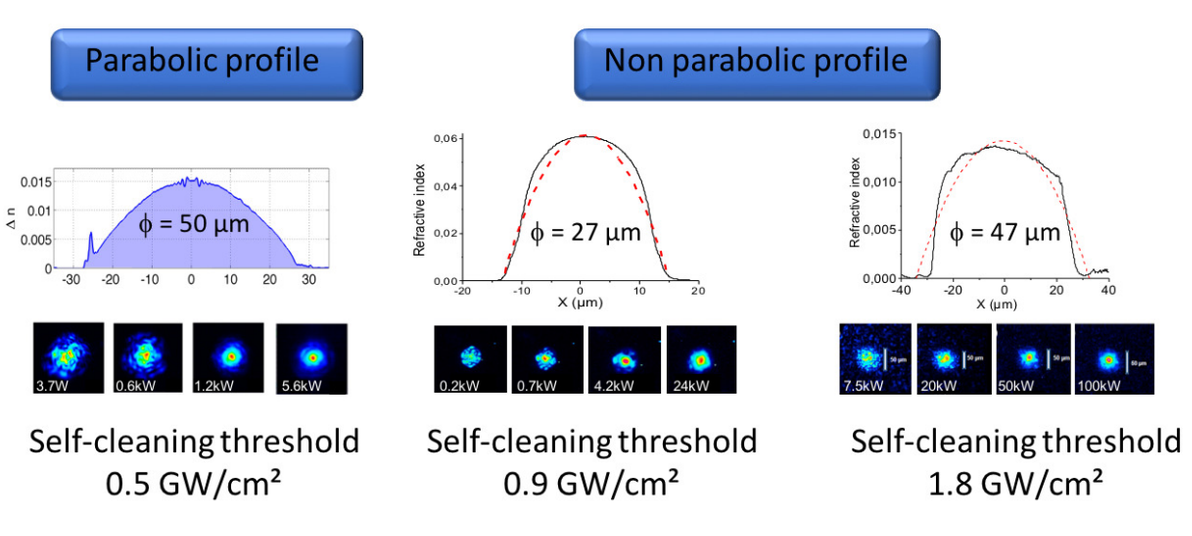

FIG. 19. Experimental results of spatial Kerr self-cleaning in three different MMFs; fiber length: 3m; wavelength: 1064 nm

number of guided modes. In our experiments, we found that the larger the number of modes over which the input beam energy is coupled, the lesser is the self-cleaning efficiency, which drastically limits the use of the cleaning process in applications. A typical example of spatial self-cleaning dynamics is shown in Figure 20, versus the initial coupling condition. The number of excited modes is changed with the spatial shift of the pump beam on the input face of the fiber.

Beyond the understanding of the physical phenomena involved in the nonlinear spatial Kerr self-cleaning effect, large perspectives are open regarding MMF technology, which have to be redesigned to boost the new demonstrated capabilities of such type of fiber. It clearly appears that multimode fibers with transverse and longitudinal micro-structuration can open a new way for high power single mode emission, for nonlinear large band conversion in visible and infrared domains, and to mimic the action of nonlinear saturable absorber able to temporally or spatially shape light structures.

2. Theory of Kerr self-cleaning

Since the first observations of the phenomenon of Kerr-induced beam self-cleaning, researchers have been working to elucidate and understand the physical mechanisms respon-

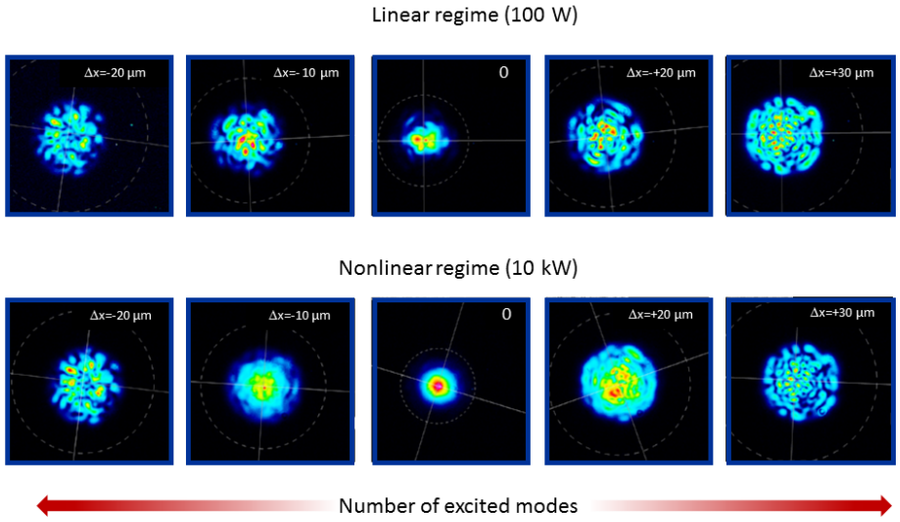

FIG. 20. Experimental results, spatial Kerr self-cleaning versus input excitation conditions driven by the transverse shift of the fundamental beam on the input face of the fiber (Fiber 50/125, 12 m length, wavelength: 1064 nm, pulse duration 500 ps).

sible for such surprising effect. Currently several hypotheses have been formulated, and all seem to agree that the self-imaging property of GRIN MMF and nonlinear mode mixing play an important role in this context. One of the hypotheses is based on nonreciprocal behavior of the nonlinear mode coupling. In fibers with a parabolic index profile, the equally-spaced propagation constants of the modes lead, through the coherent mode beating, to a periodic local intensity oscillation along the fiber, which in combination with the Kerr nonlinearity creates a periodic longitudinal modulation of the refractive index. With only two-mode excitation, such a dynamic refractive index grating was previously exploited by Hellwig et al. to demonstrate efficient mode conversion of the LP_{01} into the LP_{11} mode in a GRIN MMF[139].

In the multimode case, modal four-wave mixing (FWM) interactions introduce quasi-phase-matching conditions allowing for numerous mode-coupling processes, and thus energy exchanges among the modes, which may favor the fundamental mode of the fiber. Indeed, as already mentioned in this section, the parabolic profile of the refractive index provides the

highest value of mode overlap between the input multimode field and the fundamental mode. The energy exchanges, which involve the fundamental mode, become nonreciprocal because of its highest self-phase modulation coefficient; if the initial power distribution is in favour of the fundamental mode at a sufficiently large input power, one observes an irreversible decoupling of the fundamental mode, allowing the power to remain in this mode. Such an explanation has been proposed in ref.[20], and developed in the framework of a simplified two-mode mean-field model that describes analytically the dynamics of the interaction between the fundamental mode and a generic higher-order mode, driven by the collective presence of all fiber modes through FWM.

In the theoretical approach given in ref.[20], one of the initial phenomena allowing for spatial mode mixing and cleaning is the spatial self-imaging process, which can periodically modulate the core refractive index of the fiber when associated with the Kerr nonlinearity. Spatial self-imaging is a well-known process, and it was first observed by Talbot in 1836[6], but it remains difficult to really prove its existence and impact in multimode optical fibers. However, it is possible to work around this problem by recording the local nonlinear parametric conversion obtained in a non-collinear geometry, i.e., by using Cherenkov phase matching[140]. Thus, the periodic emission of a second harmonic wave, obtained at the core-cladding interfaces and accompanied by a wideband multi-photon fluorescence in the blue domain, can provide a clear evidence of the periodic evolution of the power density in the MMF (see Figure 21). The highlighting of that process is obtained with femtosecond excitation, in order to allow for high peak power excitation, which is maximized at the points of minimum beam waist of the periodic self-imaging process.

Beyond the indirect evidence of the periodic evolution of the light in a GRIN MMF, thanks to the observation of local nonlinear frequency conversion, it is also possible to directly measure the image of the output beam intensity pattern along a self-imaging period, or a period of the beating modes (see Figure 22). These measurements have been made for different positions in the fiber, and we clearly observe the multimodal evolution of the beam, with a significant increase of the peak power density at the nodes of periodic self-imaging. These experimental observations directly demonstrate the periodic modulation of the intensity of light guided in GRIN optical fibers, which is at the origin of the Kerr self-cleaning and GPI processes (see ref.[20]).

A very recent study by Podivilov et al. provides an interesting insight in the process of

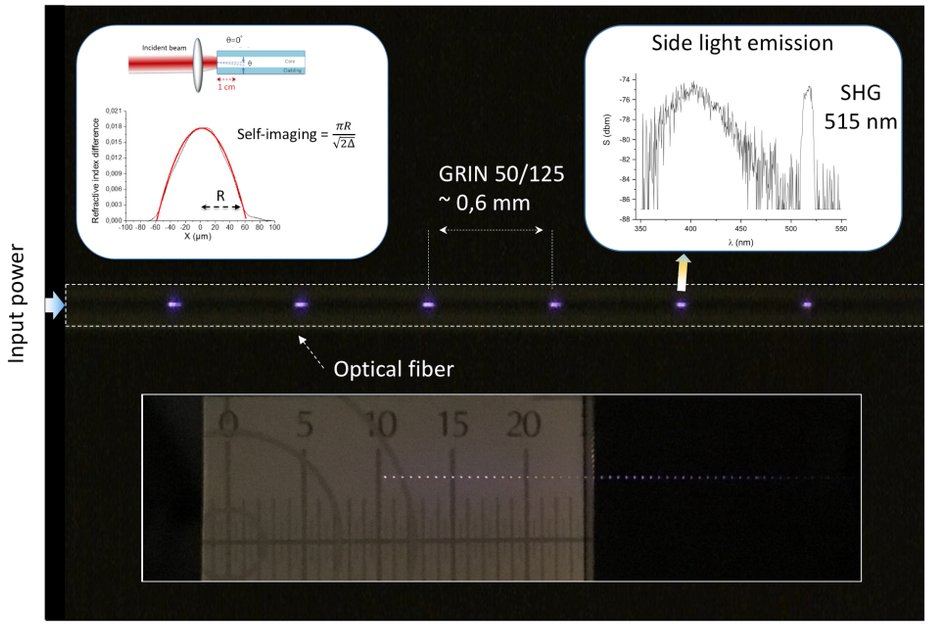

FIG. 21. Experimental evidence of periodic self-imaging, allowing for a periodic modulation of the core refractive index in 50/125 μm GRIN fiber (Pump wavelength: 1030 nm, 250 fs pulse duration, 30 kHz repetition rate). The measured periodicity is 0.6 mm, which matches well with the theoretical calculation.

beam self-cleaning in GRIN MMFs, by demonstrating that it is analogous to hydrodynamic 2D turbulence[141]. This process is characterized by a presence of a direct energy cascade towards high wave numbers, accompanied by the inverse cascade towards low wave numbers (fundamental mode). The nonlinear redistribution of energy among modes with different wave numbers occurs above a certain power threshold, due to parametric transverse mode mixing instabilities. The authors analytically predicted the power threshold for Kerr beam self-cleaning by approximating the mode coupling process by a truncated three-mode expansion involving the first three radially symmetric transverse modes only. In this case, the power threshold can be simply obtained as the power such that a bifurcation of a fixed point of the three-wave mode coupling process occurs, corresponding to the loss of spatial stability of the intermediate mode. As a result of the parametric instability, power flows in a symmetric way out of the intermediate mode, into both the fundamental and the highest order mode, respectively.

In the fully multimode case, Podivilov et al. pointed out that the spatial modes of the

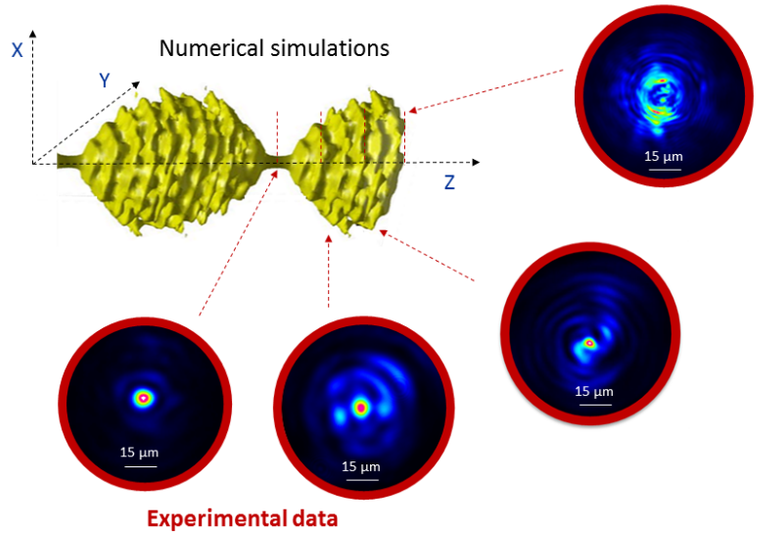

FIG. 22. Experimental evidence of the power density change along the propagation in a 50/125 μm GRIN fiber (Pump wavelength: 1030 nm, 250 fs pulse duration, 30 kHz repetition rate).

$3+1$D NLSE (Eq. (1)), with complex amplitudes $B_{p,m}$, evolve in a way to conserve both energy

$$\sum_{n=0}^{\infty} f_n = 1, \quad f_n = \sum_{p,m} |B_{p,m}|^2 \delta(n - 2p - |m|), \tag{10}$$

and average mode number

$$\sum_{n=0}^{\infty} n f_n = \overline{n} = const, \tag{11}$$

where $n = 2p + |m|$, and f_n is the energy in the group of modes with equal index n. As a result, one obtains that if the amplitude of modes with the largest wave number increases, then the amplitude of modes with intermediate wave numbers should decrease. At the same time, the fundamental mode intensity must also grow, so that the average mode number is conserved, as predicted by Eq.11. This conservation also occurs in the presence of random mode coupling, as long as its spatial correlation length is much longer than the self-imaging period in the GRIN fiber. The somewhat counter-intuitive conservation of the average mode number throughout the whole process of beam self-reshaping, which is a key ingredient of 2D hydrodynamic turbulence, was experimentally demonstrated[141].

Another hypothesis put forward by Wright et al. says that the origin of spatial beam self-cleaning in GRIN MMFs is a universal unstable attractor, whose self-organization and instability are both caused by intermodal interactions mediated by cooperating disorder, nonlinearity and dissipation. Basing on their theoretical model and experimental results, the authors show that a given initial field in a GRIN MMF self-organizes into a state that is the most unstable, and once the critical state of the attractor (i.e. a clean Gaussian beam) is reached, subsequently spatiotemporal modulation instability occurs, which in turn causes the field to evolve towards a spatiotemporally complex steady state. In the experiments sub-nanosecond duration pulses with kilowatt peak power were propagated in 100-m long normal-dispersion GRIN MMFs with tens of modes initial excitation[131].

Classical wave condensation has been theoretically demonstrated in GRIN MMFs in 2011 by P. Aschieri et al., who showed that an initial random distribution of guided modes may exhibit an irreversible evolution towards an equilibrium state, whereby the fundamental mode may grow to a dominant level of occupation while remaining immersed in a sea of small-scale fluctuations, due to a natural thermalization process in a way similar to the Bose-Einstein condensation of a gas of particles[142]. Nevertheless, the role of classical wave condensation in the Kerr beam self-cleaning, has remained so far one of the most obscure aspects, since the first experimental observation of such unexpected effect. According to ref.[142] to achieve complete thermalization and condensation of incoherent waves through nonlinear optical propagation requires prohibitive large interaction lengths.

Only very recently, Fusaro et al. have developed a theory based on a discrete kinetic equation that reveals that a structural disorder of the MMF can accelerate the process of thermalization and condensation by several orders of magnitude. Indeed, light propagation in MMFs is unavoidably affected by the structural disorder of the material, due to inherent technological imperfections and external perturbations. Such important findings can provide a natural explanation for the effect of beam self-cleaning. The discrete nature of the kinetic equation also explains why beam self-cleaning has not been observed in step-index optical fibers, owing to the absence of exact resonances. Moreover, the authors demonstrate experimentally in GRIN MMFs the transition from an incoherent thermal distribution to wave condensation, with a condensate fraction of up to 60% in the fundamental mode of the waveguide trapping potential by varying the spatial coherence of the input beams, and thus their corresponding kinetic energies[143].

By using a coupled mode model, with no temporal dependence of the fields, Sidelnikov et al. investigated beam self-cleaning in the presence of different types of random mode coupling[144]. In cases where all spatial modes are linearly coupled to each other (strong coupling regime), or where neighbouring modes (i.e., with adjacent radial and azimuthal mode numbers) are coupled, it was not possible to reproduce the highly speckled field which is obtained in the experiments in linear conditions. Moreover, when using these types of coupling in the nonlinear regime, rapid oscillations along the fiber of the fundamental mode power were observed, as in the case of the model without any random linear coupling. Finally, the model with random linear coupling between spatial modes with equal radial mode number only was considered. In this case, only degenerate modes are linearly coupled: via the linear random coupling, energy from a radially symmetric mode flows into azimuthal modes with the same number. In this situation, realistic-looking random speckled output field was obtained at low powers, and also one easily observes the appearance of the self-cleaning effect, with the fundamental mode power that quickly stabilizes upon propagation. Simulations show that power transfer into the fundamental mode always occurs within the first half meter of fiber, owing to phase-matched modal FWM. The role of random mode coupling then, is that of making this power transfer stable and irreversible, so that the fundamental mode remains essentially uncoupled from the HOMs upon further propagation, in good agreement with the experimental demonstrations[144].

3. Temporal and polarization dynamics in the regime of Kerr beam self-cleaning

In addition to its spatial aspects, polarization and temporal dynamics of nonlinear multimode beam propagation in GRIN MMFs have also attracted research attention. In ref.[145], Krupa et al. experimentally demonstrated that Kerr beam self-cleaning is accompanied by a nonlinear repolarization effect with a threefold increase of degree of linear polarization resulting from a complex nonlinear mode mixing. They observed that a linearly polarized input pump beam, which is almost depolarized when measured at the fiber output in the linear propagation regime, becomes partially re-polarized at powers close to the threshold for beam self-cleaning. They showed experimentally how the self-cleaned beam experiences nonlinear polarization rotation, which eventually causes a decrease of the time-averaged de-

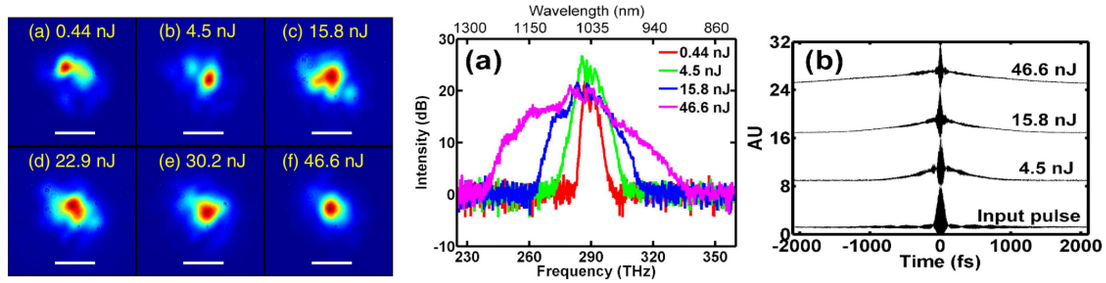

FIG. 23. Beam self-cleaning in GRIN MMF with femtosecond pulses. Left: Near-field output images versus energy (a-f). Scale bars, 13 μm. Right: Corresponding spectral (a) and temporal/autocorrelation (b) measurements of the output field. [Reprinted with permission from[146]. Copyright 2016 Optical Society of America]

gree of linear polarization of a pulsed beam, when the input power is further increased. The nonlinear polarization rotation could be used to implement an ultrafast saturable absorber mechanism for mode-locked lasers based on multimode fibers.

Krupa et al. also reported that Kerr beam self-cleaning is accompanied by significant temporal-reshaping, leading to pulse break-up, temporal compression and eventually highly irregular oscillations[133]. The complex temporal dynamics that characterizes spatially self-cleaned beams could be seen as a demonstration of the numerically predicted transfer of entropy from the spatial to the temporal degrees of freedom[132]. The observed temporal reshaping could be numerically well reproduced by a relatively simple coupled-wave model, where at each point in time the instantaneous power across the profile of quasi-CW pulse determines the total power carried by the modal expansion[133]. Krupa et al. observed that, for input powers slightly larger than the threshold value for spatial self-cleaning, sub-nanosecond laser pulses may undergo up to a four-fold temporal shortening, with a consequent peak power enhancement[133]. Temporal pulse shortening associated with a self-cleaning process in normal dispersion regime was also reported by Liu et al., as presented in Figure 23, however with femtosecond pulses and at power levels which were about two orders of magnitude larger, so that in the regime where both dispersive and self-focusing effects could play a significant role[146].

4. Many-mode Kerr beam self-cleaning

For many applications, including for instance multi-photon imaging, it is required a flexible control of a focused output beam to obtain a 3D scan across a sample. As a first step to achieve such a flexible light-activated focusing from MMFs, Deliancourt et al. investigated the possibility to self-clean towards a given mode, which is different from the fundamental mode of the fiber. They found that a proper adjustment of the input injection conditions permits to get the output shape similar to LP_{11} or other low-order modes. The excited modal distribution results in generating a Kerr-induced index grating with a spatial geometry leading to a strong overlap with the desired mode, and thus favoring the quasi phase-matching of the FWM involving that mode[147]. This proof-of-principle experiment has however the drawback of requiring a manual control of the input launching conditions, which is difficult to precisely replicate. To overcome such difficulty, in a subsequent experiment Deliancourt et al. applied, this time, an optimized adaptive wave-front shaping of the input coherent beam to control, in reliable and reproducible way, the transverse output modal distribution resulting from nonlinear propagation in MMFs[148]. As presented in Figure 24, thanks to the extra degrees of freedom brought by wave-front tailoring, an optimized and stable Kerr self-cleaning on several different low-order modes was obtained, when beam propagation took place in the nonlinear regime. Note that, for all states of spatial beam self-organization, a broad modal population was excited, and the mode expected to prevail after nonlinear propagation counts among the ones with the highest power fraction in the excited population. Moreover, the power threshold for self-cleaning was found to be increasing with the mode order[148].

5. Self-cleaning in active multimode fibers

For the use of multimode active fibers in amplifiers and lasers, it is important to investigate the possibility of Kerr self-cleaning in amplifying MMFs. In a first experiment, Guenard et al. used a 5-m long double-clad ytterbium doped multimode fiber with nearly step-index refractive index profile and uniform core doping profile. They demonstrated that spatial Kerr reshaping is of a more general nature, not being restricted only to conservative systems, since it can be also observed in dissipative configuration exhibiting either

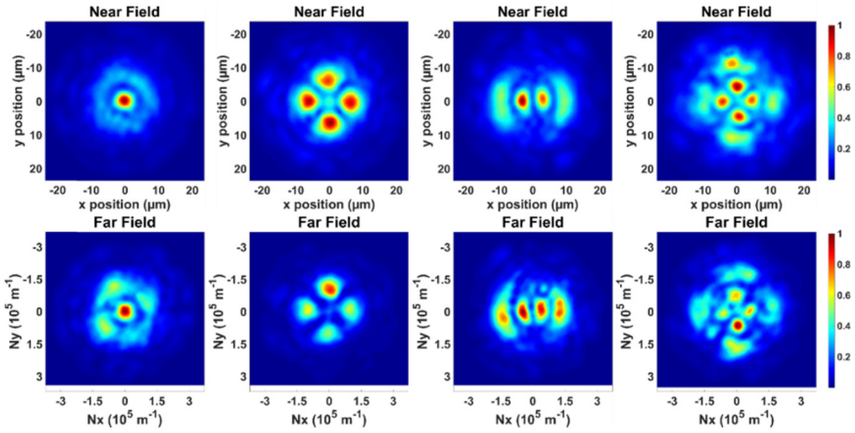

FIG. 24. Near field (top row) and far field (bottom row) images recorded after optimization of the input wave-front to obtain a desired mode profile at the MMF output (LP_{02}, LP_{21}, LP_{12} and LP_{22} from left to right, respectively) at relatively high peak powers (31 kW, 31 kW, 29 kW and 29 kW, respectively) [Reprinted with permission from[148]. Copyright 2019 Optical Society of America]

a strong attenuation or significant laser gain. More importantly, they found that amplification permits to dramatically reduce the self-cleaning power threshold; in presence of optical gain, a pulse of only 500 W of peak power was sufficient to trigger the spatial self-organization phenomenon[149]. Guenard et al. also studied self-cleaning in a composite cavity laser configuration, where a passively Q-switched Nd:YAG microchip laser was combined with an extended cavity including the same multimode Yb-doped MMF. For appropriate coupling levels with the extended cavity, they observed that beam self-cleaning was induced in the multimode fiber, leading to a quasi-single mode laser output and two-fold temporal pulse compression. They also observed a Q-switched mode-locked operation, where spatial self-cleaning was accompanied by far-detuned nonlinear frequency conversion in the active multimode fiber[150].

In more recent experiments, Niang et al. studied instead spatiotemporal dynamics of Kerr beam self-cleaning in a 10-m long tapered Ytterbium-doped MMF, with parabolic core refractive index profile, in the situation where sub-nanosecond 1064 nm pulses were propagating from the wider (120 μm) into the smaller (40 μm) diameter[151]. They demonstrated that, in addition to self-cleaning phenomenon observed in the passive lossy operation, the introduction of gain from a pump laser diode permitted the combination of spatial reshaping with SCG. Indeed, tapering leading to accelerating self-imaging allowed for a continuous

up-shift of the anti-Stokes GPI sidebands along the taper (in agreement to what already reported for undoped multimode tapers in ref.[95]), which permitted to broaden the SCG toward the visible spectral region.

The supercontinuum generated with the active GRIN MMF taper was found to extend between 520 and 2600 nm, and at the same time maintained its cleaned spatial pattern. Moreover, by cut-back measurements, the authors showed that the dissipative landscape, i.e. a non-monotonic variation of the average beam power along the MMF, might lead to modal transitions of self-cleaned beams through various low-order modes towards the fundamental mode along the taper length. Very recently, Wright at al. showed how by exploiting the multimode nature of a laser cavity with MMFs it is possible to realize very flexible light sources based on spatiotemporal mode-locking[152]. Multimode fiber lasers will be described in details in the next section VI.

VI. MULTIMODE FIBER LASERS

Fiber laser sources have enjoyed tremendous success, thanks to their high conversion efficiency and reliability, efficient thermal management and high beam quality. In many applications, it is necessary to combine high output power and high beam quality. The introduction of doubly-clad singlemode fibers has permitted to substantially increase the output power from singlemode lasers. In fact, cladding pumping can be achieved by using low-brightness semiconductor laser diodes. Diffraction-limited emission has traditionally been achieved by fiber lasers based on singlemode active fibers. This leads to small mode areas, which restrains high-power emission given the limited volume of amplifying medium, hence little quantity of doping ions. Moreover, given the tight confinement of the fundamental transverse mode, scaling of the output power from singlemode fiber lasers by means of increasing the mode field diameter remains limited by nonlinear and thermo-optic effects, power saturation, and optical damage. Although these effects can be mitigated by using large-mode-area, and low-numerical aperture active singlemode fibers, transverse instabilities remain, and provide a fundamental limitation to the output power of singlemode optical fiber lasers[153]. In this section, we overview different strategies that have been introduced to scale up the power of fiber laser sources by using multimode fiber amplifiers, and at the same time maintain a quasi-singlemode output beam quality.

A. Transverse and total mode-locking

So far, most of research on laser sources delivering diffraction-limited, ultrashort optical pulses has involved the phase-locking of a single transverse mode. With the notable exception of high-average power laser sources, where incoherent mode superposition can be exploited at the expense of a dramatic reduction of the output beam quality, mode-locked short pulse fiber laser sources have also been largely limited to using singlemode optical fibers.

As is well known, the electromagnetic field in laser cavities can be expressed in terms of a set of orthogonal transverse modes, with different oscillation frequencies. Mode-locking of lasers is a standard technique to obtain short pulses from lasers: typically it involves phase-locking the longitudinal (or axial modes) with the same fundamental transverse mode profile. In 1968, D. Auston theoretically investigated the possibility of transverse mode-locking, i.e., phase locking a set of Hermite-Gauss transverse modes of a laser, in the context of gas lasers. By using the analogy with the oscillating wave packet motion as described by the quantum-mechanical harmonic oscillator, he showed that if a transverse mode set having a Poisson intensity distribution can be phase locked, one obtains a scanning laser beam (that is, a beam which moves in an elliptic or circular motion in the transverse plane)[154]. Moreover, if one can lock various sets of transverse modes that belong to different longitudinal orders (total mode-locking), then one simultaneously obtains a scanning beam in the transverse plane (with a scan rate given by the transverse mode spacing) and a pulse that bounces back and forth in a cavity (with a rate given by the longitudinal mode spacing).

Shortly thereafter, by using a discharge tube filled with pure neon as a nonlinear element, P.W. Smith experimentally demonstrated total mode-locking, that is, the locking of both longitudinal and transverse modes of a 632 nm He-Ne laser. In a first configuration, he observed that each transverse mode has all its longitudinal resonances phase locked to form a narrow pulse. However, pulses corresponding to the various transverse mode orders do not coincide in time. Whenever the frequency spacing between transverse modes ($\Delta\nu_T$) is a simple fraction of the longitudinal mode spacing ($\Delta\nu_L$), e.g. $\Delta\nu_T/\Delta\nu_L = 1/3$, a coherent superposition in time of all transverse modes occurs, which leads to transverse beam scanning. In other words, a 3-D light spot traces out a zig-zag path in the laser cavity[155].

Thirty years later, total mode locking of TEM_{00} and TEM_{01} modes was observed in a Kerr-lens mode-locked Ti:sapphire laser operated at 830 nm[156]. Since the longitudinal

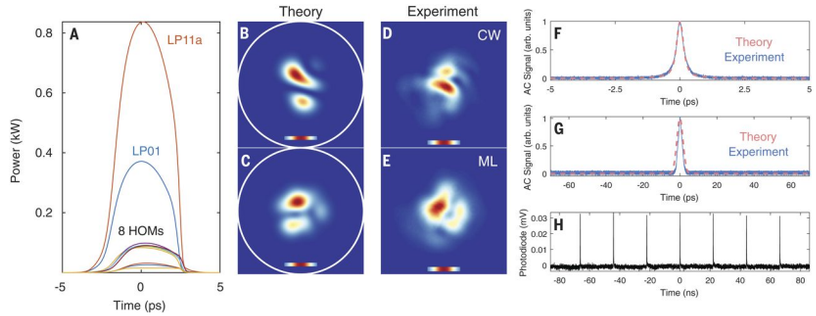

FIG. 25. Simulated decomposition of totally mode-locked pulse in GRIN fiber modes (A), and theoretical (B,C) or experimental (D,E) output near field profiles in the CW or mode-locked state, respectively, in a MMF laser. Autocorrelations of de-chirped (F) and chirped (G) pulses and their oscilloscope trace (H). [From ref.[152]. Reprinted with permission from AAAS]

frequencies of TEM_{01} modes occur exactly in the middle of the TEM_{00} frequencies (i.e., $\Delta\nu_T/\Delta\nu_L = 1/2$), locking of both transverse modes leads to period doubling, i.e., subsequent pulses in the 84-MHz repetition-rate pulse train exhibit different amplitudes, and the pulse train repeats itself every second pulse. This corresponds to a spatial sweeping action of a single-peaked pulse at 42 MHz. Period tripling and quadrupling was also observed, indicating that more higher-order transverse modes were involved in the mode-locking[156]. Gain saturation was mentioned as the likely mechanism to couple the fundamental and high-order modes, which is necessary to initiate the beating and the subsequent locking. Moreover, it was pointed out that if transverse locking of Hermite-Gauss modes leads to periodic beam sweeping in the transverse plane, phase-locking of the cylindrically symmetric Laguerre-Gauss modes would lead to periodic waist modulation, or beam breathing.

This type of self-organized transverse mode locking was experimentally observed in 2002 in a micro-cavity vertical-cavity surface-emitting laser (VCSEL), which supports evenly spaced Laguerre-Gauss transverse modes. In fact, a VCSEL with a ring-geometry injection pattern has a parabolic index profile. A low jitter train of 2.1 ps pulses with 11 ps repetition rate was observed[157].

Ding et al. have studied mode-locking of dissipative soliton fiber lasers using large mode area fibers, supporting multiple transverse modes[158]. In the modeling, mode-locking dynamics was studied by a distributed model, involving a system of coupled Ginzburg-Landau equations. Although simulations show that stable and robust mode-locked pulses can be

produced, both numerics and experiments involving different types of MMFs showed that mode-locking can be destabilized by excessive HOM content, which restrains the maximum single-pulse energy.

The principle of total mode-locking (also called spatiotemporal mode-locking) was recently applied by Wright et al. to a MMF laser[152]. The fiber ring laser was composed by offset splicing a GRIN fiber (supporting the propagation of $\simeq$ 100 modes) to a few-mode (3 modes were supported) Yb-doped fiber amplifier, which leads to spatial filtering action. Self-starting mode-locking in the normal chromatic dispersion regime was achieved by using a combination of spectral filtering and intracavity nonlinear polarization rotation.

As shown by Figure 25, the resulting ultrashort pulses comprise multiple phase-locked transverse (from 10 to 100) and longitudinal modes. Similar results were also obtained when using a MMF laser composed by a single, highly multimode Yb-doped gain fiber[152]. Total-mode locking permits, on the one hand, to substantially scale-up the pulse energy in fiber lasers. On the other hand, as shown in Figure 25, because of the multimode laser output, the spatial beam quality remains relatively low. In the next sub-sections, we outline different approaches to obtain at the same time high-beam quality, and high-power output beams from optical fiber lasers using multimode fiber amplifiers.

In 2018, Wang et al. reported total or spatiotemporal mode-locking at 2 μm of a fiber laser using a step-index few-mode thulium fiber amplifier, using a semiconductor saturable absorber[159]. Record average power ($> 10W$), pulse energy (500 nJ) and peak power (>16 kW) were achieved for Tm fiber laser by exploiting multimode-locking. By increasing the 793 nm pump power up to 35 W, the transition from CW to stable mode locking occurred through different stages. In a first low power stage, the laser output exhibited three distinct spectral peaks, associated with different transverse modes. Temporal synchronization of pulses in different modes can be achieved in this regime by compensating modal dispersion via chromatic dispersion. Whereas at high powers, the three peaks merge in a single spectral feature. At the same time, pulse narrowing both in the temporal and in the spatial domains indicated the possible occurrence of beam self-cleaning in the multimode fiber amplifier[159]

By using a laser cavity similar to that of Wright et al.[152], Qin et al. reported observations of soliton molecules in a spatiotemporal mode-locked (via nonlinear polarization rotation and spatial/spectral filtering) Yb-doped MMF laser[160]. Single pulses as well as pulse pairs,

triplets and quadruplets with varying temporal separation were obtained by simply adjusting the intra-cavity waveplates, or by varying the pump power.

Recently, total-mode locking of TEM_{00} and TEM_{01} modes in $Yb:CaF_2$ laser, leading to a sweeping output beam, was exploited by Kowalczyk et al.[161] to induce time-varying pulse coupling in a photonic-crystal fiber, for subsequent generation of frequency-shifted Raman solitons. Since the SSFS depends on its intensity, a high-speed wavelength-swept source covering the 1300 nm and 1700 nm bio-imaging windows was obtained. The sweeping rate was adjustable between 7 and 21.5 MHz.

B. High-order mode MMF lasers

The technique of SDM is attracting much attention for its potential increase of the capacity of optical communication channels. In this context, it could be interesting to develop laser sources of HOMs with high modal purity. HOM generation is also of interest for laser material processing. Many methods of HOM generation using fiber lasers have been introduced: they are mostly based on mode conversion of the output from a laser oscillator operating in the fundamental transverse mode. In 2018, Wang et al have demonstrated direct high-order LP_{11} mode oscillation in a few-mode fiber laser[162]. Their laser is based on the use of a WDM mode-selective coupler, which permits mode conversion of the diode pump from LP_{01} to the LP_{11} mode (hence efficient and high-purity LP_{11} mode amplification in a few-mode Erbium doped fiber), and at the same time inhibits fundamental mode oscillation.

In a subsequent experiment, Huang et al. demonstrated the generation of both CW and mode-locked (via nonlinear polarization rotation) HOMs at 1.0 μm in all-fiber Yb-doped lasers, again based on mode selective couplers, in order to convert the pump mode into the desired signal mode[163]. Efficient generation of dissipative solitons with spatial LP_{11}, LP_{02} and LP_{21} modal profiles was obtained, along with cylindrical vector and orbital angular momentum beams. Mode switching was simply obtained by means of intracavity polarization controllers.

By using a Sagnac interferometer as wavelength selector, switchable multi-wavelength optical vortex beams have been recently experimentally generated in a few-mode Erbium fiber ring laser cavity[164]. By inserting a carbon-nanotube saturable absorber in combination

with nonlinear polarization rotation as saturable absorber elements, Q-switched operation with cylindrical vector beam generation emission was obtained in the few-mode fiber laser.

A different method to achieve multimode and wavelength switchable oscillation in a few-mode fiber cavity is to exploit fiber Bragg grating (FBG) mirrors that couple, at different reflection wavelengths, different counter-propagating transverse modes. Han et al. demonstrated a Q-switched erbium-doped fiber laser with pulses exhibiting different hybrid transverse mode compositions, corresponding to the various operating wavelengths permitted by the few-mode FBGs[165].

C. Single-mode emission from MMF laser

In order to increase the diffraction-limited output power from fiber lasers, it is necessary to employ a multimode active optical fiber, which permits the use of a multimode pump laser. However, this should be combined with a mode-selection mechanism that filters out all fiber modes except for the fundamental at the laser output. We are interested here in transverse mode selection mechanisms based on the nonlinearity of the MMF. One way to do that is to exploit the nonlinear beam-cleanup effect such as that provided by Raman scattering[118,166], as we will see in the next subsection.

1. Multimode Raman fiber lasers based on beam cleanup

In 2003, Baek and Roh achieved for the first time nearly single-mode emission from a Raman MMF laser, by exploiting the Raman beam cleanup effect[121]. The Raman laser was pumped by a multimode beam from Nd:YAG laser, and used Raman gain in a 40 m long, $50\mu m$-core GRIN MMF, coupled with MMF FBGs. Raman beam cleanup led to Stokes wave oscillation in the fundamental LP_{01} mode, with a beam quality factor $M^2 = 1.66$, and nearly perfect correlation with a Gaussian beam, as shown in Figure 26.

Although a significant beam quality improvement as compared with that for the pump laser (M^2=7) has been achieved in the first demonstration[121], the efficiency was rather low (6%), which means that insignificant brightness enhancement at the Raman conversion of the pump beam was obtained. In order to make the Raman cleanup effect practically feasible and multimode Raman lasers comparable in performance with conventional fiber

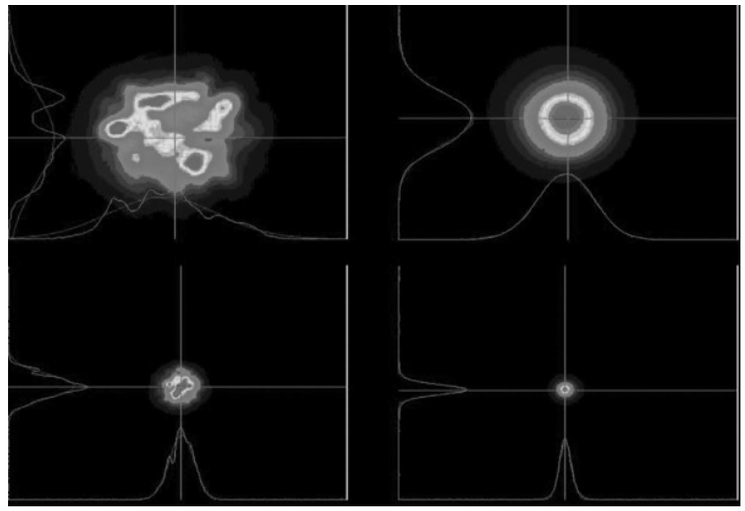

FIG. 26. Near-field (top) and far-field (bottom) images of the pump (left) and Stokes beams (right) from a GRIN MMF Raman laser [Reprinted with permission from[121]. Copyright 2004 Optical Society of America]

lasers, much higher efficiencies as well as direct pumping of multimode fibers by high-power multimode laser diodes (LDs) in robust all-fiber configuration are desired. These problems were in the focus of further developments on multimode Raman fiber lasers (RFLs).

Raman lasing in a directly diode-pumped 62.5 μm- core GRIN MMF with a cavity formed by a highly-reflective (HR) fiber Bragg grating (FBG) and 4% reflection from the output fiber end, was first demonstrated by Kablukov et al.[167]. In addition to the significant beam quality improvement in comparison with that for commercial 940-nm LD used for pumping, the developed 3-W Raman laser operates at the wavelength of 980 nm, that is problematic for conventional rare-earth-doped fiber lasers. Output power scaling to 20 W and then to 154 W for a 1020-nm RFL based on 980-nm LD pumped 62.5 μm- core GRIN MMF and bulk-optics cavity, has been demonstrated by Tao el al.[168] and Glick et al.[169], respectively. Though the pump-to-Stokes conversion efficiency reaches 65%[169], the output beam quality in such configuration is far from the diffraction-limited one, and it worsens with increasing power, namely, M^2=4-8 was obtained.

The generation of a near-diffraction-limited beam in LD-pumped multimode fiber Raman lasers was demonstrated in 2017 by Zlobina et al.[170]. Using a 1.1- km long 62.5 μm- core GRIN MMF pumped by a multimode 915-nm diode, Raman lasing at 954 nm with beam quality $M^2 \leq 1.27$ and output power P>10 W has been obtained. The laser cavity here

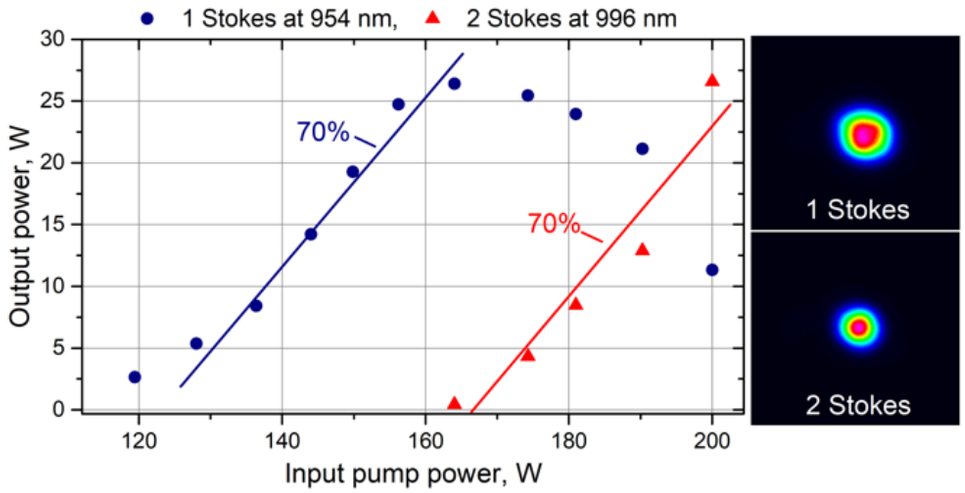

FIG. 27. Output power of GRIN-fiber Raman laser as a function of input pump power of LDs at 915 nm (M^2≃30) for the 1st Stokes wave at 954 nm with linear cavity and for the 2nd Stokes wave at 996 nm with half-open cavity. At the right panels corresponding beam profiles at 954 nm (M^2=2.5) and 996 nm (M^2=1.6) are shown.

involves an output FBG inscribed by a femtosecond laser in the central part of the GRIN MMF, which provides mode-selective feedback, hence securing fundamental mode generation. Beam brightness $B = P/(M^2\lambda)^2$ is enhanced by more than 20 times with respect to the laser diode pump beam (M^2≃20).

As a next important step, an all-fiber configuration of the LD-pumped GRIN MMF Raman laser has been developed in ref.[171]. Output power of the 954-nm RFL pumped by 915-nm laser diodes via fiber pump combiner increased to 50 W with the replacement of the 62.5 μm by a 85 μm- core GRIN MMF, at the expense of slight beam quality reduction to M^2≃2.5. In that case, the maximum power at 954-nm in 1-km long 85 μm-core GRIN MMF with an in-fiber cavity made of UV-inscribed HR FBG and fs-inscribed output FBG was limited by the second-Stokes generation at 996 nm, arising due to the random distributed feedback via Rayleigh backscattering in the GRIN MMF.

To explore this effect for cascaded Raman lasing, an additional HR FBG forming a half-open cavity for 996-nm radiation was inserted[172]. In such cavity configuration, a 100 μm-core GRIN MMF provides an output power larger than 60 W (depleted to ≃ 30 W at cascaded generation) for the 1st Stokes component at 954 nm with M^2 ≃ 2.5 (out of a LD

pump with $M^2 \simeq 30$), and about 30 W for the 2nd Stokes component at 996 nm, with nearly diffraction-limited beam quality ($M^2 \simeq 1.6$). Moreover, as can be seen in Figure 27, the two Stokes components have the same pump-to-Stokes slope efficiency (70%).

Therefore, beam quality at cascaded Raman generation in GRIN MMFs could be gradually improved by means of the Raman cleanup effect, supported by the mode-selective properties of the cavity FBGs and Rayleigh backscattering at the 1st and 2nd stages, respectively. It was also shown that 2nd-order Stokes generation in this scheme is broadly tunable by means of a FBG selecting the 2-order wavelength (tunability in the 978-996 nm range was demonstrated), while the efficiency and beam quality were kept nearly unchanged throughout the tuning.

Power scaling capabilities in multimode all-fiber Raman lasers have been explored in a tandem pumping configuration, when fiber-combined LD-pumped Yb-doped fiber lasers pump a 62.5 μm- core GRIN MMF with in-fiber cavity FBGs similar to those used in ref.[170]. 135 W output power at 1080 nm with beam quality M^2<2.5 and optical-to-optical conversion efficiency of 68% was achieved by Glick et al.[173]. Kilowatt power levels have recently been reached in GRIN MMF Raman amplifiers, similarly pumped by Yb-doped fiber lasers being seeded by a 1060-nm laser. Here a beam quality improvement from $M^2 \simeq 10$ (pump) to $M^2 \simeq 5$ (Stokes) could be achieved solely via the Raman cleanup effect (i.e., in the absence of FBGs)[174],[175]. The development of mode-selective FBGs immune to high powers may improve the beam quality at kilowatt level, thus making high-power GRIN MMF Raman lasers comparable in performance with high-power double-clad rare-earth doped fiber lasers.

2. Self-imaging based MMF lasers

In 2008, Zhu et al. introduced an alternative approach to achieve single-transverse-mode emission from a fiber laser by using an active MMF[176], based on multimode interference (MMI) resulting from self-imaging in the MMF. Their linear fiber cavity was constructed by simply splicing a standard passive singlemode fiber with a short piece of active, $25\mu m$ core diameter MMF, with a precisely controlled length. Self-imaging at points Z_s along the MMF, such that

$$(\beta_n - \beta_1)Z_s = m_n 2\pi \tag{12}$$

where β_n and β_1 are the propagation constants of higher-order modes with index n and of the fundamental mode, respectively, and m_n is an integer. Because of the self-imaging resulting from MMI in a MMF, any input field profile is reproduced at periodic intervals along the propagation of the MMF. Therefore, an input diffraction-limited field is periodically recovered along the MMF: a diffraction-limited beam will tunnel through the MMF, whenever its length is exactly equal to an integer multiple of the self-imaging period.

Since MMI depends on the in-phase combination of the MMF modes, the self-imaging condition depends on wavelength. In fact, for a MMF of length L, Eq. (12) can be written as

$$\Delta n_{eff,n} L = m_n \lambda_0 \tag{13}$$

with $\Delta n_{eff,n} = (\beta_n - \beta_1)\lambda_0/2\pi = n_{eff,n} - n_{eff,1}$. Relatively low cavity losses are only obtained at wavelengths λ_0, which lead to spatial singlemode emission. Hence, both spatial and spectral filtering occur in a MMI-based fiber laser, which result in high beam quality and narrowband emission. A limitation of this approach is that the singlemode fiber must sustain the entire power delivered by the laser, hence a very high intensity results, which could lead to fiber damage. Moreover, the length of the active MMF is limited to a few cm to avoid mode conversion, and permit a control of the MMF length with micrometric precision, which is necessary to ensure in-phase MMI. Hence very high levels of doping are required.

Shortly thereafter, Shalaby et al. demonstrated an improved architecture of the MMI-based fiber laser[177]. In their theoretical scheme, a ring cavity is considered where the laser output is obtained at the end of the active MMF. A small portion of the laser output is fed into a singlemode fiber, which provides mode-selective feedback. As a result, the laser self-adjusts its frequency to ensure self-imaging between input and output ends of the active MMF. In this way, one has the extra flexibility to select a particular laser output transverse pattern and set of longitudinal modes, by simply adjusting the position of the singlemode fiber end face with respect to the axis of the MMF amplifier. Moreover, a precise control of the fiber length is not required, since the ring cavity self-adjusts, via chromatic dispersion, its lasing wavelength in order to achieve self-imaging at the MMF output, a condition that minimizes round-trip loss. In their proof-of-principle demonstration, the active MMF was replaced by 1 m long passive MMF with $50\mu m$ core diameter supporting up to six modes,

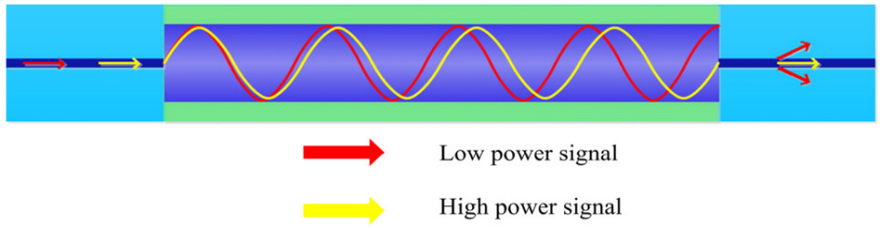

FIG. 28. Schematic of SMS based saturable absorber [Reprinted with permission from[179]. Copyright 2017 Optical Society of America]

and gain was provided by a single-mode erbium doped amplifier[177].

The design of MMI fiber lasers using multimode active fibers with core diameters up to $100\mu m$, which is desirable for high power single-transverse-mode emission, was studied in details by simulations and experiments[178]. It was also found that increasing the mode diameter of the singlemode fiber improves the self-imaging quality and length accuracy tolerance of the active MMF. Self-imaging in the MMF was directly observed by tuning the wavelength of the input signal, and measuring the transmission spectrum of the MMI structure.

In 2013, Nazemosadat and Mafi proposed to use the differential phase shift among transverse modes owing to the Kerr effect, in order to obtain nonlinear MMI in a short length of GRIN MMF[180]. In the presence of an intensity dependent refractive index, the self-imaging period changes (see Figure 28) according to

$$(\beta_n(I) - \beta_1(I))Z_I = m_n 2\pi \tag{14}$$

Correspondingly, the self-imaging wavelength is also intensity-dependent

$$\Delta n_{eff,n}(I)L = m_n \lambda_I \tag{15}$$

Hence, at high intensities, the wavelength of self-imaging λ_I will differ from the wavelength λ_0 from Eq. (13). When the MMF is sandwiched between singlemode fibers in a singlemode-multimode-singlemode (SMS) fiber configuration, a structure that has been extensively studied in the linear regime (see, e.g., ref.[181]), nonlinear MMI can act as a fast saturable absorber mechanism to obtain mode-locking in high-pulse energy fiber lasers. In other words, the nonlinear MMI can be adjusted so that low power signals are strongly at-

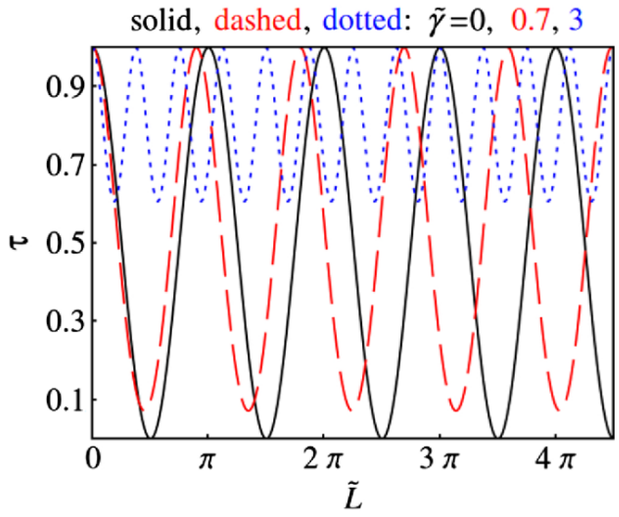

FIG. 29. Theoretical relative power transmission from SMS structure vs. length of GRIN fiber for equal excitation of LG00 and LG10 modes and increasing values of nonlinearity. [Reprinted with permission from[180]. Copyright 2013 Optical Society of America]

tenuated when propagating through the sequence of the three fibers, whereas high intensity pulses experience nearly unit transmission.

Let us consider nonlinear coupling between the Laguerre-Gauss LG_{00} and LG_{10} modes only, and their equal excitation at the input of the GRIN MMF. The nonlinear transmission curves of the SMS structure reported in Figure 29 show that, as the input power is increased, not only the period of the transmission changes, but the depth of the oscillation strongly decreases. In fact, the differential nonlinear phase shift of the two modes leads to a nonlinear nonreciprocity of the mode coupling process: as a result, power exchanges are suppressed at high powers. Hence, at high intensities the average transmission remains relatively high when compared with linear case. In this regime, saturable absorber action occurs, irrespective of the precise length of the GRIN fiber.

Nonlinear MMI can be thought of as a multimode generalization of nonlinear polarization rotation, which is a commonly used mechanism for passive mode locking in fiber lasers. However, nonlinear MMI-based saturable absorber permits to operate at much higher pulse energies and peak powers than all other saturable absorber mechanisms, that have been used so far in fiber lasers. Moreover, it has the advantage of high damage threshold, low cost, simple structure, and mechanical robustness. Note that nonlinear MMI in a GRIN MMF also performs the spectral filtering operation which is required to stabilize mode-locking in

fiber lasers operating in the normal dispersion regime.

Based on the Kerr-effect induced change to the self-imaging wavelength (or period), a Q-switched Er3+/Yb3+ co-doped fiber laser at 1559.5 nm using the SMS configuration acting as a nonlinear saturable absorber was demonstrated in 2015[182]. A maximum pulse energy of 0.8 μJ for the average output power of 27.6 mW was obtained. The gain medium was provided by 5 m of gain fiber in the ring cavity, whereas the MMF in the SMS device was a piece of 4.9 cm, 50 μm core diameter passive fiber.

Interestingly, a different mechanism of saturable absorber action of a mixed passive/active SMS structure can be exploited for Q-switching and at the same time to suppress nonlinear effects (such as SRS and SPM induced spectral broadening) in a high-power (1kW peak power) Yb-doped fiber laser[183]. In that configuration, the SMS device was composed by a piece of passive singlemode fiber, 3 m of MMF Yb-doped gain fiber (with 20 μm core diameter), and 1.2 m of singlemode Yb-doped section (with 10 μm core diameter), which acted as saturable absorber to induce Q-switching. In fact, for sufficiently strong pumping, the high loss of the singlemode Yb-fiber is bleached by the amplified spontaneous emission from the gain fiber. As a result, a sudden increase of the Q factor occurs, and a pulse is generated owing to population inversion in the MM gain fiber. The large mode area of the active MMF was responsible for suppressing SRS and mitigating SPM-induced spectral broadening.

Two cascaded SMS structures with MMFs of different lengths were exploited to realize a stable dual-wavelength Tm3+:Ho3+ co-doped fiber laser operating above 2 μm. The SMS device with a short MMF acts as a long-pass filter to suppress laser emission below 2 μm. Instead, the SMF with long MMF works as a band-pass filter to select the specific operating laser wavelengths[184].

In 2017, the mode-locked operation of a Er-doped fiber laser based on nonlinear MMI using a modified SMS device, based on splicing a short length (431 μm) of step-index MMF and a 12.7 cm long GRIN MMF in between the two singlemode fibers, was proposed and experimentally demonstrated[185]. The introduction of the short span of step-index MMF leads to an additional degree of freedom: its bending radius. A slight amount of bending in the step-index MMF permits to largely modify the input modal excitation content into the GRIN MMF, and generate a substantial amount of higher-order modes (HOMs). Exciting HOMs permits relaxation of the restriction on the length of the GRIN MMF from the

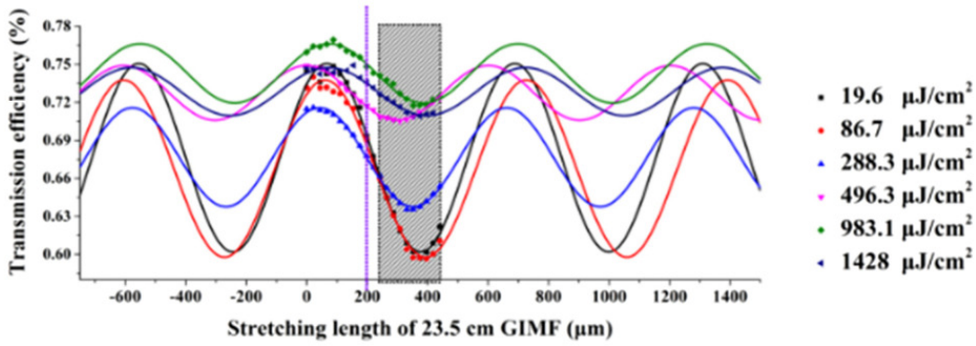

FIG. 30. Transmission of SMS structure vs. stretching length for different input fluences [Reprinted with permission from[187]. Copyright 2018 Optical Society of America]

condition to be precisely equal to a multiple of the self-imaging period in the SMS structure (as previously discussed with reference to Figure 29). By exploiting nonlinear MMI in this type of SMS structure, mode-locked laser output pulses with 446 fs duration and up to 47 pJ energies could be generated. Based on the same device, a stable mode-locked all-fiber Tm laser using a SMS structure including a step-index MMF as a nonlinear saturable absorber, emitting 1.4 ps soliton pulses at 1888 nm, was also demonstrated[179].

A variant of the previous SMS structure was demonstrated for saturable absorber action in a Er-doped mode-locked fiber laser[186]. The step-index MMF was replaced by a inner micro-cavity, obtained by etching with hydrofluoric acid one end face of a cleaved GRIN MMF. Bending the modified GRIN fiber also leads to HOMs excitation, which in turn is able to activate a stable saturable absorber action. Pulses with 528 fs temporal duration and 26 pJ energy were generated. Harmonic mode-locking (up to 6th order) operation was also achieved.

The two modified SMS structures, involving either a piece of step-index MMF, or an inner micro-cavity to generate HOMs in the GRIN fiber, lead to significant insertion loss, and require a control of the bending that is necessary to obtain stable saturable absorber action, which makes them not so practical. To circumvent this, Wang et al. have shown that mode-locking could be achieved by using a SMS structure including 23.5 cm of stretched GRIN fiber as nonlinear saturable absorber[187]. In this case, the operating point of the saturable absorber may be simply controlled by adjusting the strength of the applied stretching. In fact, varying the stretching is equivalent to adjusting the length of the GRIN fiber up to the optimal operating point of the saturable absorber.

Interestingly, the measurement of the transmission of the SMS structure as a function of the stretching length for different input fluences was carried out[187]. As can be seen from Figure 30, at high intensities ($\simeq 1000\ \mu J/cm^2$) the self-imaging induced beam oscillations occur with much smaller amplitude, and with average (i.e., over one self-imaging period) transmission that is significantly increased ($\simeq 75\%$) with respect to the low intensity case ($\simeq 68\%$ at $\simeq 20\ \mu J/cm^2$). This is in excellent agreement with the theoretical prediction in Figure 29, and indicates that nonlinear mode coupling and beam reshaping, akin to spatial beam cleaning, is the main mode-locking mechanism at play, rather than the nonlinear variation of the self-imaging period. This supposition is supported by previous experiments, where the excitation of HOMs in the GRIN fiber was necessary to obtain saturable absorber action[179,185]. In fact, saturable absorber action of nonlinear MMI requires that HOMs are present along with the fundamental mode. A ring Er-doped fiber laser based on this device could be mode-locked, generating 500-400 fs pulses at 1572.5 nm and 416 fs at 1591.4 nm, respectively, with up to 110 pJ energy[187].

Previous experiments demonstrated mode-locking in fiber lasers operating in the anomalous dispersion regime. In 2018, Teğin and Ortaç demonstrated, nonlinear MMI induced mode locking in a normal-dispersion ytterbium-doped fiber laser, generating highly stable 5 ps dissipative soliton pulses at 1030 nm[188]. Note that nonlinear MMI included a step-index and a GRIN MMF, and provided both saturable absorber action and bandpass filtering action, both required to sustain dissipative soliton mode locking.

Using the same saturable absorber structure, and bending it to control the multimode excitation in the GRIN fiber, Zhao et al. demonstrated a mode-locked soliton Er-doped fiber laser emitting 960 fs pulses with energy increased to 2.44 nJ[189]. The impact of the GRIN core diameter (ranging from 20 to 62.5 μm) was studied, showing that larger diameters (hence larger proportions of excited HOMs) increase the output laser power.

For mode-locking a fiber Tm laser using the SMS saturable absorber, the short step-index MMF was substituted by a no-core fiber, which had the same purpose of controlling the HOM excitation into the GRIN MMF via bending. Stable 1.25 ps soliton mode-locking operation at 1895.7 nm was obtained[190].

Again based on bending the SMS structure including a short ($\simeq 100\ \mu m$) step-index MMF to excite HOMs in a 20 cm long GRIN MMF as saturable absorber, Zhao et al. have shown the possibility to simultaneously generate both solitons (with 1 ps duration and

3.6 nm spectral bandwidth) and stretched-pulses (with 300 fs duration and with a smooth bandwidth increased to 14.2 nm) at 1600 nm, by simply increasing the pump power above 420 mW[191]. Similar observations were later reported by Chen et al.[192]: however in their experiment no step-index MMF was included, nor any bending was exploited to generate HOMs. The precise control of the length of the GRIN fiber could be achieved by stretching it, with a precision of 20 μm. In both experiments, the observed transition from the soliton to the stretched pulse regime remains yet to be fully explained.

Chen et al. proposed and demonstrated nonlinear MMI based passive mode locking on a SMS structure, where the GRIN fiber is replaced by a step-index MMF[193], as it was used by Fu et al. to show Q-switching[182]. Since the self-imaging period Z_l is increased up to 10-43 mm in a step-index MMF with 50-105 μm core diameter, with respect to about 1 mm or less for a GRIN MMF, with this fiber it is much easier to control the MMF length to ensure the optimal operating point of the SA. It was shown that the length of the step-index MMF is critical for proper mode-locking operation: reducing its length from 59 mm ($6Z_l$) to 49 mm ($5Z_l$) permits to change the operation from Q-switching to soliton mode-locking, in agreement with the theoretical prediction, which requires an odd multiple of Z_l. The influence of total cavity dispersion was also studied, by adding different lengths of singlemode and dispersion compensating fiber in the cavity[193].

VII. PERSPECTIVES AND CONCLUSIONS

In this final section, we outline our perspectives for further research, as well for application technologies, involving nonlinear multimode optical fibers.

A. Open problems

While the structural disorder inherent to MMFs with a parabolic index profile has been proposed as a powerful accelerator for the optical condensation process, much remains to be explored to better understand the link between the phenomenon of wave condensation and the beam self-cleaning effect in MMFs. So far, models of disorder that have been studied originate from polarization fluctuations, or from random coupling between nearly degenerate modes with the same radial number. By applying theories of wave turbulence, it would be

interesting to compare different models of disorder and different refractive index profiles, in order to better understand, for example, why beam self-cleaning has not yet been observed in step-index MMFs. It would also be interesting to consider the case where the nonlinear length associated with nonlinear effects is decreased, until it becomes comparable (resonance condition) with the correlation length associated with random mode coupling, or structural disorder.

B. Laser technology

The beam cleanup effect in Raman conversion of multimode radiation in GRIN MMF opens a new approach for the development of high-power diode-pumped fiber lasers. High-beam-quality (M^2=1.2-2.5) Raman lasing has been demonstrated at tens to hundred Watts output powers with the help of in-fiber fs-inscribed FBGs, providing mode-selective feedback in the MMF cavity. Similar beam cleaning effect is observed when random Rayleigh backscattering is used for the feedback. Therefore, the technological challenge consists in the development of a mode-selective fiber cavity, stably operating at high powers. A still open theoretical problem is the development of a realistic GRIN MMF Raman laser model, involving both Raman gain cleanup and cavity mode selection effects. Note that the explanation proposed by Terry et al[25] is qualitative only, and it fails when we take into consideration multimode pump depletion, which is significant in realistic Raman lasers based on GRIN MMFs.

Pump depletion is inhomogeneous in the transverse coordinate depending on the generated Stokes beam profile: this complicates mode analysis at Raman conversion. Additional complications arise when we include a transverse-mode dependent feedback, as that provided by fs-inscribed FBGs (or Rayleigh backscattering). It should also be noted that the Kerr beam cleaning effect may be significant for hundred-Watts Stokes beams propagating in hundred-meters long MMF cavities. Therefore, the interplay of Kerr beam cleaning and Raman beam cleanup remains to be studied, both theoretically and experimentally. The idea of using a MMF to clean and combine several laser modes or beams is expected to have a long-term technological impact on the laser community, with the possibility of leading to a new generation of lasers for industrial applications.

A full new range of spatiotemporal dynamics, including transverse multimode locking,

temporal field redistributions from beam cleaning, as well as the formation of spatiotemporal soliton molecules could be explored in MMF laser cavities. In addition to MMF laser cavities, passive MMF cavities could be a topic for further investigations as well. Indeed, ultrafast pulses with a coherent localized transverse multimode profile belong to the category of optical light bullets, which consist of stable traveling light pulses confined in both longitudinal (in the temporal moving frame) and transverse (spatial) dimensions. These photonic objects, which have been in the top list of holy grail nonlinear optics endeavors for the past 20 years, have remained quite elusive in spite of the experimental efforts. Beyond their fundamental interest, optical light bullets could be used as complex data bits in the frame of high-capacity optical communication and parallel processing devices.

In ultrafast laser cavities, the notion of soliton (usually associated with solutions of integrable conservative nonlinear wave systems) has been extended to include the concept of dissipative soliton. This object is a localized pulse originating from a balanced process, involving the presence of gain/loss, nonlinearity, dispersion and/or diffraction[194]. This general concept finds a vast number of applications in nonlinear photonics and other fields of physics. Within a certain range of laser cavity parameters, a dissipative soliton manifests itself as a stable attracting state, leading to a long-term stability and robustness of the traveling pulse. The flexible design of dissipative soliton laser systems allows for stable mode locking in counterintuitive parameter ranges, such as in the normal dispersion regime, leading to record high-energy pulse generation in fiber oscillators[195].

In our perspective, major advances will stem from the combining of the two advanced soliton concepts, that is, dissipative solitons and MMSs. This will lead to dissipative light bullets. Precisely, light bullets in active and dissipative media should be found. These spatiotemporally extended solitary waves will benefit from the existence of dynamical attractors that will regenerate them every cavity roundtrip, allowing their propagation in the laser cavity during virtually unlimited times. Owing to the increased number of spatiotemporal degrees of freedom as well as that of relevant cavity parameters, one may anticipate that dissipative light bullets might form in both cavity dispersion regimes, while unveiling a wide range of new pattern formations[196].

Spatiotemporal soliton molecules are fascinating new photonic objects. Until recently, ultrafast soliton molecules were formed as one-dimensional objects of single transverse mode cavities. Therefore, opening the transverse dimensions represents a way to unfold opti-

cal pattern self-organization, as well as to deepen the analogies between matter and optical molecules. For instance, three-dimensional optical soliton molecular complexes[197] and other supramolecular structures[198] could be formed and interact among themselves, through nonlinear interaction processes of various range and magnitude. Note that the study of optical soliton molecule dynamics is currently driving a lot of focus among the scientific community[199–201], and may lead to discoveries of original pattern-forming dynamics in ultrafast Raman lasers as well.

Moving gradually out of the stable region of spatiotemporal mode locking, by shifting the laser cavity parameters, we expect to find a new intermediate region where the coherence will be gradually reduced, whereas pulsating and chaotic dynamics will progressively become prominent. We anticipate the existence of novel fundamental spatiotemporal structures such as: moving soliton molecules, spatiotemporal vortices, incoherent dissipative solitons, and optical rogue waves. Spatiotemporal optical rogue waves are particularly interesting: until recently, optical rogue waves have been investigated mostly either in the temporal domain (guided wave propagation) or in the spatial domain (transverse modes, speckle etc.)[202]. Whereas there is a strong analogy between the optical and oceanic rogue waves, we are generally lacking experimental optical systems that have both spatial and temporal dimensions, as experienced by waves in the ocean.

C. Fiber technology

It is worth noticing that, if from the one side MMFs open new perspectives for many applications (as amplifier medium, saturable absorber component, spatial and temporal reshaping system, nonlinear frequency converter, etc), it is still difficult to properly design and control the fabrication of doped fibers with accurate transverse and longitudinal structuration, with scale details ranging from micrometer to centimeter. In order to be convinced about this statement, we can remember the results on self-cleaning in a doped optical fiber taper, recently published by Niang et al.[151]. Although the refractive index profile of the taper fiber follows a parabolic evolution, the transverse distribution of the active doping ion (Yb) follows a quasi-step profile, which prevents any additional gain filtering, that could help to control the output beam pattern (see Figure 31). A better control of the fiber fabrication could certainly improve our capability to shape in time and in space the light propagating

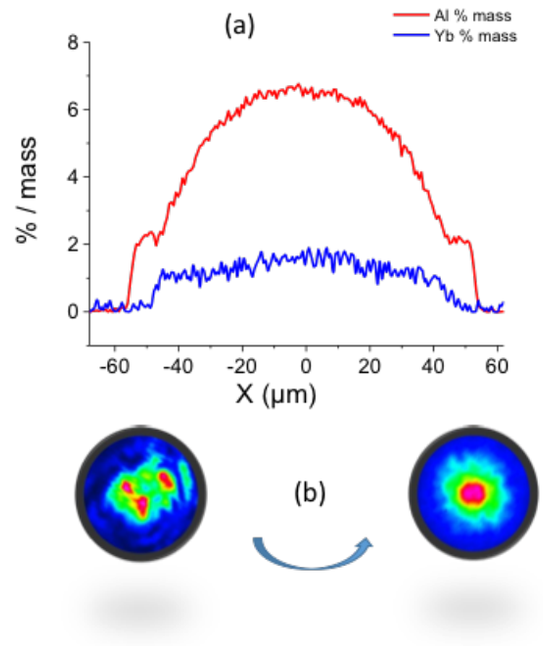

FIG. 31. Experimental results: (a) measure of the transverse doping repartition in an Yb doped taper amplifier MMF used for Kerr-beam self-cleaning (see ref.[151]); (b) example of spatial self-cleaning obtained in that particular multimode taper.

in such type of fiber. A first technological effort has to be made on the fiber design and drawing with particular structures, and doping from the micrometer to the centimeter scale.

Infrared MMFs are not easily accessible, unlike silica MMFs. So an important perspective is to develop efficient MMFs made with tellurite and chalcogenide, ZBLAN glasses with a fine control of the refractive index profile. MMFs using these new infrared materials should be targeted to obtain powerful laser emission between 3 and 12 m. Infrared active imaging, micromachining and microspectroscopy are the main applications which could be significantly boosted by the new multicomponents MMFs. Moreover, fibered optical components as multimode couplers, isolators, nonlinear saturable absorbers, etc. could benefit from the renewed interest for multimodal propagation.

D. Nonlinear frequency conversion

Efficient nonlinear conversion in multimode fibers is also a very important concept to give an alternative to current OPO, supercontinua, harmonic generators, frequency comb sys-

tems, which are largely used in a variety of applications. Among them, we can, for example, underline the potentiality to generate, by using GPI or intermodal four-wave mixing, tunable infrared Stokes lines to obtain, after amplification with Tm and Ho doped multimode fibers, powerful infrared laser sources. Optical poling can be used to write a periodic quadratic nonlinear coefficient in multimode fibers, and the SH generation could be sufficiently efficient to be used in microspectroscopy and for nonlinear imaging systems.

Previously mentioned MIR glasses present nonlinearities 10 to 1000 times higher than silica glass and their infrared transparency extends from 6 μm to more than 12 μm, depending on the compositions, while silica is limited to 2.4 μm. So beam self-cleaning, parametric conversion and supercontinuum generation could be investigated in the MIR using specially designed infrared MMFs.

E. Characterization techniques

On the characterization side, it would be interesting to access the mode content of the MMF output under Kerr beam self-cleaning regime, i.e. to be able to decompose in experiments the output field on the fiber eigenmode base (in a narrow spectral range). The development of reliable and accurate 2D optical sampling techniques with high temporal resolution for the observation of ultrafast spatiotemporal dynamics in highly MMF systems would also be of major importance.

Novel characterization techniques for multimode fields need to be developed. In amplified ultrafast lasers, shot-to-shot pulse characterization for above-μJ pulses at repetition rates up to 100 kHz can be performed, using both single-shot optical autocorrelation and ultrafast cameras. The situation is naturally different for laser oscillators mode-locked at repetition rates that are typically tens of MHz, with single pulse energy in the nJ range or below. The usual average spectral and autocorrelation measurements can hide complex laser dynamics where the features of the output pulses change significantly over successive cavity roundtrips. Currently there is a surge of real-time characterization techniques adapted to the low-to-moderate average powers of ultrafast laser oscillators dynamics, taking advantage of a simple real-time time-stretch technique, also termed dispersive Fourier-transform characterization[203]. This technique maps the optical spectrum of the laser output onto a temporal waveform that is readout on a real-time oscilloscope, which is achieved by prop-

agating linearly the attenuated laser output pulses through a highly-dispersive medium. The spectro-temporal approach needs to be combined with a spatial characterization. Advanced spatiotemporal characterization in real time should be developed, by combining various tools, such as spatial multiplexing and demultiplexing, time-stretch and hyperspectral imaging techniques.

F. Spatial beam shaping for microscopy, micro-spectroscopy and remote sensing applications

Currently, MMFs appear as a potential good solution for high power single-mode laser emission, even if important progresses in the understanding of nonlinear multimode propagation remains to be done. Additionally, large-band conversion covering the entire spectral windows of the fibers can also be obtained which open new potentialities for medical diagnostic, remote sensing and imaging systems. To illustrate this statement, we demonstrated the potentiality to obtain images of kidney of mouse with very good spatial resolution by using a multimode beam shaped by means of the Kerr self-cleaning process. The nonlinear fluorescence technique has been used with the two-photon absorption process from the 1064 nm wavelength, mixed with staining by different dyes (Alexa 568, Alexa 488 and Dapi to label actin, tubules and nucleus, respectively). The measured maximum resolution was 0.6 μm (see Figure 32).

It is also important to highlight that the same images have been obtained in the endoscopy configuration, and by using the same multimode fiber in which we obtained Kerr-beam self-cleaning. In that experiment, no double-clad fiber is needed to deliver a single-mode pump beam and to collect the emitted fluorescence.

The high potentiality of multimode doped fibers to deliver supercontinuum beams with high peak power opens also new applications regarding hyperspectral remote sensing experiments. Supercontinuum spectra emitted by large core MMF will be crucial for flow cytometry and nonlinear spectroscopy, where the chemical and biological samples under test have transverse dimensions of tens or hundreds of microns and, as a consequence, they cannot be uniformly illuminated by the beam emitted by singlemode fibers.

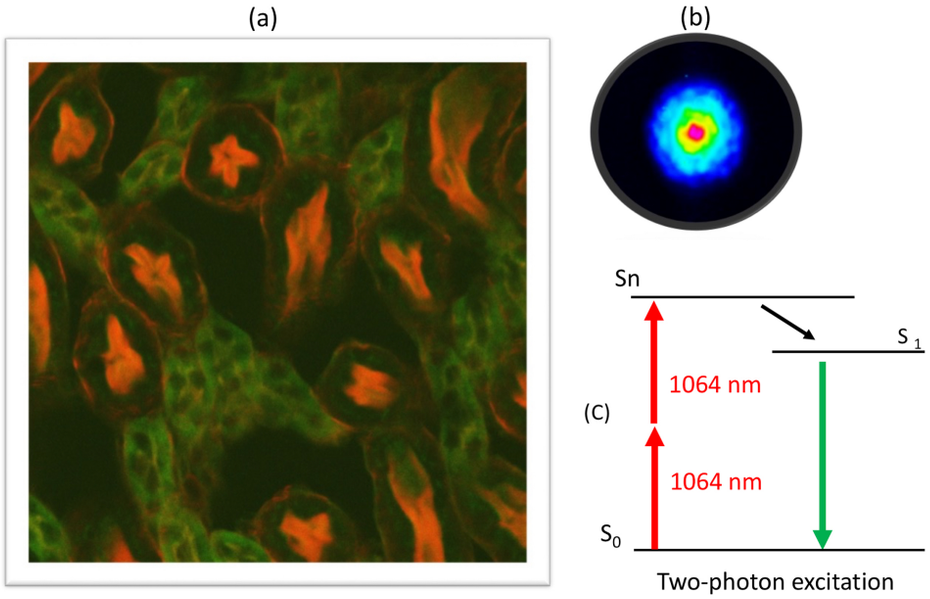

FIG. 32. (a) image of kidney of mouse obtained by using two photon absorption from a cleaned beam at 1064 nm after propagation in a GRIN multimode optical fiber. Red color: signature of actin labeled with Alexa 568; Green color: signature of tubules labeled with Alexa 488. (b) Image of the output cleaned beam after propagation in a GRIN MMF 50/125 μm. (c) energy level scheme for two-photon absorption. Spatial transverse resolution in that experiment: 0.6 μm.

G. Spatial beam shaping for beam delivery applications

It is worth underlying the potential breakthrough impact that beam cleaning in MMFs can have on laser beam-delivery technologies. Large mode area passive delivery fibers usually play a very important role in the construction of high performance, high power fiber lasers, particularly in delivering efficiently the generated power into the work-piece. The possibility of beam cleaning in MMFs represents an interesting alternative to overcome the limits of standard step-index fiber technology. Beam cleaning and combining architectures based on standard MMFs could be designed to work for any laser emitting in the visible or near infrared. In particular, Tm-doped fiber lasers operating around the eye-safe 2 μm region have been recently scaled up to kilowatt level, and appear to be promising for new industrial applications.

H. Spatial division multiplexing

The study of nonlinear effects in MMFs is not only innovative but also very timely for the photonics community: in fact, many research groups and telecom companies are working on the approach of taking into account the modes within a MMF to define spatially distinct channels, using SDM to increase optical fiber capacity. Transmission through multimode fibers can be an effective way to overcome the capacity crunch in data centers and in long-haul transmission systems.

I. Optical computing and machine learning

Multimode fibers and nonlinear propagation within them could be an option also to perform and enhance the performance of all optical data processing devices (combining linear random mixing with nonlinear interactions), such as neuromorphic and reservoir computers, which can be aided by nonlinear components in their input or output layers. Reservoir computing is a machine learning platform, that is able to expand the dimensionality of a problem by mapping an input signal into a higher-dimensional reservoir space, which is able to can capture and predict the features of complex and nonlinear temporal dynamical systems. A recent study by Pauwels et al. investigated the role of distributed Kerr nonlinearity in a passive coherent photonic reservoir computer, based on a passive coherent singlemode optical fiber-ring cavity[204]. They found that the optical Kerr nonlinearity of the fiber enhances the task solving capability of the reservoir. This suggests that by combining nonlinearity with MMFs in the cavity will further enhance the performances of future coherent all-optical reservoir computers. On the other hand, speckles generated by propagating a laser beam modulated with a spatial light modulator through a MMF have been exploited by Paudel et al. to demonstrate the operation of an analog reservoir computer[205]. In that setup, the laser beam propagated in the MMF in the linear regime, and nonlinear activation was obtained through the saturation of a 2D camera array. A multivariate audio classification task was successfully performed, by using the Japanese vowel speakers public data set.

ACKNOWLEDGMENTS

This work was supported by the European Research Council (ERC) under the European Union's Horizon 2020 research and innovation programme (Advanced research grant No. 740355); the Russian Ministry of Science and Education (Grant 14.Y26.31.0017); the Institut Universitaire de France; the french Investissements d'Avenir program, project ISITE-BFC (contract ANR-15-IDEX-0003); XLIM has received funding from Agence Nationale de la Recherche (ANR) (TRAFIC project : ANR-18-CE080016-01), and from CILAS Company (ArianeGroup) by means of the shared X-LAS laboratory.

REFERENCES

[1]R.-J. Essiambre, R. W. Tkach, and R. Ryf, "Chapter 1 - fiber nonlinearity and capacity: Single-mode and multimode fibers," in *Optical Fiber Telecommunications (Sixth Edition)*, Optics and Photonics, edited by I. P. Kaminow, T. Li, and A. E. Willner (Academic Press, Boston, 2013) sixth edition ed., pp. 1 – 43.

[2]A. Picozzi, G. Millot, and S. Wabnitz, "Nonlinear virtues of multimode fibre," Nat. Photonics **9**, 289–291 (2015).

[3]B. Crosignani, A. Cutolo, and P. D. Porto, "Coupled-mode theory of nonlinear propagation in multimode and single-mode fibers: envelope solitons and self-confinement," J. Opt. Soc. Am. **72**, 1136–1141 (1982).

[4]A. Hasegawa, "Self-confinement of multimode optical pulse in a glass fiber," Opt. Lett. **5**, 416–417 (1980).

[5]J. T. Manassah, P. L. Baldeck, and R. R. Alfano, "Self-focusing and self-phase modulation in a parabolic graded-index optical fiber," Opt. Lett. **13**, 589–591 (1988).

[6]H. Talbot, "LXXVI. Facts relating to optical science. No. IV," The London, Edinburgh, and Dublin Philosophical Magazine and Journal of Science **9**, 401–407 (1836).

[7]S. Longhi and D. Janner, "Self-focusing and nonlinear periodic beams in parabolic index optical fibres," Journal of Optics B: Quantum and Semiclassical Optics **6**, S303–S308 (2004).

[8]F. Poletti and P. Horak, "Description of ultrashort pulse propagation in multimode optical fibers," J. Opt. Soc. Am. B **25**, 1645–1654 (2008).

[9]F. Poletti and P. Horak, "Dynamics of femtosecond supercontinuum generation in multimode fibers," Opt. Express **17**, 6134–6147 (2009).

[10]A. Mafi, "Pulse propagation in a short nonlinear graded-index multimode optical fiber," Journal of Lightwave Technology **30**, 2803–2811 (2012).

[11]M. E. V. Pedersen, J. Cheng, C. Xu, and K. Rottwitt, "Transverse field dispersion in the generalized nonlinear Schrödinger equation: four wave mixing in a higher order mode fiber," Journal of Lightwave Technology **31**, 3425–3431 (2013).

[12]R. Khakimov, I. Shavrin, S. Novotny, M. Kaivola, and H. Ludvigsen, "Numerical solver for supercontinuum generation in multimode optical fibers," Opt. Express **21**, 14388–14398 (2013).

[13]F. Tani, J. C. Travers, and P. S. Russell, "Multimode ultrafast nonlinear optics in optical waveguides: numerical modeling and experiments in kagomé photonic-crystal fiber," J. Opt. Soc. Am. B **31**, 311–320 (2014).

[14]J. Lægsgaard, "Efficient simulation of multimodal nonlinear propagation in step-index fibers," J. Opt. Soc. Am. B **34**, 2266–2273 (2017).

[15]L. G. Wright, Z. M. Ziegler, P. M. Lushnikov, Z. Zhu, M. A. Eftekhar, D. N. Christodoulides, and F. W. Wise, "Multimode nonlinear fiber optics: Massively parallel numerical solver, tutorial, and outlook," IEEE Journal of Selected Topics in Quantum Electronics **24**, 1–16 (2018).

[16]S. Longhi, "Modulational instability and space time dynamics in nonlinear parabolic-index optical fibers," Opt. Lett. **28**, 2363–2365 (2003).

[17]W. H. Renninger and F. W. Wise, "Optical solitons in graded-index multimode fibres," Nat. Commun. **4**, 1719 (2012).

[18]S.-S. Yu, C.-H. Chien, Y. Lai, and J. Wang, "Spatio-temporal solitary pulses in graded-index materials with Kerr nonlinearity," Opt. Commun. **119**, 167–170 (1995).

[19]K. Krupa, A. Tonello, A. Barthélémy, V. Couderc, B. M. Shalaby, A. Bendahmane, G. Millot, and S. Wabnitz, "Observation of geometric parametric instability induced by the periodic spatial self-imaging of multimode waves," Phys. Rev. Lett. **116**, 183901 (2016).

[20]K. Krupa, A. Tonello, B. M. Shalaby, M. Fabert, A. Barthélémy, G. Millot, S. Wabnitz, and V. Couderc, "Spatial beam self-cleaning in multimode fibres," Nat. Photonics **11**, 234–241 (2017).

[21]B. Crosignani and P. D. Porto, "Soliton propagation in multimode optical fibers," Opt. Lett. **6**, 329–330 (1981).

[22]D. Gloge, "Optical power flow in multimode fibers," Bell System Technical Journal **51**, 1767–1783 (1972).

[23]A. B. Grudinin, E. Dianov, D. Korbkin, M. P. A, and D. Khaidarov, "Nonlinear mode coupling in multimode optical fibers; excitation of femtosecond-range stimulated-Raman-scattering solitons," J. Exp. Theor. Phys. Lett **47**, 356–359 (1988).

[24]E. Fermi, J. Pasta, and S. Ulam, "Studies of nonlinear problems," Document LA-1940. Los Alamos National Laboratory (1955).

[25]N. B. Terry, T. G. Alley, and T. H. Russell, "An explanation of SRS beam cleanup in graded-index fibers and the absence of SRS beam cleanup in step-index fibers," Opt. Express **15**, 17509–17519 (2007).

[26]A. Mecozzi, C. Antonelli, and M. Shtaif, "Soliton trapping in multimode fibers with random mode coupling," arXiv e-prints , arXiv:1207.6506 (2012), arXiv:1207.6506 [physics.optics].

[27]A. Mecozzi, C. Antonelli, and M. Shtaif, "Coupled Manakov equations in multimode fibers with strongly coupled groups of modes," Opt. Express **20**, 23436–23441 (2012).

[28]C. R. Menyuk, "Stability of solitons in birefringent optical fibers. i: Equal propagation amplitudes," Opt. Lett. **12**, 614–616 (1987).

[29]C. R. Menyuk, "Stability of solitons in birefringent optical fibers. ii. arbitrary amplitudes," J. Opt. Soc. Am. B **5**, 392–402 (1988).

[30]L. G. Wright, W. H. Renninger, D. N. Christodoulides, and F. W. Wise, "Spatiotemporal dynamics of multimode optical solitons," Opt. Express **23**, 3492–3506 (2015).

[31]Z. Zhu, L. G. Wright, D. N. Christodoulides, and F. W. Wise, "Observation of multimode solitons in few-mode fiber," Opt. Lett. **41**, 4819–4822 (2016).

[32]D. J. Richardson, J. M. Fini, and L. Nelson, "Space-division multiplexing in optical fibres," Nat. Photonics **7**, 354–362 (2013).

[33]N. Akhmediev and M. Karlsson, "Cherenkov radiation emitted by solitons in optical fibers," Phys. Rev. A **51**, 2602–2607 (1995).

[34]L. G. Wright, D. N. Christodoulides, and F. W. Wise, "Controllable spatiotemporal nonlinear effects in multimode fibres," Nat. Photonics **9**, 1–5 (2015).

[35]L. G. Wright, S. Wabnitz, D. N. Christodoulides, and F. W. Wise, "Ultrabroadband dispersive radiation by spatiotemporal oscillation of multimode waves," Phys. Rev. Lett. **115**, 223902 (2015).

[36]Y. Kodama, M. Romagnoli, S. Wabnitz, and M. Midrio, "Role of third order dispersion on soliton instabilities and interactions in optical fibers," Opt. Lett. **19**, 165–167 (1994).

[37]F. Poletti and P. Horak, "Description of ultrashort pulse propagation in multimode optical fibers," J. Opt. Soc. Am. B **25**, 1645–1654 (2008).

[38]M. Conforti, C. M. Arabi, A. Mussot, and A. Kudlinski, "Fast and accurate modeling of nonlinear pulse propagation in graded-index multimode fibers," Opt. Lett. **42**, 4004–4007 (2017).

[39]M. Karlsson, D. Anderson, and M. Desaix, "Dynamics of self-focusing and self-phase modulation in a parabolic index optical fiber," Opt. Lett. **17**, 22–24 (1992).

[40]A. S. Ahsan and G. P. Agrawal, "Graded-index solitons in multimode fibers," Opt. Lett. **43**, 3345–3348 (2018).

[41]A. Hasegawa and Y. Kodama, "Guiding-center soliton in optical fibers," Opt. Lett. **15**, 1443–1445 (1990).

[42]Z. Deng, Y. Chen, J. Liu, C. Zhao, and D. Fan, "Graded-index breathing solitons from Airy pulses in multimode fibers," Opt. Express **27**, 483–493 (2019).

[43]S. Buch and G. P. Agrawal, "Soliton stability and trapping in multimode fibers," Opt. Lett. **40**, 225–228 (2015).

[44]S. Buch and G. P. Agrawal, "Intermodal soliton interaction in nearly degenerate modes of a multimode fiber," J. Opt. Soc. Am. B **33**, 2217–2224 (2016).

[45]A. Antikainen, L. Rishøj, B. Tai, S. Ramachandran, and G. P. Agrawal, "Fate of a soliton in a high order spatial mode of a multimode fiber," Phys. Rev. Lett. **122**, 023901 (2019).

[46]L. Rishøj, B. Tai, P. Kristensen, and S. Ramachandran, "Soliton self-mode conversion: revisiting Raman scattering of ultrashort pulses," Optica **6**, 304–308 (2019).

[47]K. D. Moll, A. L. Gaeta, and G. Fibich, "Self-similar optical wave collapse: Observation of the Townes profile," Phys. Rev. Lett. **90**, 203902 (2003).

[48]Y. Silberberg, "Collapse of optical pulses," Opt. Lett. **15**, 1282–1284 (1990).

[49]S. Raghavan and G. P. Agrawal, "Spatiotemporal solitons in inhomogeneous nonlinear media," Optics Communications **180**, 377 – 382 (2000).

[50]Y. Kong, "Spatiotemporal soliton solution to generalized nonlinear Schrödinger equation with a parabolic potential in Kerr media," Optics Communications **371**, 27 – 33 (2016).

[51]O. V. Shtyrina, M. P. Fedoruk, Y. S. Kivshar, and S. K. Turitsyn, "Coexistence of collapse and stable spatiotemporal solitons in multimode fibers," Phys. Rev. A **97**, 013841 (2018).

[52]V. Serkin and T. Belyaeva, "Nonlinear solitonic analogues of coherent and squeezed states: Graded-index fiber solitons and breathing spherically symmetric BEC clouds," Optik **176**, 38 – 48 (2019).

[53]D. Popmintchev, C. Hernández-García, F. Dollar, C. Mancuso, J. A. Pérez-Hernández, M.-C. Chen, A. Hankla, X. Gao, B. Shim, A. L. Gaeta, M. Tarazkar, D. A. Romanov, R. J. Levis, J. A. Gaffney, M. Foord, S. B. Libby, A. Jaron-Becker, A. Becker, L. Plaja, M. M. Murnane, H. C. Kapteyn, and T. Popmintchev, "Ultraviolet surprise: Efficient soft x-ray high-harmonic generation in multiply ionized plasmas," Science **350**, 1225–1231 (2015), http://science.sciencemag.org/content/350/6265/1225.full.pdf.

[54]X. Gao, G. Patwardhan, B. Shim, T. Popmintchev, H. C. Kapteyn, M. M. Murnane, and A. L. Gaeta, "Ionization-assisted spatiotemporal localization in gas-filled capillaries," Opt. Lett. **43**, 3112–3115 (2018).

[55]B. A. López-Zubieta, E. C. Jarque, I. J. Sola, and J. S. Roman, "Spatiotemporal-dressed optical solitons in hollow-core capillaries," OSA Continuum **1**, 930–938 (2018).

[56]R. H. Stolen, J. E. Bjorkholm, and A. Ashkin, "Phase-matched three-wave mixing in silica fiber optical waveguides," Appl. Phys. Lett. **24**, 308–310 (1974).

[57]R. Stolen, "Phase-matched-stimulated four-photon mixing in silica-fiber waveguides," IEEE Journal of Quantum Electronics **11**, 100–103 (1975).

[58]R. Stolen and J. Bjorkholm, "Parametric amplification and frequency conversion in optical fibers," IEEE Journal of Quantum Electronics **18**, 1062–1072 (1982).

[59]K. O. Hill, B. S. Kawasaki, Y. Fujii, and D. C. Johnson, "Efficient sequence-frequency generation in a parametric fiber-optic oscillator," Appl. Phys. Lett. **36**, 888–890 (1980), https://doi.org/10.1063/1.91372.

[60]K. O. Hill, D. C. Johnson, and B. S. Kawasaki, "Efficient conversion of light over a wide spectral range by four-photon mixing in a multimode graded-index fiber," Appl. Opt. **20**, 1075–1079 (1981).

[61]C. Lin and M. A. Bosch, "Large-Stokes-shift stimulated four-photon mixing in optical fibers," Appl. Phys. Lett. **38**, 479–481 (1981), https://doi.org/10.1063/1.92424.

[62]R. Pini, R. Salimbeni, M. Matera, and C. Lin, "Ultraviolet four-photon mixing in a multimode silica fiber Raman amplifier," Opt. Commun. **47**, 226 – 229 (1983).

[63]J. K. Ranka, R. S. Windeler, and A. J. Stentz, "Optical properties of high-delta air–silica microstructure optical fibers," Opt. Lett. **25**, 796–798 (2000).

[64]H. Tu, Z. Jiang, D. L. Marks, and S. A. Boppart, "Intermodal four-wave mixing from femtosecond pulse-pumped photonic crystal fiber," Appl. Phys. Lett. **94**, 101109 (2009), https://doi.org/10.1063/1.3094127.

[65]J. Cheng, M. E. V. Pedersen, K. Charan, K. Wang, C. Xu, L. Grüner-Nielsen, and D. Jakobsen, "Intermodal four-wave mixing in a higher-order-mode fiber," Appl. Phys. Lett. **101**, 161106 (2012), https://doi.org/10.1063/1.4759038.

[66]J. Cheng, M. E. V. Pedersen, K. Charan, K. Wang, C. Xu, L. Grüner-Nielsen, and D. Jakobsen, "Intermodal Cherenkov radiation in a higher-order-mode fiber," Opt. Lett. **37**, 4410–4412 (2012).

[67]R. Essiambre, M. A. Mestre, R. Ryf, A. H. Gnauck, R. W. Tkach, A. R. Chraplyvy, Y. Sun, X. Jiang, and R. Lingle, "Experimental investigation of inter-modal four-wave mixing in few-mode fibers," IEEE Photonics Technology Letters **25**, 539–542 (2013).

[68]S. M. M. Friis, I. Begleris, Y. Jung, K. Rottwitt, P. Petropoulos, D. J. Richardson, P. Horak, and F. Parmigiani, "Inter-modal four-wave mixing study in a two-mode fiber," Opt. Express **24**, 30338–30349 (2016).

[69]Y. Xiao, R.-J. Essiambre, M. Desgroseilliers, A. M. Tulino, R. Ryf, S. Mumtaz, and G. P. Agrawal, "Theory of intermodal four-wave mixing with random linear mode coupling in few-mode fibers," Opt. Express **22**, 32039–32059 (2014).

[70]M. Esmaeelpour, R. Essiambre, N. K. Fontaine, R. Ryf, J. Toulouse, Y. Sun, and R. Lingle, "Power fluctuations of intermodal four-wave mixing in few-mode fibers," Journal of Lightwave Technology **35**, 2429–2435 (2017).

[71]H. Pourbeyram, E. Nazemosadat, and A. Mafi, "Detailed investigation of intermodal four-wave mixing in smf-28: blue-red generation from green," Opt. Express **23**, 14487–14500 (2015).

[72]H. Pourbeyram and A. Mafi, "Four-wave mixing of a laser and its frequency-doubled version in a multimode optical fiber," Photonics **2**, 906–915 (2015).

[73]S. R. Petersen, T. T. Alkeskjold, C. B. Olausson, and J. Lægsgaard, "Intermodal and cross-polarization four-wave mixing in large-core hybrid photonic crystal fibers," Opt.

Express **23**, 5954–5971 (2015).

[74]J. Yuan, X. Sang, Q. Wu, G. Zhou, F. Li, X. Zhou, C. Yu, K. Wang, B. Yan, Y. Han, H. Y. Tam, and P. K. A. Wai, "Enhanced intermodal four-wave mixing for visible and near-infrared wavelength generation in a photonic crystal fiber," Opt. Lett. **40**, 1338–1341 (2015).

[75]J. Yuan, Z. Kang, F. Li, G. Zhou, X. Sang, Q. Wu, B. Yan, X. Zhou, K. Zhong, L. Wang, K. Wang, C. Yu, C. Lu, H. Y. Tam, and P. K. A. Wai, "Polarization-dependent intermodal four-wave mixing in a birefringent multimode photonic crystal fiber," Opt. Lett. **42**, 1644–1647 (2017).

[76]J. Yuan, Z. Kang, F. Li, X. Zhang, X. Sang, G. Zhou, Q. Wu, B. Yan, K. Wang, C. Yu, H. Y. Tam, and P. K. A. Wai, "Demonstration of intermodal four-wave mixing by femtosecond pulses centered at 1550 nm in an air-silica photonic crystal fiber," Journal of Lightwave Technology **35**, 2385–2390 (2017).

[77]B. Sévigny, A. Cassez, O. Vanvincq, Y. Quiquempois, and G. Bouwmans, "High-quality ultraviolet beam generation in multimode photonic crystal fiber through nondegenerate four-wave mixing at 532 nm," Opt. Lett. **40**, 2389–2392 (2015).

[78]J. Yuan, Z. Kang, F. Li, X. Zhang, C. Mei, G. Zhou, X. Sang, Q. Wu, B. Yan, X. Zhou, K. Zhong, K. Wang, C. Yu, G. Farrell, C. Lu, H. Y. Tam, and P. K. A. Wai, "Experimental generation of discrete ultraviolet wavelength by cascaded intermodal four-wave mixing in a multimode photonic crystal fiber," Opt. Lett. **42**, 3537–3540 (2017).

[79]J. Demas, P. Steinvurzel, B. Tai, L. Rishøj, Y. Chen, and S. Ramachandran, "Intermodal nonlinear mixing with Bessel beams in optical fiber," Optica **2**, 14–17 (2015).

[80]E. Nazemosadat, H. Pourbeyram, and A. Mafi, "Phase matching for spontaneous frequency conversion via four-wave mixing in graded-index multimode optical fibers," J. Opt. Soc. Am. B **33**, 144–150 (2016).

[81]J. Demas, G. Prabhakar, T. He, and S. Ramachandran, "Wavelength-agile high-power sources via four-wave mixing in higher-order fiber modes," Opt. Express **25**, 7455–7464 (2017).

[82]R. Dupiol, A. Bendahmane, K. Krupa, A. Tonello, M. Fabert, B. Kibler, T. Sylvestre, A. Barthelemy, V. Couderc, S. Wabnitz, and G. Millot, "Far-detuned cascaded intermodal four-wave mixing in a multimode fiber," Opt. Lett. **42**, 1293–1296 (2017).

[83]A. Bendahmane, K. Krupa, A. Tonello, D. Modotto, T. Sylvestre, V. Couderc, S. Wabnitz, and G. Millot, "Seeded intermodal four-wave mixing in a highly multimode fiber," J. Opt. Soc. Am. B **35**, 295–301 (2018).

[84]S. K. Chatterjee and R. Vijaya, "Degenerate intermodal four-wave mixing with Q-switched nanosecond pulses in SMF-28 for the generation of discrete ultraviolet-visible wavelengths," OSA Continuum **1**, 1360–1369 (2018).

[85]H. Pourbeyram and A. Mafi, "Saturable mode conversion of parametric amplification in a multimode optical fiber," APL Photonics **4**, 022805 (2019), https://doi.org/10.1063/1.5048514.

[86]J. Demas, L. Rishøj, X. Liu, G. Prabhakar, and S. Ramachandran, "Intermodal group-velocity engineering for broadband nonlinear optics," Photon. Res. **7**, 1–7 (2019).

[87]H. Pourbeyram and A. Mafi, "Photon pair generation with tailored frequency correlations in graded-index multimode fibers," Opt. Lett. **43**, 2018–2021 (2018).

[88]L. Yin, Z. Han, H. Shen, and R. Zhu, "Suppression of inter-modal four-wave mixing in high-power fiber lasers," Opt. Express **26**, 15804–15818 (2018).

[89]G. Millot, S. Pitois, P. T. Dinda, and M. Haelterman, "Observation of modulational instability induced by velocity-matched cross-phase modulation in a normally dispersive bimodal fiber," Opt. Lett. **22**, 1686–1688 (1997).

[90]A. Tonello, S. Pitois, S. Wabnitz, G. Millot, T. Martynkien, W. Urbanczyk, J. Wojcik, A. Locatelli, M. Conforti, and C. DeAngelis, "Frequency tunable polarization and intermodal modulation instability in high birefringence holey fiber," Opt. Express **14**, 397–404 (2006).

[91]R. Dupiol, A. Bendahmane, K. Krupa, J. Fatome, A. Tonello, M. Fabert, V. Couderc, S. Wabnitz, and G. Millot, "Intermodal modulational instability in graded-index multimode optical fibers," Opt. Lett. **42**, 3419–3422 (2017).

[92]M. Guasoni, "Generalized modulational instability in multimode fibers: Wideband multimode parametric amplification," Phys. Rev. A **92**, 033849 (2015).

[93]L. Li, J. Leng, P. Zhou, and J. Chen, "Modulation instability induced by intermodal cross-phase modulation in step-index multimode fiber," Appl. Opt. **58**, 4283–4287 (2019).

[94]Z. S. Eznaveh, M. A. Eftekhar, J. E. A. Lopez, M. Kolesik, A. Schülzgen, F. W. Wise, D. N. Christodoulides, and R. A. Correa, "Tailoring frequency generation in uniform and concatenated multimode fibers," Opt. Lett. **42**, 1015–1018 (2017).

[95]M. A. Eftekhar, Z. Sanjabi-Eznaveh, H. E. Lopez-Aviles, S. Benis, J. E. Antonio-Lopez, M. Kolesik, F. Wise, R. Amezcua-Correa, and D. N. Christodoulides, "Accelerated nonlinear interactions in graded-index multimode fibers," Nature Communications **10**, 1638 (2019).

[96]H. E. L. Aviles, F. O. Wu, Z. Eznaveh, M. A. Eftekhar, F. Wise, R. Correa, and D. N. Christodoulides, "A systematic analysis of parametric instabilities in nonlinear parabolic multimode fibers," APL Photonics **4**, 022803 (2019), https://doi.org/10.1063/1.5044659.

[97]C. Mas Arabí, A. Kudlinski, A. Mussot, and M. Conforti, "Geometric parametric instability in periodically modulated graded-index multimode fibers," Phys. Rev. A **97**, 023803 (2018).

[98]U. Teğin and B. Ortaç, "Spatiotemporal instability of femtosecond pulses in graded-index multimode fibers," IEEE Photonics Technology Letters **29**, 2195–2198 (2017).

[99]A. Mussot, T. Sylvestre, L. Provino, and H. Maillotte, "Generation of a broadband single-mode supercontinuum in a conventional dispersion-shifted fiber by use of a subnanosecond microchip laser," Opt. Lett. **28**, 1820–1822 (2003).

[100]A. Efimov, A. J. Taylor, F. G. Omenetto, J. C. Knight, W. J. Wadsworth, and P. S. J. Russell, "Nonlinear generation of very high-order UV modes in microstructured fibers," Opt. Express **11**, 910–918 (2003).

[101]H. Pourbeyram, G. P. Agrawal, and A. Mafi, "Stimulated Raman scattering cascade spanning the wavelength range of 523 to 1750 nm using a graded-index multimode optical fiber," Appl. Phys. Lett. **102**, 201107 (2013), https://doi.org/10.1063/1.4807620.

[102]M. A. Eftekhar, L. G. Wright, M. S. Mills, M. Kolesik, R. A. Correa, F. W. Wise, and D. N. Christodoulides, "Versatile supercontinuum generation in parabolic multimode optical fibers," Opt. Express **25**, 9078–9087 (2017).

[103]G. L. Galmiche, Z. S. Eznaveh, M. A. Eftekhar, J. A. Lopez, L. G. Wright, F. Wise, D. Christodoulides, and R. A. Correa, "Visible supercontinuum generation in a graded index multimode fiber pumped at 1064 nm," Opt. Lett. **41**, 2553–2556 (2016).

[104]K. Krupa, C. Louot, V. Couderc, M. Fabert, R. Guenard, B. M. Shalaby, A. Tonello, D. Pagnoux, P. Leproux, A. Bendahmane, R. Dupiol, G. Millot, and S. Wabnitz, "Spatiotemporal characterization of supercontinuum extending from the visible to the mid-infrared in a multimode graded-index optical fiber," Opt. Lett. **41**, 5785–5788 (2016).

[105]U. Teğin and B. Ortaç, "Cascaded Raman scattering based high power octave-spanning supercontinuum generation in graded-index multimode fibers," Scientific Reports **8**, 12470 (2018).

[106]S. Perret, G. Fanjoux, L. Bigot, J. Fatome, G. Millot, J. M. Dudley, and T. Sylvestre, "Supercontinuum generation by intermodal four-wave mixing in a step-index few-mode fibre," APL Photonics **4**, 022905 (2019), https://doi.org/10.1063/1.5045645.

[107]U. Österberg and W. Margulis, "Dye laser pumped by Nd:YAG laser pulses frequency doubled in a glass optical fiber," Opt. Lett. **11**, 516–518 (1986).

[108]R. H. Stolen and H. W. K. Tom, "Self-organized phase-matched harmonic generation in optical fibers," Opt. Lett. **12**, 585–587 (1987).

[109]E. M. Dianov and D. S. Starodubov, "Photoinduced generation of the second harmonic in centrosymmetric media," Quantum Electron. **25**, 395–407 (1995).

[110]D. Z. Anderson, V. Mizrahi, and J. E. Sipe, "Model for second-harmonic generation in glass optical fibers based on asymmetric photoelectron emission from defect sites," Opt. Lett. **16**, 796–798 (1991).

[111]V. Dominic and J. Feinberg, "Light-induced second-harmonic generation in glass via multiphoton ionization," Phys. Rev. Lett. **71**, 3446–3449 (1993).

[112]D. Ceoldo, K. Krupa, A. Tonello, V. Couderc, D. Modotto, U. Minoni, G. Millot, and S. Wabnitz, "Second harmonic generation in multimode graded-index fibers: spatial beam cleaning and multiple harmonic sideband generation," Opt. Lett. **42**, 971–974 (2017).

[113]M. A. Eftekhar, Z. S. Eznaveh, J. E. A. Lopez, F. W. Wise, D. N. Christodoulides, and R. Amezcua-Correa, "Instant and efficient second-harmonic generation and downconversion in unprepared graded-index multimode fibers," Opt. Lett. **42**, 3478–3481 (2017).

[114]O. Tzang, A. M. Caravaca-Aguirre, K. Wagner, and R. Piestun, "Adaptive wavefront shaping for controlling nonlinear multimode interactions in optical fibres," Nat. Photonics **12**, 368–374 (2018).

[115]R. N. Mahalati, D. Askarov, J. P. Wilde, and J. M. Kahn, "Adaptive control of input field to achieve desired output intensity profile in multimode fiber with random mode coupling," Opt. Express **20**, 14321–14337 (2012).

[116]I. N. Papadopoulos, S. Farahi, C. Moser, and D. Psaltis, "Focusing and scanning light through a multimode optical fiber using digital phase conjugation," Opt. Express **20**, 10583–10590 (2012).

[117]M. Plöschner, T. Tyc, and T. Cizmár, "Seeing through chaos in multimode fibres," Nature Photonics **9**, 529 EP – (2015), article.

[118]K. S. Chiang, "Stimulated Raman scattering in a multimode optical fiber: evolution of modes in Stokes waves," Opt. Lett. **17**, 352–354 (1992).

[119]H. Bruesselbach, "Beam cleanup using stimulated Brillouin scattering in multimode fibers," in *Conference on Lasers and Electro-Optics* (Optical Society of America, 1993) p. CThJ2.

[120]L. Lombard, A. Brignon, J.-P. Huignard, E. Lallier, and P. Georges, "Beam cleanup in a self-aligned gradient-index Brillouin cavity for high-power multimode fiber amplifiers," Opt. Lett. **31**, 158–160 (2006).

[121]S. H. Baek and W. B. Roh, "Single-mode Raman fiber laser based on a multimode fiber," Opt. Lett. **29**, 153–155 (2004).

[122]A. G. Kuznetsov, E. V. Podivilov, and S. A. Babin, "Actively Q-switched Raman fiber laser," Laser Physics Letters **12**, 035102 (2015).

[123]N. B. Terry, K. T. Engel, T. G. Alley, and T. H. Russell, "Use of a continuous wave Raman fiber laser in graded-index multimode fiber for SRS beam combination," Opt. Express **15**, 602–607 (2007).

[124]B. C. Rodgers, T. H. Russell, and W. B. Roh, "Laser beam combining and cleanup by stimulated Brillouin scattering in a multimode optical fiber," Opt. Lett. **24**, 1124–1126 (1999).

[125]K. C. Brown, T. H. Russell, T. G. Alley, and W. B. Roh, "Passive combination of multiple beams in an optical fiber via stimulated Brillouin scattering," Opt. Lett. **32**, 1047–1049 (2007).

[126]A. Polley and S. E. Ralph, "Raman amplification in multimode fiber," IEEE Photonics Technology Letters **19**, 218–220 (2007).

[127]B. Steinhausser, A. Brignon, E. Lallier, J. P. Huignard, and P. Georges, "High energy, single-mode, narrow-linewidth fiber laser source using stimulated Brillouin scattering beam cleanup," Opt. Express **15**, 6464–6469 (2007).

[128]Q. Gao, Z. Lu, C. Zhu, and J. Zhang, "Mechanism of beam cleanup by stimulated Brillouin scattering in multimode fibers," Applied Physics Express **8**, 052501 (2015).

[129]C. Y. Zhu, J. H. Zhang, Y. B. Yuan, D. X. Ba, J. Yan, Q. L. Gao, and Z. W. Lu, "Beam cleanup of 20 kW peak power laser pulses by SBS in 105 μm large core diameter fiber with

high beam quality ($M^2 \simeq 1.5$)," in *2013 International Conference on Optoelectronics and Microelectronics (ICOM)* (2013) pp. 248–250.

[130]P. M. Lushnikov and N. Vladimirova, "Nonlinear combining of laser beams," Opt. Lett. **39**, 3429–3432 (2014).

[131]L. G. Wright, Z. Liu, D. A. Nolan, M.-J. Li, D. N. Christodoulides, and F. W. Wise, "Self-organized instability in graded-index multimode fibres," Nat. Photonics **10**, 771–776 (2016).

[132]J. Lægsgaard, "Spatial beam cleanup by pure Kerr processes in multimode fibers," Opt. Lett. **43**, 2700–2703 (2018).

[133]K. Krupa, A. Tonello, V. Couderc, A. Barthélémy, G. Millot, D. Modotto, and S. Wabnitz, "Spatiotemporal light-beam compression from nonlinear mode coupling," Phys. Rev. A **97**, 043836 (2018).

[134]C. K. Asawa and H. F. Taylor, "Propagation of light trapped within a set of lowest-order modes of graded-index multimode fiber undergoing bending," Appl. Opt. **39**, 2029–2037 (2000).

[135]D. E. Boonzajer Flaes, J. Stopka, S. Turtaev, J. F. de Boer, T. Tyc, and T. Čižmár, "Robustness of light-transport processes to bending deformations in graded-index multimode waveguides," Phys. Rev. Lett. **120**, 233901 (2018).

[136]Y. Leventoux, A. Parriaux, O. Sidelnikov, G. Granger, M. Jossent, L. Lavoute, D. Gaponov, M. Fabert, A. Tonello, K. Krupa, A. Desfarges-Berthelemot, V. Kermene, G. Millot, S. Février, S. Wabnitz, and V. Couderc, "Kerr beam self-cleaning in the multimode fiber anomalous dispersion regime," arXiv e-prints , arXiv:1810.05878 (2018), arXiv:1810.05878 [physics.optics].

[137]R. Dupiol, K. Krupa, A. Tonello, M. Fabert, D. Modotto, S. Wabnitz, G. Millot, and V. Couderc, "Interplay of Kerr and Raman beam cleaning with a multimode microstructure fiber," Opt. Lett. **43**, 587–590 (2018).

[138]K. Krupa, V. Couderc, A. Tonello, D. Modotto, A. Barthélémy, G. Millot, and S. Wabnitz, "Refractive index profile tailoring of multimode optical fibers for the spatial and spectral shaping of parametric sidebands," J. Opt. Soc. Am. B **36**, 1117–1126 (2019).

[139]T. Hellwig, T. Walbaum, and C. Fallnich, "Optically induced mode conversion in graded-index fibers using ultra-short laser pulses," Applied Physics B **112**, 499–505 (2013).

[140]P. Cerenkov, "Visible glow under exposure of gamma radiation," Dokl, Akad, Nauk, SSSR **2**, 451 (1934).

[141]E. V. Podivilov, D. S. Kharenko, V. A. Gonta, K. Krupa, O. S. Sidelnikov, S. Turitsyn, M. P. Fedoruk, S. A. Babin, and S. Wabnitz, "Hydrodynamic 2D turbulence and spatial beam condensation in multimode optical fibers," Phys. Rev. Lett. **122**, 103902 (2019).

[142]P. Aschieri, J. Garnier, C. Michel, V. Doya, and A. Picozzi, "Condensation and thermalization of classsical optical waves in a waveguide," Phys. Rev. A **83**, 033838 (2011).

[143]A. Fusaro, J. Garnier, K. Krupa, G. Millot, and A. Picozzi, "Dramatic acceleration of wave condensation mediated by disorder in multimode fibers," Phys. Rev. Lett. **122**, 123902 (2019).

[144]O. S. Sidelnikov, E. V. Podivilov, M. P. Fedoruk, and S. Wabnitz, "Random mode coupling assists Kerr beam self-cleaning in a graded-index multimode optical fiber," Optical Fiber Technology **53**, 101994 (2019).

[145]K. Krupa, G. G. Castañeda, A. Tonello, A. Niang, D. S. Kharenko, M. Fabert, V. Couderc, G. Millot, U. Minoni, D. Modotto, and S. Wabnitz, "Nonlinear polarization dynamics of Kerr beam self-cleaning in a graded-index multimode optical fiber," Opt. Lett. **44**, 171–174 (2019).

[146]Z. Liu, L. G. Wright, D. N. Christodoulides, and F. W. Wise, "Kerr self-cleaning of femtosecond-pulsed beams in graded-index multimode fiber," Opt. Lett. **41**, 3675–3678 (2016).

[147]E. Deliancourt, M. Fabert, A. Tonello, K. Krupa, A. Desfarges-Berthelemot, V. Kermene, G. Millot, A. Barthélémy, S. Wabnitz, and V. Couderc, "Kerr beam self-cleaning on the LP_{11} mode in graded-index multimode fibers," OSA Continuum **2**, 1089–1096 (2019).

[148]E. Deliancourt, M. Fabert, A. Tonello, K. Krupa, A. Desfarges-Berthelemot, V. Kermene, G. Millot, A. Barthélémy, S. Wabnitz, and V. Couderc, "Wavefront shaping for optimized many-mode Kerr beam self-cleaning in graded-index multimode fiber," Opt. Express **27**, 17311–17321 (2019).

[149]R. Guenard, K. Krupa, R. Dupiol, M. Fabert, A. Bendahmane, V. Kermene, A. Desfarges-Berthelemot, J. L. Auguste, A. Tonello, A. Barthélémy, G. Millot, S. Wabnitz, and V. Couderc, "Kerr self-cleaning of pulsed beam in an ytterbium doped multimode fiber," Opt. Express **25**, 4783–4792 (2017).

[150]R. Guenard, K. Krupa, R. Dupiol, M. Fabert, A. Bendahmane, V. Kermene, A. Desfarges-Berthelemot, J. L. Auguste, A. Tonello, A. Barthélémy, G. Millot, S. Wabnitz, and V. Couderc, "Nonlinear beam self-cleaning in a coupled cavity composite laser based on multimode fiber," Opt. Express **25**, 22219–22227 (2017).

[151]A. Niang, T. Mansuryan, K. Krupa, A. Tonello, M. Fabert, P. Leproux, D. Modotto, O. N. Egorova, A. E. Levchenko, D. S. Lipatov, S. L. Semjonov, G. Millot, V. Couderc, and S. Wabnitz, "Spatial beam self-cleaning and supercontinuum generation with yb-doped multimode graded-index fiber taper based on accelerating self-imaging and dissipative landscape," Opt. Express **27**, 24018–24028 (2019).

[152]L. G. Wright, D. N. Christodoulides, and F. W. Wise, "Spatiotemporal mode-locking in multimode fiber lasers," Science **358**, 94–97 (2017).

[153]J. W. Dawson, M. J. Messerly, R. J. Beach, M. Y. Shverdin, E. A. Stappaerts, A. K. Sridharan, P. H. Pax, J. E. Heebner, C. W. Siders, and C. Barty, "Analysis of the scalability of diffraction-limited fiber lasers and amplifiers to high average power," Opt. Express **16**, 13240–13266 (2008).

[154]D. Auston, "Transverse mode locking," IEEE Journal of Quantum Electronics **4**, 420–422 (1968).

[155]P. W. Smith, "Simultaneous phase-locking of longitudinal and transverse laser modes," Appl. Phys. Lett. **13**, 235–237 (1968), https://doi.org/10.1063/1.1652586.

[156]D. Côté and H. M. van Driel, "Period doubling of a femtosecond Ti:sapphire laser by total mode locking," Opt. Lett. **23**, 715–717 (1998).

[157]R. Gordon, A. P. Heberle, and J. R. A. Cleaver, "Transverse mode-locking in microcavity lasers," Appl. Phys. Lett. **81**, 4523–4525 (2002), https://doi.org/10.1063/1.1528287.

[158]E. Ding, S. Lefrancois, J. N. Kutz, and F. W. Wise, "Scaling fiber lasers to large mode area: An investigation of passive mode-locking using a multi-mode fiber," IEEE Journal of Quantum Electronics **47**, 597–606 (2011).

[159]Y. Wang, Y. Tang, S. Yan, and J. Xu, "High-power mode-locked 2 μm multimode fiber laser," Laser Physics Letters **15**, 085101 (2018).

[160]H. Qin, X. Xiao, P. Wang, and C. Yang, "Observation of soliton molecules in a spatiotemporal mode-locked multimode fiber laser," Opt. Lett. **43**, 1982–1985 (2018).

[161]M. Kowalczyk, T. Martynkien, P. Mergo, G. Soboń, and J. Sotor, "Ultrabroadband wavelength-swept source based on total mode-locking of an $Yb : CaF_2$ laser," Photon.

Res. **7**, 182–186 (2019).

[162]T. Wang, F. Shi, Y. Huang, J. Wen, Z. Luo, F. Pang, T. Wang, and X. Zeng, "High-order mode direct oscillation of few-mode fiber laser for high-quality cylindrical vector beams," Opt. Express **26**, 11850–11858 (2018).

[163]Y. Huang, F. Shi, T. Wang, X. Liu, X. Zeng, F. Pang, T. Wang, and P. Zhou, "High-order mode Yb-doped fiber lasers based on mode-selective couplers," Opt. Express **26**, 19171–19181 (2018).

[164]T. Wang, A. Yang, F. Shi, Y. Huang, J. Wen, and X. Zeng, "High-order mode lasing in all-FMF laser cavities," Photon. Res. **7**, 42–49 (2019).

[165]S.-m. Han, K. Yang, Z.-h. Wang, Y.-g. Liu, and Z. Wang, "Multimode oscillation Q-switched erbium-doped fiber laser with a few-mode fiber cavity," Optoelectronics Letters **14**, 417–420 (2018).

[166]J. T. Murray, W. L. Austin, and R. C. Powell, "Intracavity Raman conversion and Raman beam cleanup," Optical Materials **11**, 353 – 371 (1999).

[167]S. I. Kablukov, E. I. Dontsova, E. A. Zlobina, I. N. Nemov, A. A. Vlasov, and S. A. Babin, "An LD-pumped Raman fiber laser operating below 1 μm," Laser Physics Letters **10**, 085103 (2013).

[168]T. Yao, A. V. Harish, J. K. Sahu, and J. Nilsson, "High-power continuous-wave directly-diode-pumped fiber Raman lasers," Applied Sciences **5**, 1323–1336 (2015).

[169]Y. Glick, V. Fromzel, J. Zhang, N. Ter-Gabrielyan, and M. Dubinskii, "High-efficiency, 154 W CW diode-pumped Raman fiber laser with brightness enhancement," Appl. Opt. **56**, B97–B102 (2017).

[170]E. A. Zlobina, S. I. Kablukov, A. A. Wolf, A. V. Dostovalov, and S. A. Babin, "Nearly single-mode Raman lasing at 954 nm in a graded-index fiber directly pumped by a multimode laser diode," Opt. Lett. **42**, 9–12 (2017).

[171]E. A. Zlobina, S. I. Kablukov, A. A. Wolf, I. N. Nemov, A. V. Dostovalov, V. A. Tyrtyshnyy, D. V. Myasnikov, and S. A. Babin, "Generating high-quality beam in a multimode LD-pumped all-fiber Raman laser," Opt. Express **25**, 12581–12587 (2017).

[172]E. A. Evmenova, A. G. Kuznetsov, I. N. Nemov, A. A. Wolf, A. V. Dostovalov, S. I. Kablukov, and S. A. Babin, "2nd-order random lasing in a multimode diode-pumped graded-index fiber," Scientific Reports **8**, 17945 (2018).

[173]Y. Glick, Y. Shamir, A. A. Wolf, A. V. Dostovalov, S. A. Babin, and S. Pearl, "Highly efficient all-fiber continuous-wave Raman graded-index fiber laser pumped by a fiber laser," Opt. Lett. **43**, 1027–1030 (2018).

[174]Y. Chen, J. Leng, H. Xiao, T. Yao, J. Xu, and P. Zhou, "High-efficiency all-fiber Raman fiber amplifier with record output power," Laser Physics Letters **15**, 085104 (2018).

[175]Y. Chen, J. Leng, H. P. Xiao, T. Yao, and P. F. Zhou, "Pure passive fiber enabled highly efficient Raman fiber amplifier with record kilowatt power," IEEE Access **7**, 28334–28339 (2019).

[176]X. Zhu, A. Schülzgen, H. Li, L. Li, Q. Wang, S. Suzuki, V. L. Temyanko, J. V. Moloney, and N. Peyghambarian, "Single-transverse-mode output from a fiber laser based on multimode interference," Opt. Lett. **33**, 908–910 (2008).

[177]B. M. Shalaby, V. Kermene, D. Pagnoux, and A. Barthelemy, "Transverse mode control by a self-imaging process in a multimode fibre laser using a single-mode feedback loop," Journal of Optics A: Pure and Applied Optics **10**, 115303 (2008).

[178]X. Zhu, A. Schülzgen, H. Li, L. Li, L. Han, J. V. Moloney, and N. Peyghambarian, "Detailed investigation of self-imaging in large core multimode optical fibers for application in fiber lasers and amplifiers," Opt. Express **16**, 16632–16645 (2008).

[179]H. Li, Z. Wang, C. Li, J. Zhang, and S. Xu, "Mode-locked Tm fiber laser using SMF-SIMF-GIMF-SMF fiber structure as a saturable absorber," Opt. Express **25**, 26546–26553 (2017).

[180]E. Nazemosadat and A. Mafi, "Nonlinear multimodal interference and saturable absorption using a short graded-index multimode optical fiber," J. Opt. Soc. Am. B **30**, 1357–1367 (2013).

[181]Q. Wang, G. Farrell, and W. Yan, "Investigation on single-mode-multimode-single-mode fiber structure," Journal of Lightwave Technology **26**, 512–519 (2008).

[182]S. Fu, Q. Sheng, X. Zhu, W. Shi, J. Yao, G. Shi, R. A. Norwood, and N. Peyghambarian, "Passive Q-switching of an all-fiber laser induced by the Kerr effect of multimode interference," Opt. Express **23**, 17255–17262 (2015).

[183]J. Zhou, Y. Lu, B. He, and X. Gu, "Q-switched laser in an SMS cavity for inhibiting nonlinear effects," Appl. Opt. **54**, 6080–6084 (2015).

[184]S. Fu, G. Shi, Q. Sheng, W. Shi, X. Zhu, J. Yao, R. A. Norwood, and N. Peyghambarian, "Dual-wavelength fiber laser operating above 2 μm based on cascaded single-mode-

multimode-single-mode fiber structures," Opt. Express **24**, 11282–11289 (2016).

[185]Z. Wang, D. N. Wang, F. Yang, L. Li, C. Zhao, B. Xu, S. Jin, S. Cao, and Z. Fang, "Er-doped mode-locked fiber laser with a hybrid structure of a step-index-graded-index multimode fiber as the saturable absorber," Journal of Lightwave Technology **35**, 5280–5285 (2017).

[186]F. Yang, D. N. Wang, Z. Wang, L. Li, C.-L. Zhao, B. Xu, S. Jin, S.-Y. Cao, and Z.-J. Fang, "Saturable absorber based on a single mode fiber-graded index fiber-single mode fiber structure with inner micro-cavity," Opt. Express **26**, 927–934 (2018).

[187]Z. Wang, D. N. Wang, F. Yang, L. Li, C.-L. Zhao, B. Xu, S. Jin, S.-Y. Cao, and Z.-J. Fang, "Stretched graded-index multimode optical fiber as a saturable absorber for erbium-doped fiber laser mode locking," Opt. Lett. **43**, 2078–2081 (2018).

[188]U. Teğin and B. Ortaç, "All-fiber all-normal-dispersion femtosecond laser with a nonlinear multimodal interference-based saturable absorber," Opt. Lett. **43**, 1611–1614 (2018).

[189]F. Zhao, Y. Wang, H. Wang, X. Hu, W. Zhang, T. Zhang, and Y. Cai, "High-energy solitons generation with a nonlinear multimode interference-based saturable absorber," Laser Physics **28**, 085104 (2018).

[190]H. Li, Z. Wang, C. Li, Y. Tian, Z. Xiao, J. Zhang, and S. Xu, "Self-starting mode-locked Tm-doped fiber laser using a hybrid structure of no core - graded index multimode fiber as the saturable absorber," Optics and Laser Technology **113**, 317 – 321 (2019).

[191]F. Zhao, Y. Wang, H. Wang, Z. Yan, X. Hu, W. Zhang, T. Zhang, and K. Zhou, "Ultrafast soliton and stretched-pulse switchable mode-locked fiber laser with hybrid structure of multimode fiber based saturable absorber," Scientific Reports. **8**, 16369 (2018).

[192]G. Chen, W. Li, G. Wang, W. Zhang, C. Zeng, and W. Zhao, "Generation of coexisting high-energy pulses in a mode-locked all-fiber laser with a nonlinear multimodal interference technique," Photon. Res. **7**, 187–192 (2019).

[193]T. Chen, Q. Zhang, Y. Zhang, X. Li, H. Zhang, and W. Xia, "All-fiber passively mode-locked laser using nonlinear multimode interference of step-index multimode fiber," Photon. Res. **6**, 1033–1039 (2018).

[194]P. Grelu and N. Akhmediev, "Dissipative solitons for mode-locked lasers," Nat. Photonics **6**, 84–92 (2012).

[195]A. Chong, W. H. Renninger, and F. W. Wise, "All-normal-dispersion femtosecond fiber laser with pulse energy above 20nJ," Opt. Lett. **32**, 2408–2410 (2007).

[196]P. Grelu, J. M. Soto-Crespo, and N. Akhmediev, "Light bullets and dynamic pattern formation in nonlinear dissipative systems," Opt. Express **13**, 9352–9360 (2005).

[197]Z. Q. Wang, K. Nithyanandan, A. Coillet, P. Tchofo-Dinda, and P. Grelu, "Optical soliton molecular complexes in a passively mode-locked fibre laser," Nat. Commun. **10**, 830 (2019).

[198]W. He, M. Pang, D. H. Yeh, J. Huang, C. R. Menyuk, and P. S. J. Russell, "Supramolecular transmission of soliton-encoded bit streams over astronomical distances," (2017), arXiv:1710.01034 [physics.optics].

[199]K. Krupa, K. Nithyanandan, U. Andral, P. Tchofo-Dinda, and P. Grelu, "Real-time observation of internal motion within ultrafast dissipative optical soliton molecules," Phys. Rev. Lett. **118**, 243901 (2017).

[200]G. Herink, F. Kurtz, B. Jalali, D. R. Solli, and C. Ropers, "Real-time spectral interferometry probes the internal dynamics of femtosecond soliton molecules," Science **356**, 50–54 (2017).

[201]J. Peng and H. Zeng, "Build-up of dissipative optical soliton molecules via diverse soliton interactions," Laser & Photonics Reviews **12**, 1800009 (2018).

[202]N. Akhmediev, B. Kibler, F. Baronio, M. Belić, W.-P. Zhong, Y. Zhang, W. Chang, J. M. Soto-Crespo, P. Vouzas, P. Grelu, C. Lecaplain, K. Hammani, S. Rica, A. Picozzi, M. Tlidi, K. Panajotov, A. Mussot, A. Bendahmane, P. Szriftgiser, G. Genty, J. Dudley, A. Kudlinski, A. Demircan, U. Morgner, S. Amiraranashvili, C. Bree, G. Steinmeyer, C. Masoller, N. G. R. Broderick, A. F. J. Runge, M. Erkintalo, S. Residori, U. Bortolozzo, F. T. Arecchi, S. Wabnitz, C. G. Tiofack, S. Coulibaly, and M. Taki, "Roadmap on optical rogue waves and extreme events," Journal of Optics **18**, 063001 (2016).

[203]K. Goda and B. Jalali, "Dispersive fourier transformation for fast continuous single-shot measurements," Nat. Photonics **7**, 102–112 (2013).

[204]J. Pauwels, G. Verschaffelt, S. Massar, and G. V. der Sande, "Distributed Kerr nonlinearity in a coherent all-optical fiber-ring reservoir computer," (2019), arXiv:1908.11210 [physics.app-ph].

[205]U. Paudel, M. Luengo-Kovac, J. Pilawa, T. J. Shaw, and G. C. Valley, "Classification of time-domain waveforms using a speckle-based optical reservoir computer," (2019), arXiv:1909.12489 [physics.optics].

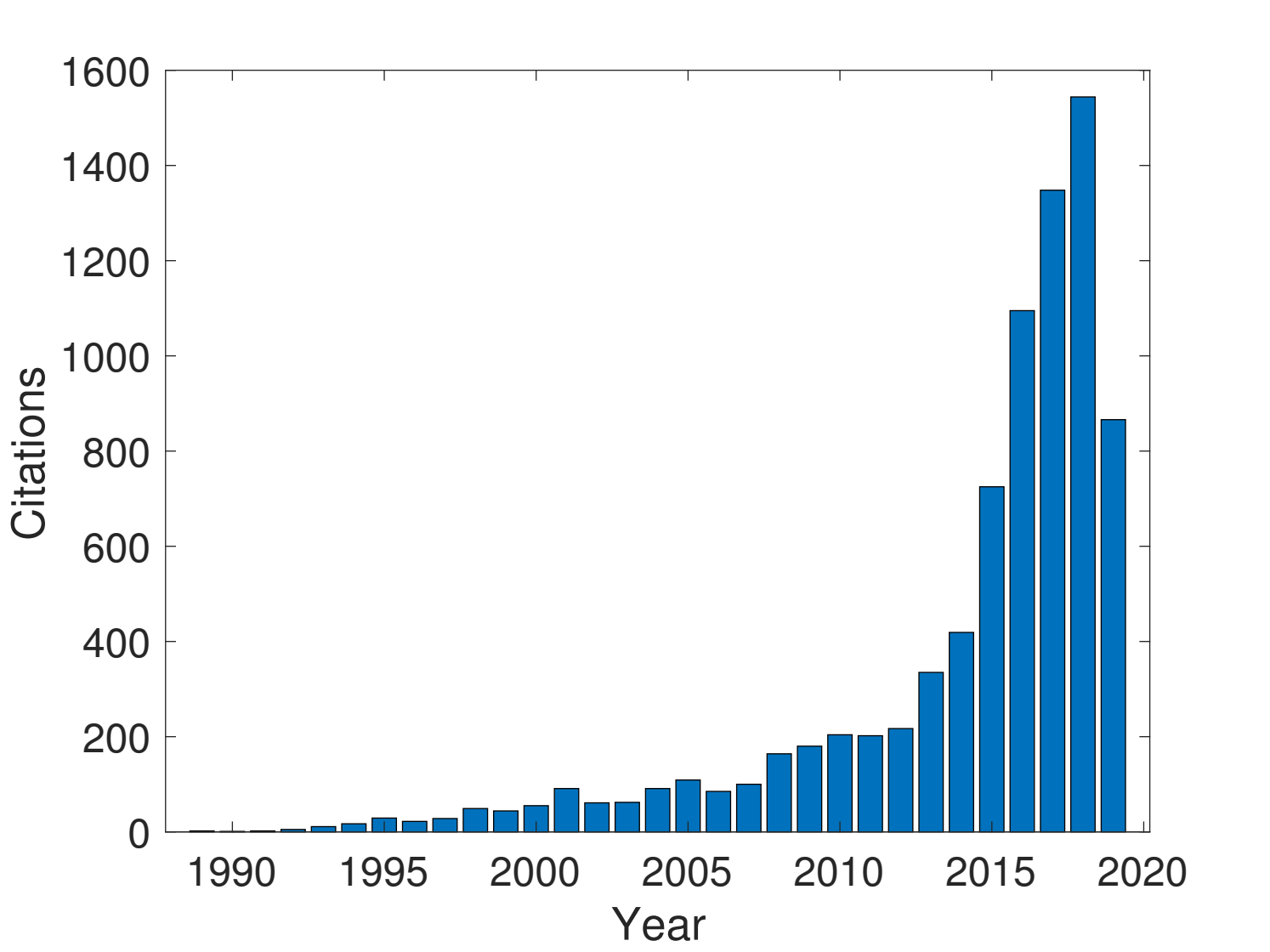
1600
1400
1200
1000
800
600
400
200
0
Citations
1990
1995
2000
2005
2010
2015
2020
Year

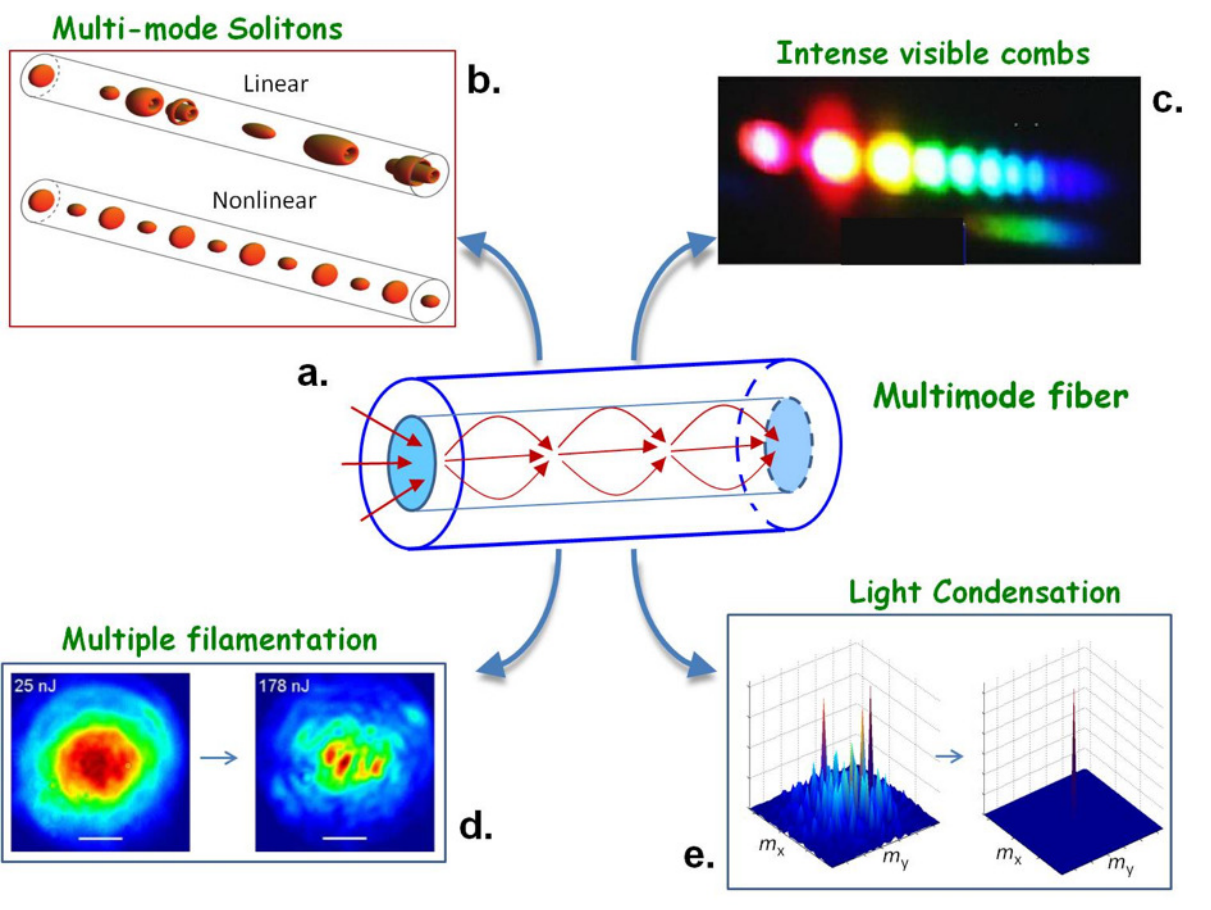
Multi-mode Solitons
Linear
Nonlinear
b.
Intense visible combs
c.
a.
Multimode fiber
Multiple filamentation
25 nJ
178 nJ
d.
Light Condensation
m_x
m_y
m_x
m_y
e.

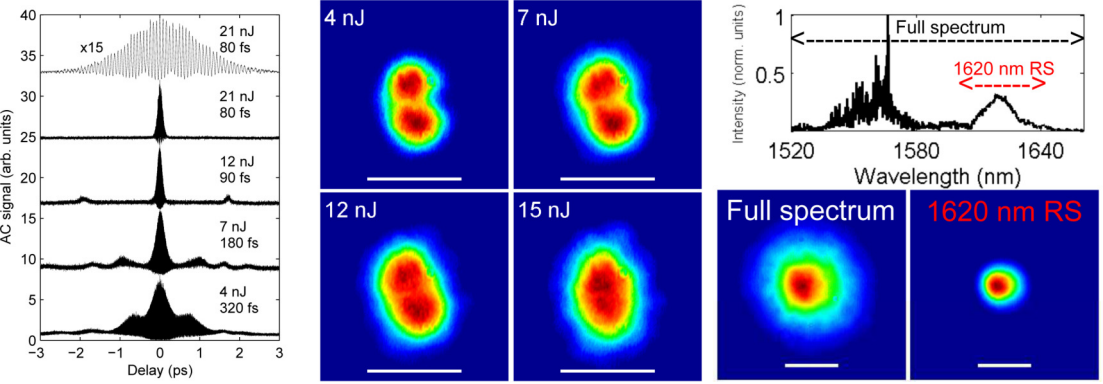
x15
21 nJ
80 fs
21 nJ
80 fs
12 nJ
90 fs
7 nJ
180 fs
4 nJ
320 fs
AC signal (arb. units)
Delay (ps)
4 nJ
7 nJ
12 nJ
15 nJ
Full spectrum
1620 nm RS
Intensity (norm. units)
Wavelength (nm)
Full spectrum
1620 nm RS

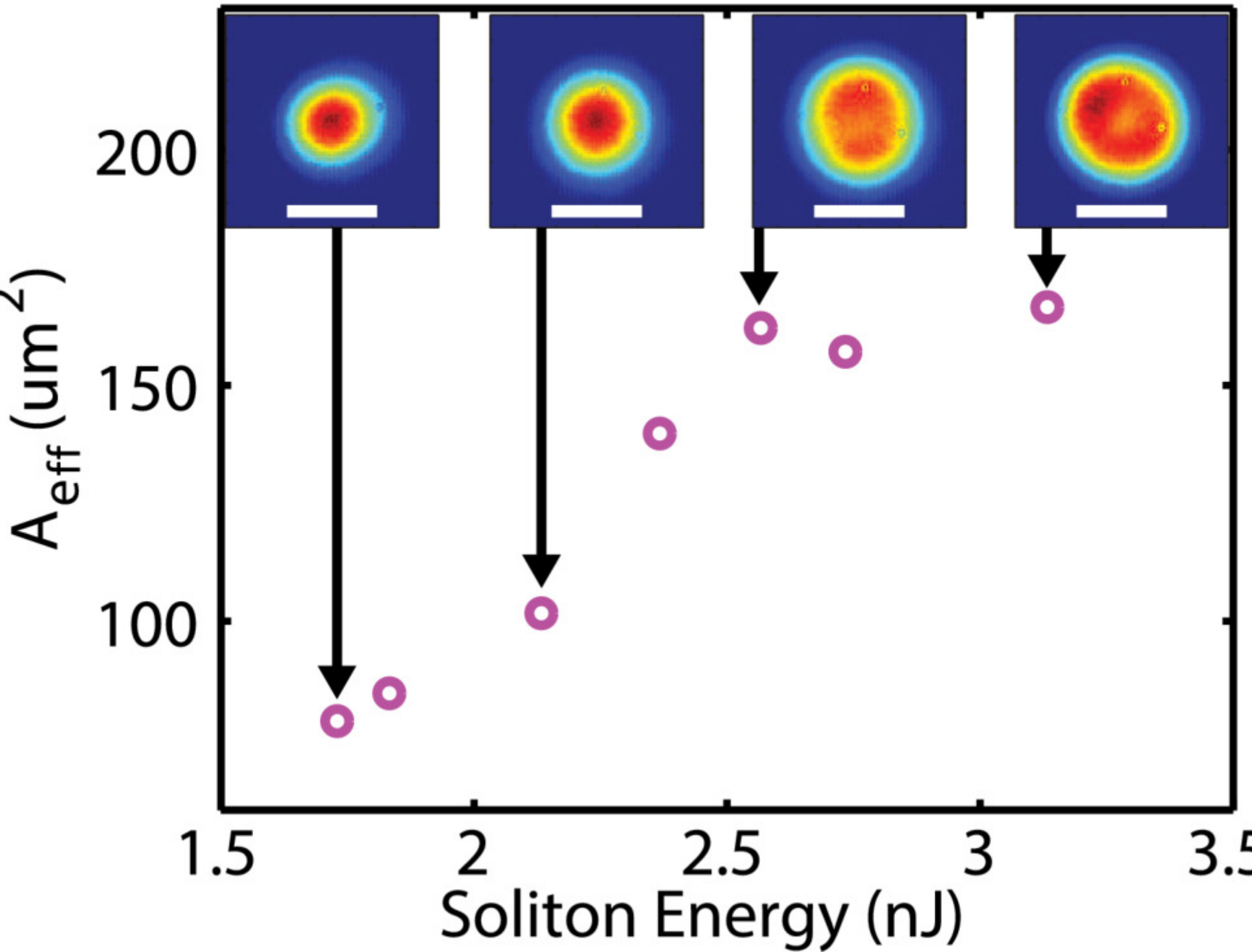
200
150
100
A_{eff} (um^2)
1.5
2
2.5
3
3.5
Soliton Energy (nJ)

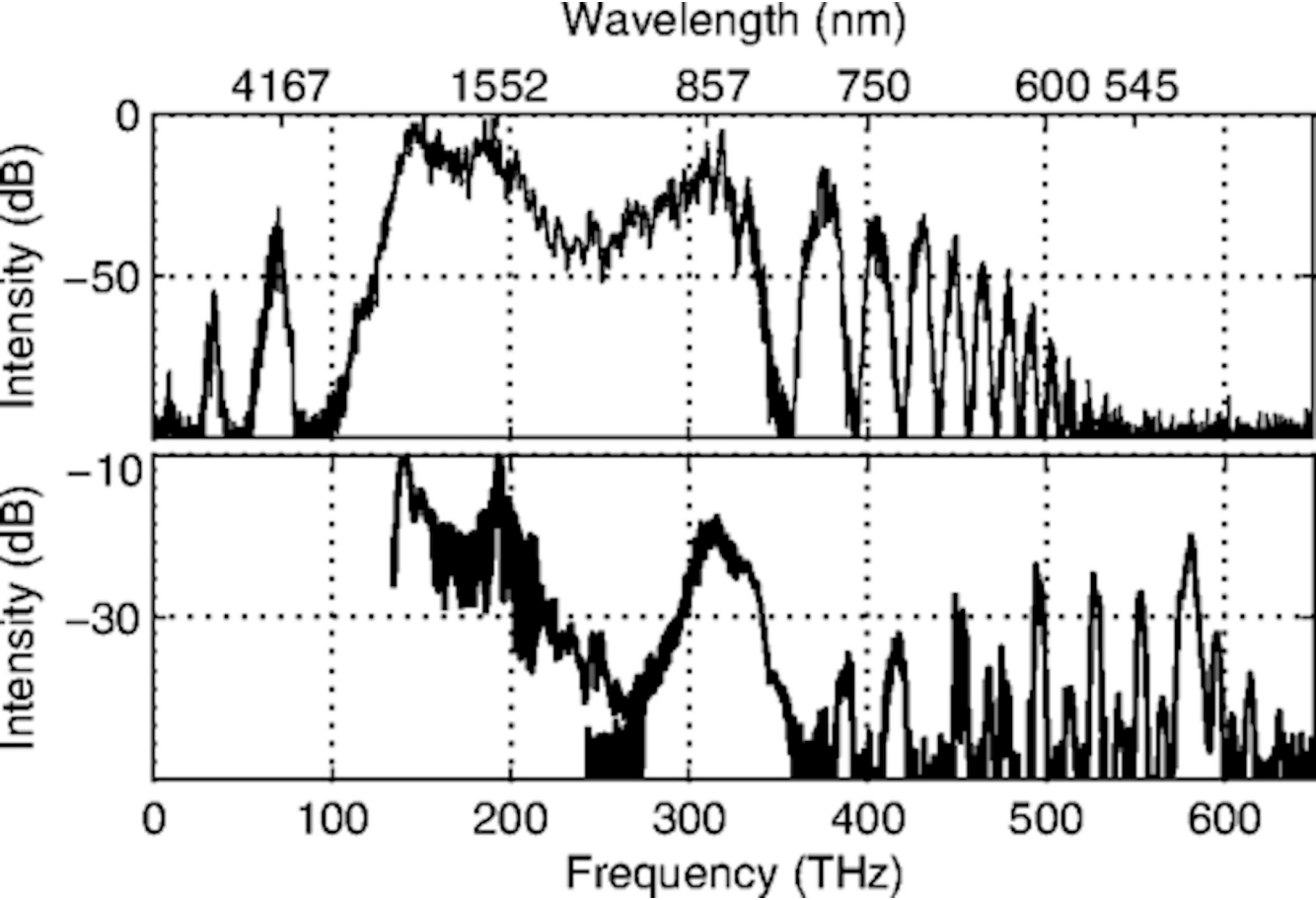
Wavelength (nm)
4167
1552
857
750
600 545
0
−50
Intensity (dB)
−10
−30
Intensity (dB)
0
100
200
300
400
500
600
Frequency (THz)

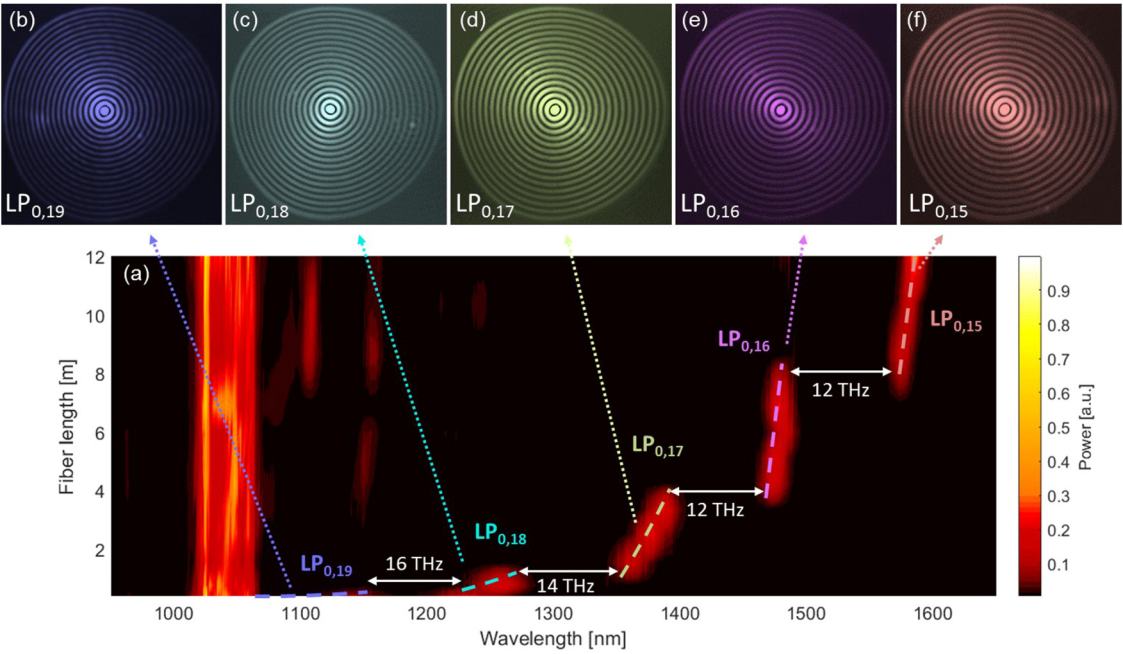
(b)
LP0,19
(c)
LP0,18
(d)
LP0,17
(e)
LP0,16
(f)
LP0,15
(a)
Fiber length [m]
Wavelength [nm]
Power [a.u.]
LP0,19
LP0,18
LP0,17
LP0,16
LP0,15
16 THz
14 THz
12 THz
12 THz

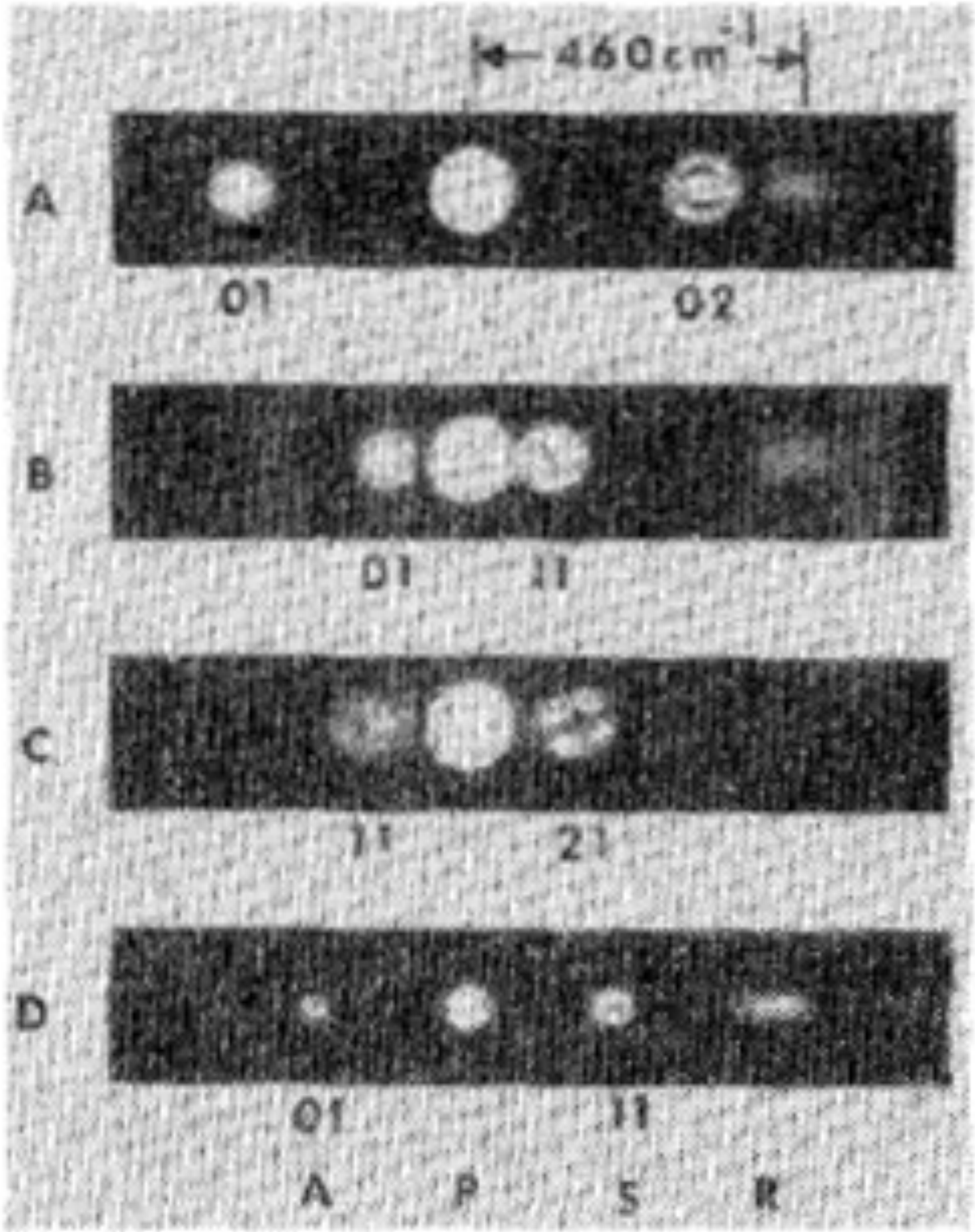
460cm⁻¹
A
O1
O2
B
D1
I1
C
I1
2I
D
O1
I1
A
P
S
R

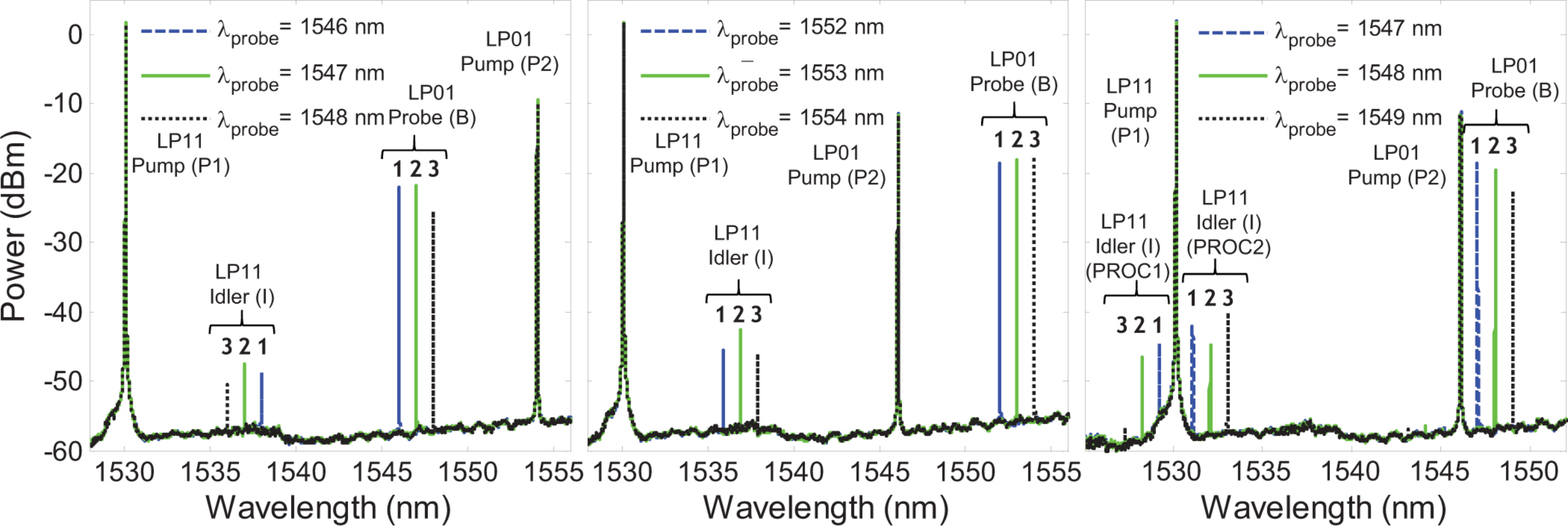
Power (dBm)
0
-10
-20
-30
-40
-50
-60
λprobe= 1546 nm
λprobe= 1547 nm
λprobe= 1548 nm
LP11
Pump (P1)
LP11
Idler (I)
3 2 1
LP01
Probe (B)
1 2 3
LP01
Pump (P2)
1530
1535
1540
1545
1550
1555
Wavelength (nm)
(a)
λprobe= 1552 nm
λprobe= 1553 nm
λprobe= 1554 nm
LP11
Pump (P1)
LP11
Idler (I)
1 2 3
LP01
Pump (P2)
LP01
Probe (B)
1 2 3
1530
1535
1540
1545
1550
1555
Wavelength (nm)
(b)
λprobe= 1547 nm
λprobe= 1548 nm
λprobe= 1549 nm
LP11
Pump
(P1)
LP11
Idler (I)
(PROC1)
3 2 1
LP11
Idler (I)
(PROC2)
1 2 3
LP01
Pump (P2)
LP01
Probe (B)
1 2 3
1530
1535
1540
1545
1550
Wavelength (nm)
(c)

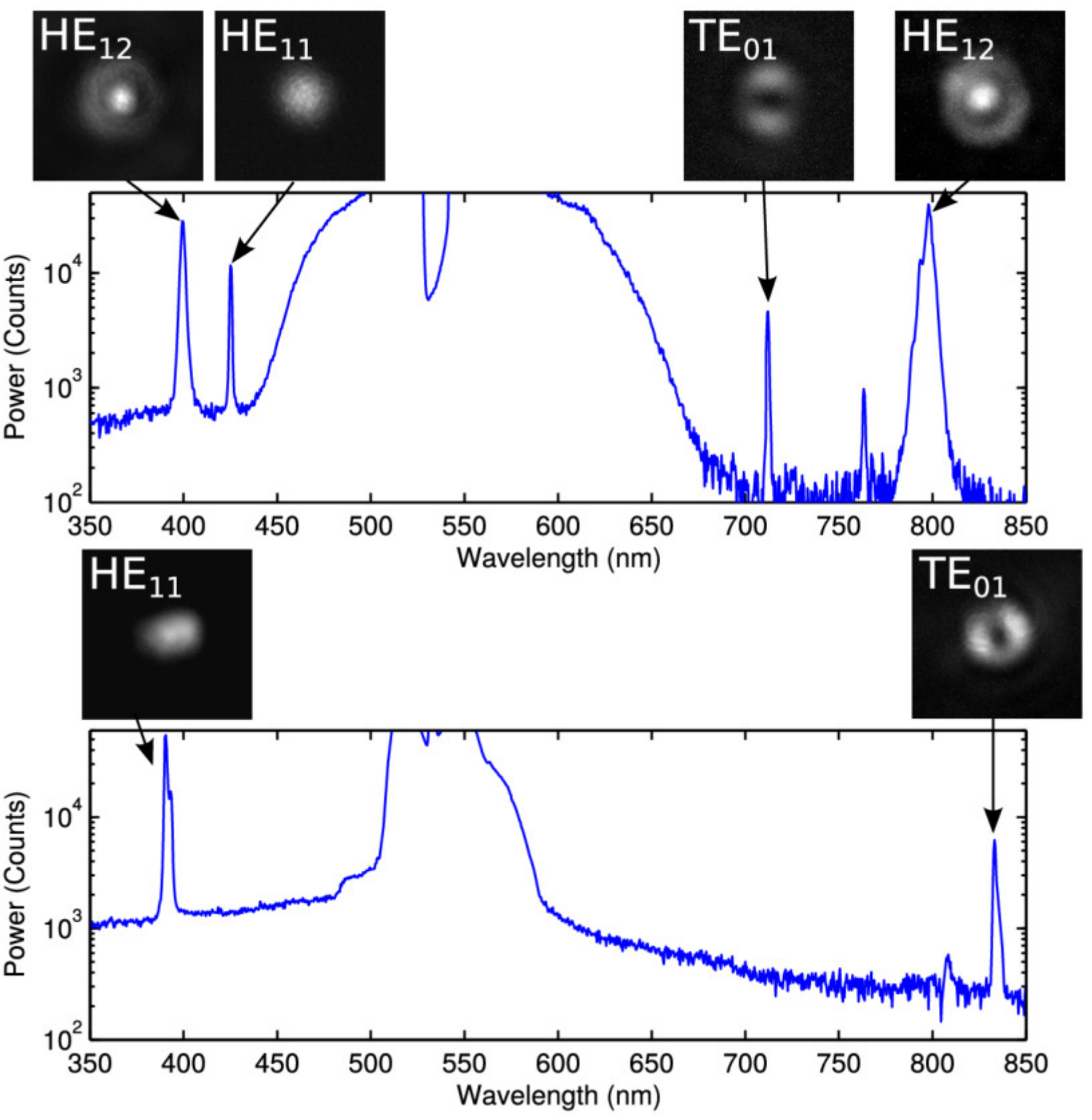
HE12
HE11
TE01
HE12
Power (Counts)
10^4
10^3
10^2
350
400
450
500
550
600
650
700
750
800
850
Wavelength (nm)
HE11
TE01
Power (Counts)
10^4
10^3
10^2
350
400
450
500
550
600
650
700
750
800
850
Wavelength (nm)

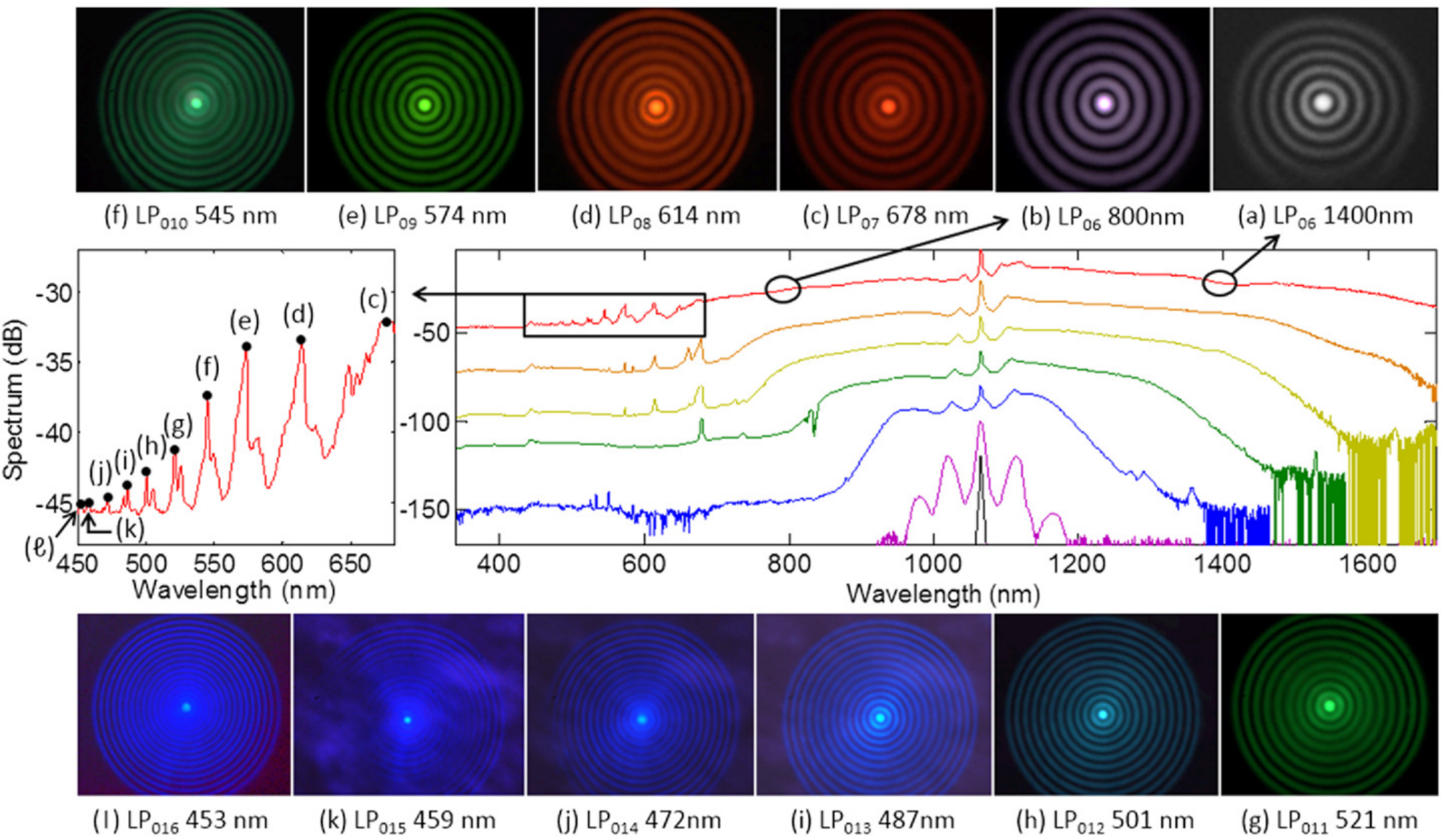
(f) LP010 545 nm
(e) LP09 574 nm
(d) LP08 614 nm
(c) LP07 678 nm
(b) LP06 800nm
(a) LP06 1400nm
Spectrum (dB)
-30
-35
-40
-45
(c)
(d)
(e)
(f)
(g)
(h)
(i)
(j)
(k)
(ℓ)
450
500
550
600
650
Wavelength (nm)
-50
-100
-150
400
600
800
1000
1200
1400
1600
Wavelength (nm)
(l) LP016 453 nm
(k) LP015 459 nm
(j) LP014 472nm
(i) LP013 487nm
(h) LP012 501 nm
(g) LP011 521 nm

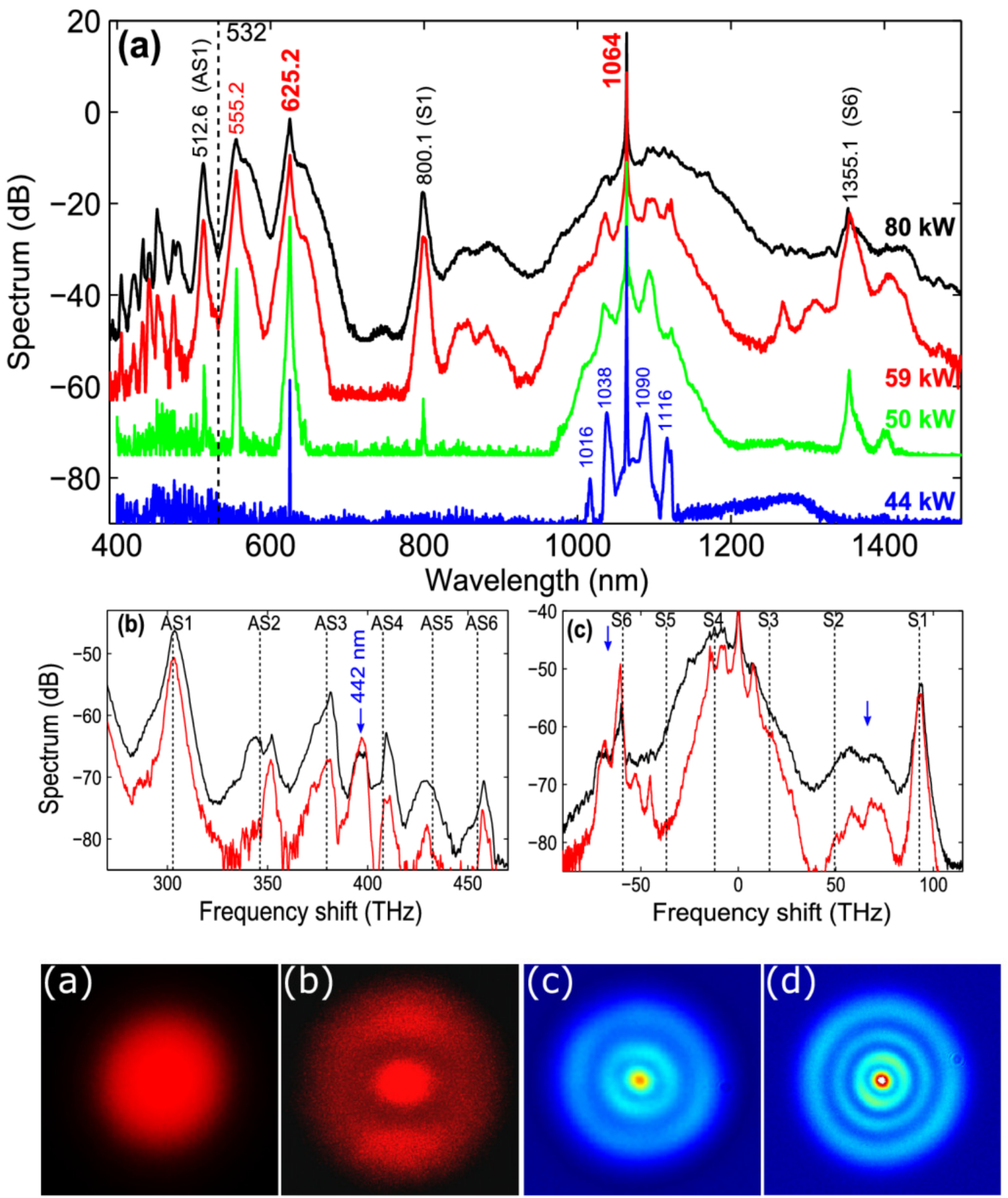
(a)
532
512.6 (AS1)
555.2
625.2
800.1 (S1)
1064
1355.1 (S6)
80 kW
59 kW
50 kW
44 kW
1016
1038
1090
1116
Spectrum (dB)
Wavelength (nm)
(b)
AS1
AS2
AS3
AS4
AS5
AS6
442 nm
Spectrum (dB)
Frequency shift (THz)
(c)
S6
S5
S4
S3
S2
S1
Frequency shift (THz)
(a)
(b)
(c)
(d)

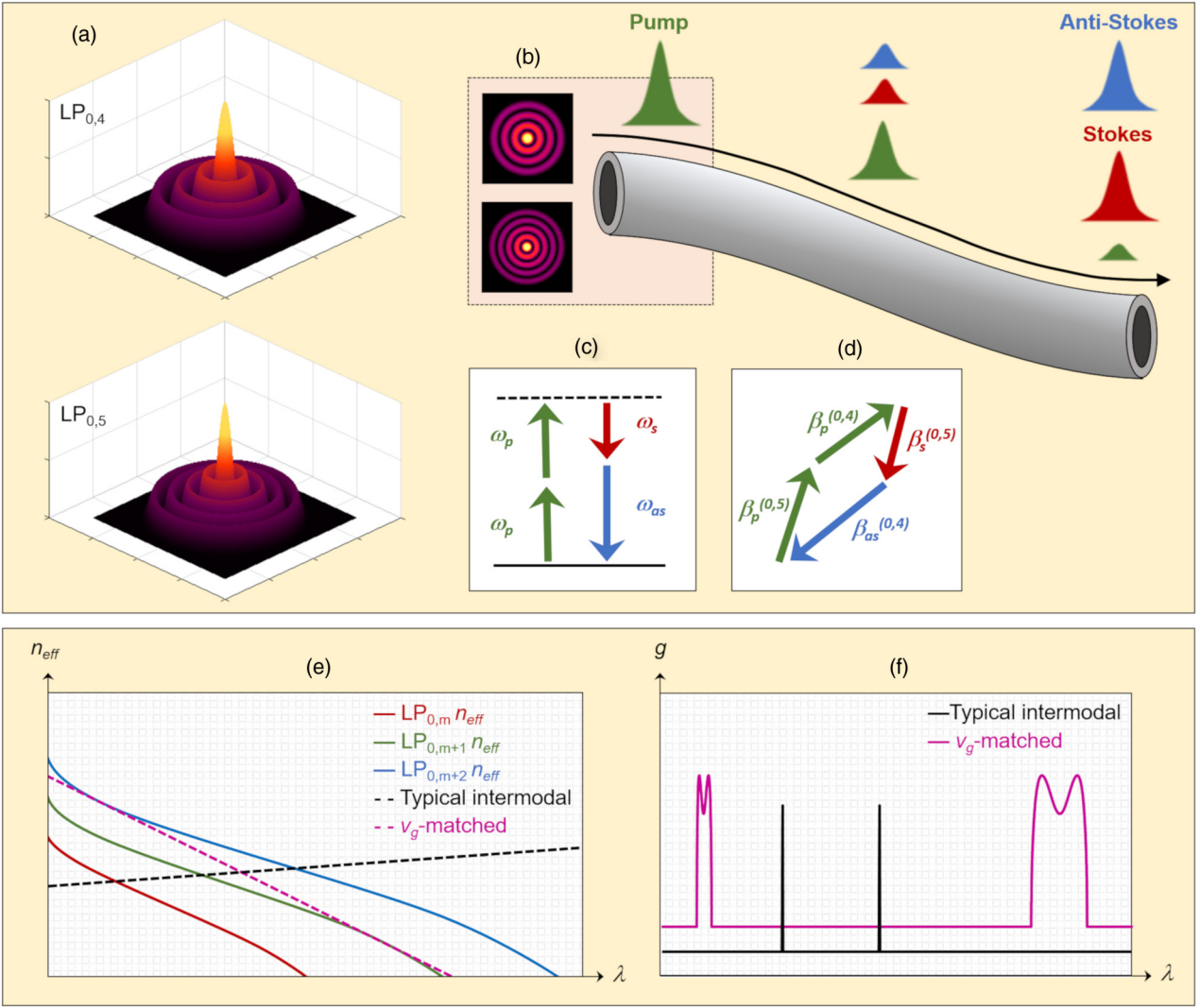
(a)
LP0,4
LP0,5
(b)
Pump
Anti-Stokes
Stokes
(c)
ωp
ωs
ωp
ωas
(d)
βp(0,4)
βs(0,5)
βp(0,5)
βas(0,4)
neff
(e)
LP0,m neff
LP0,m+1 neff
LP0,m+2 neff
Typical intermodal
vg-matched
λ
g
(f)
Typical intermodal
vg-matched
λ

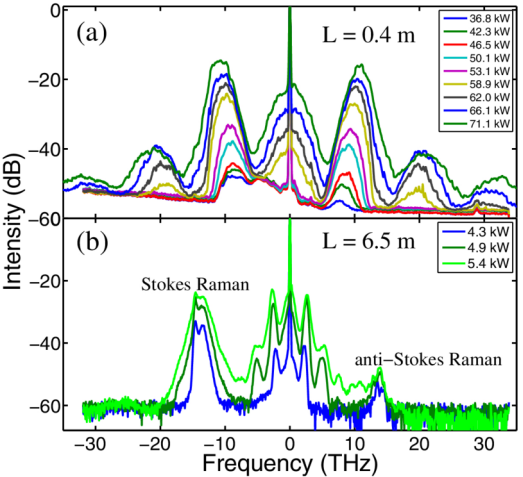
(a)
L = 0.4 m
36.8 kW
42.3 kW
46.5 kW
50.1 kW
53.1 kW
58.9 kW
62.0 kW
66.1 kW
71.1 kW
(b)
L = 6.5 m
4.3 kW
4.9 kW
5.4 kW
Stokes Raman
anti−Stokes Raman
Intensity (dB)
Frequency (THz)

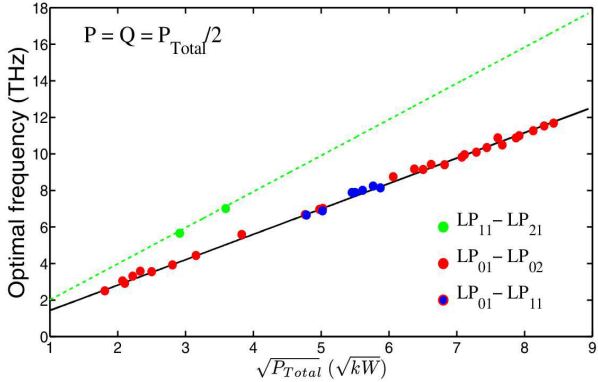
P = Q = P_Total/2
LP11 − LP21
LP01 − LP02
LP01 − LP11
Optimal frequency (THz)
√P_Total (√kW)

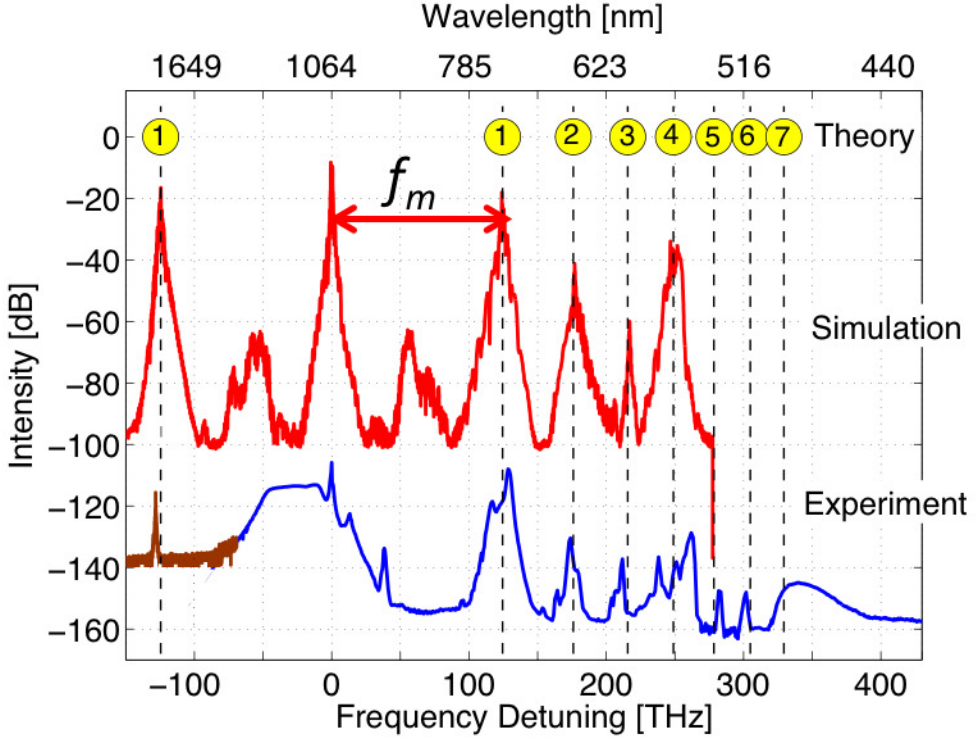
Wavelength [nm]
1649
1064
785
623
516
440
1
1
2
3
4
5
6
7
Theory
f_m
Simulation
Experiment
Intensity [dB]
0
−20
−40
−60
−80
−100
−120
−140
−160
−100
0
100
200
300
400
Frequency Detuning [THz]

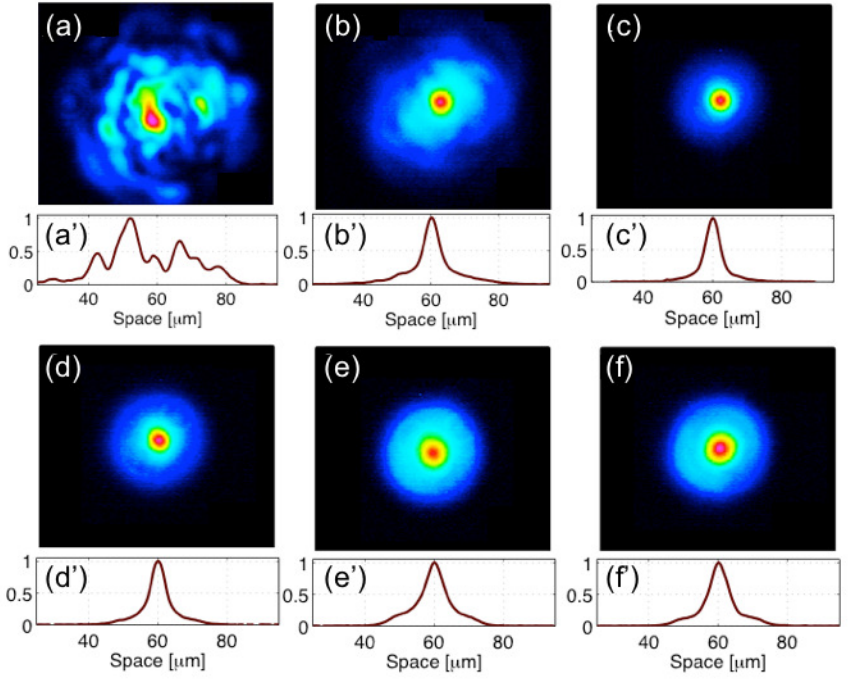
(a)
(b)
(c)
(a')
(b')
(c')
(d)
(e)
(f)
(d')
(e')
(f')
1
0.5
0
40
60
80
Space [μm]

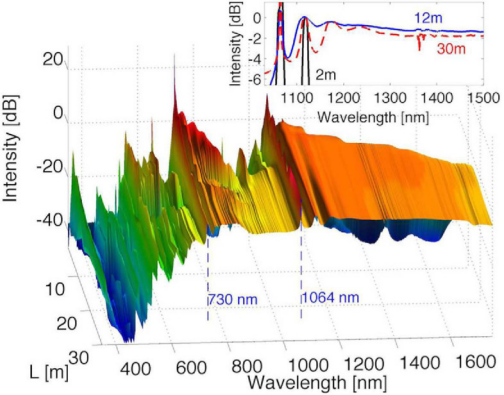
Intensity [dB]
20
0
-20
-40
10
20
30
L [m]
400
600
800
1000
1200
1400
1600
Wavelength [nm]
730 nm
1064 nm
Intensity [dB]
0
-2
-4
-6
12m
30m
2m
1100
1200
1300
1400
1500
Wavelength [nm]

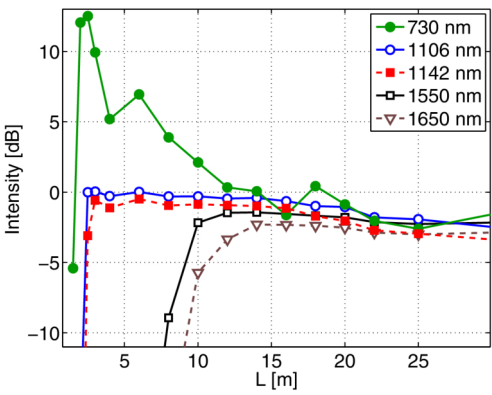
730 nm
1106 nm
1142 nm
1550 nm
1650 nm
Intensity [dB]
10
5
0
−5
−10
5
10
15
20
25
L [m]

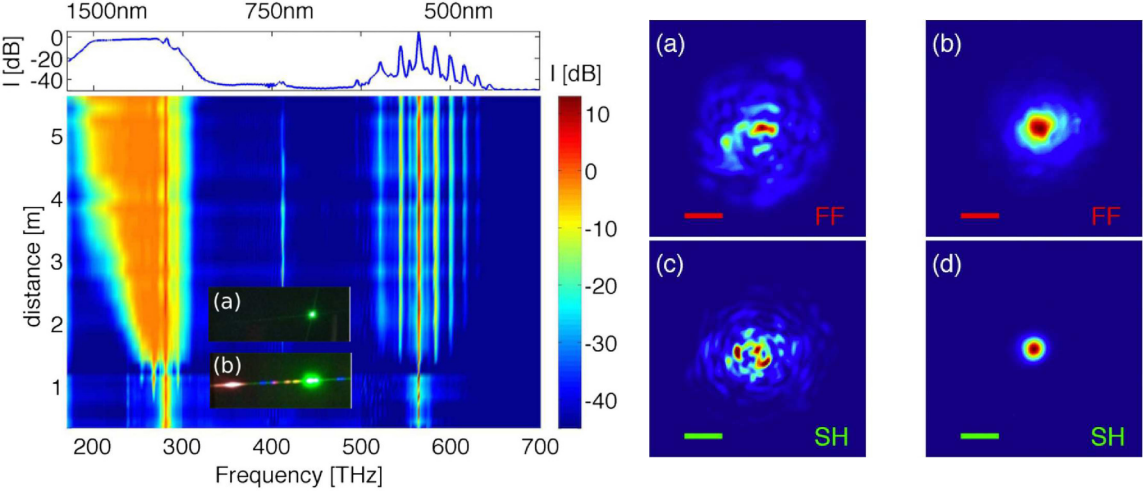
1500nm
750nm
500nm
I [dB]
0
-20
-40
I [dB]
10
0
-10
-20
-30
-40
distance [m]
5
4
3
2
1
(a)
(b)
200
300
400
500
600
700
Frequency [THz]
(a)
FF
(b)
FF
(c)
SH
(d)
SH

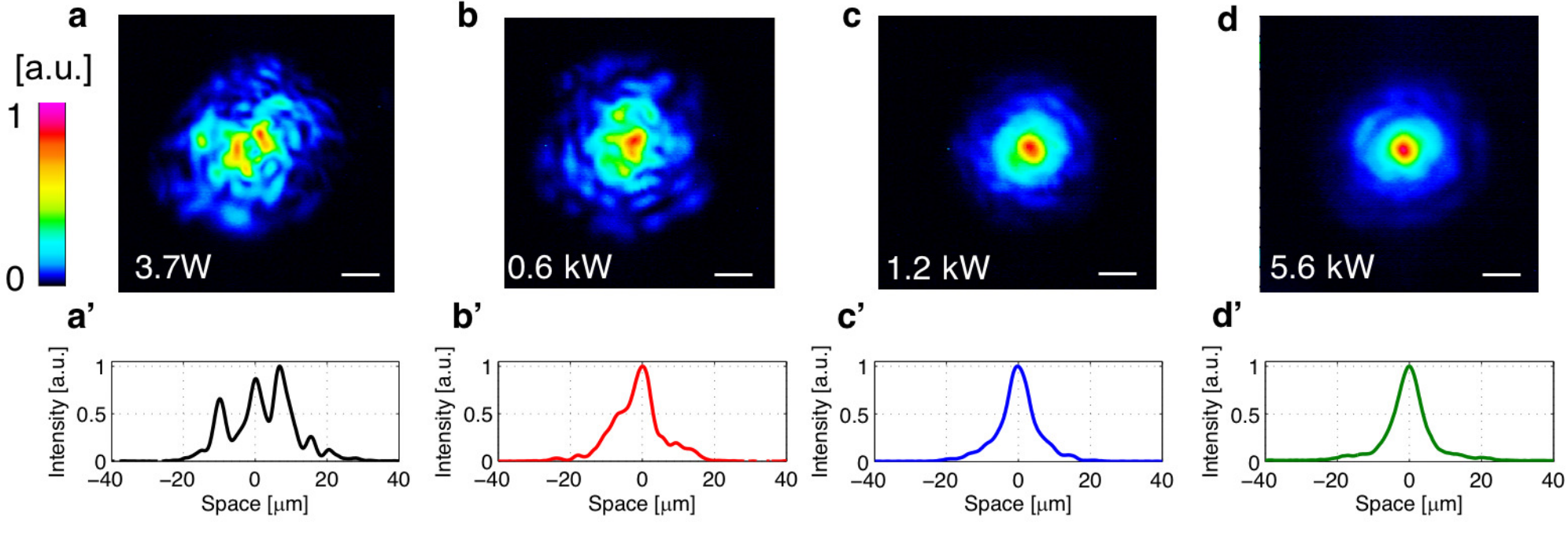
a
[a.u.]
1
0
3.7W
b
0.6 kW
c
1.2 kW
d
5.6 kW
a'
b'
c'
d'
Intensity [a.u.]
Space [μm]
1
0.5
0
−40
−20
0
20
40

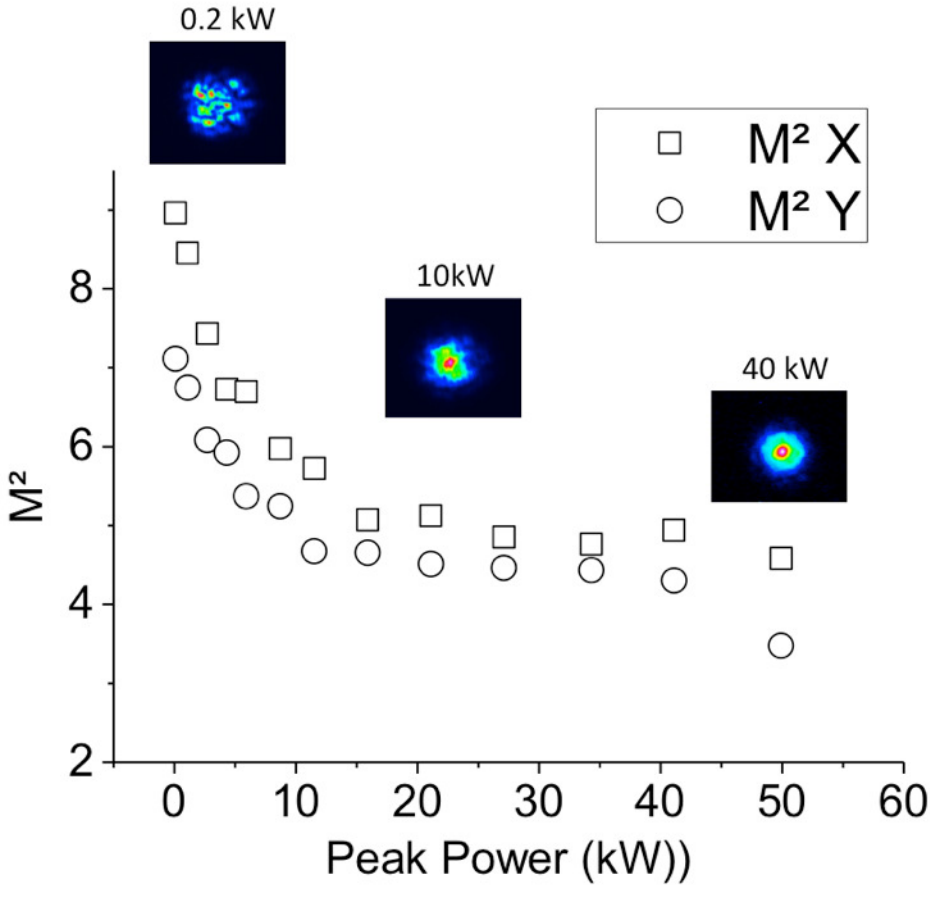
0.2 kW
10kW
40 kW
M² X
M² Y
M²
8
6
4
2
0
10
20
30
40
50
60
Peak Power (kW))

Parabolic profile

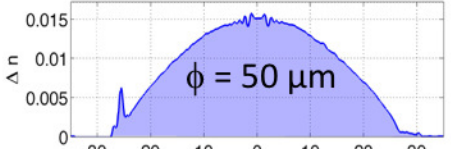

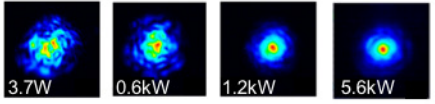

Self-cleaning threshold
0.5 GW/cm²

Non parabolic profile

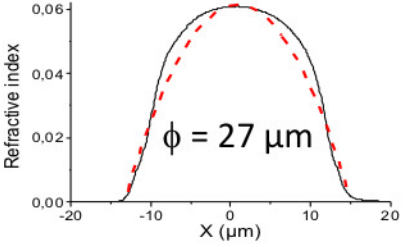

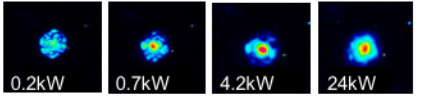

Self-cleaning threshold
0.9 GW/cm²

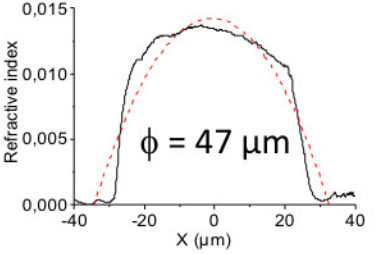

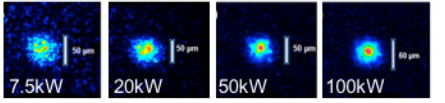

Self-cleaning threshold
1.8 GW/cm²

Linear regime (100 W)

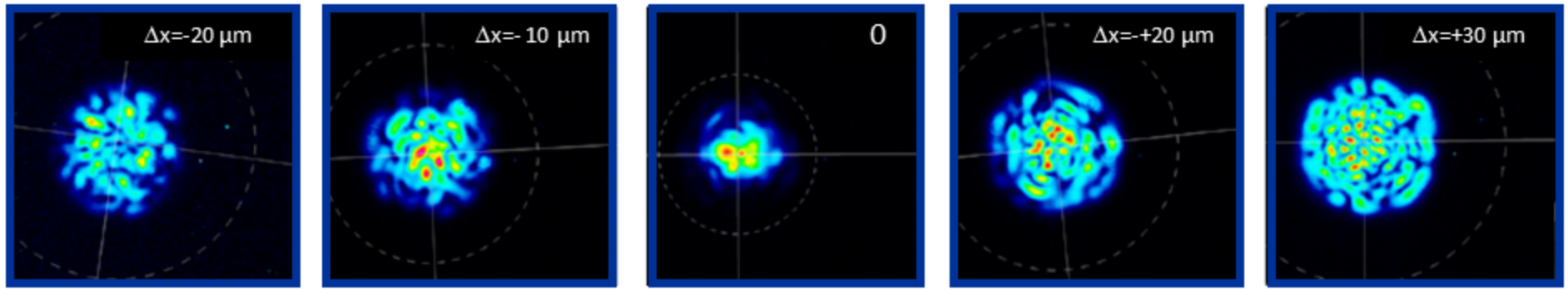

Nonlinear regime (10 kW)

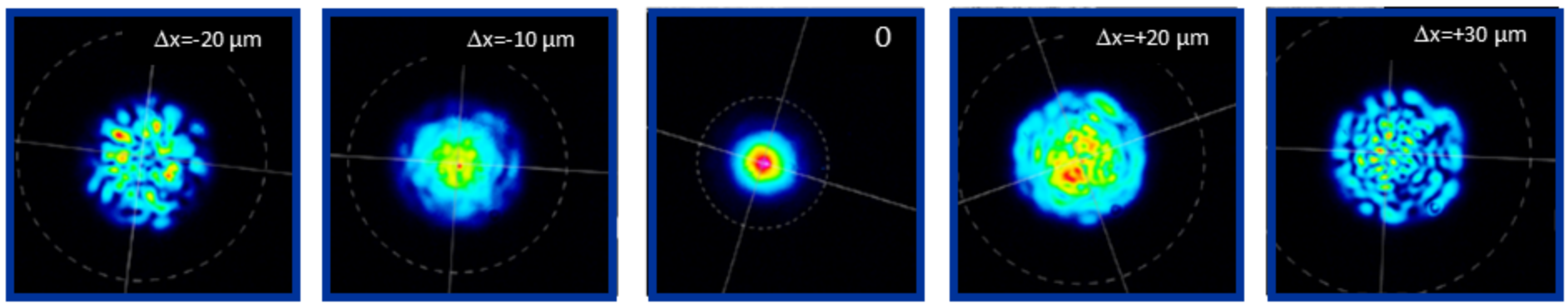

Number of excited modes

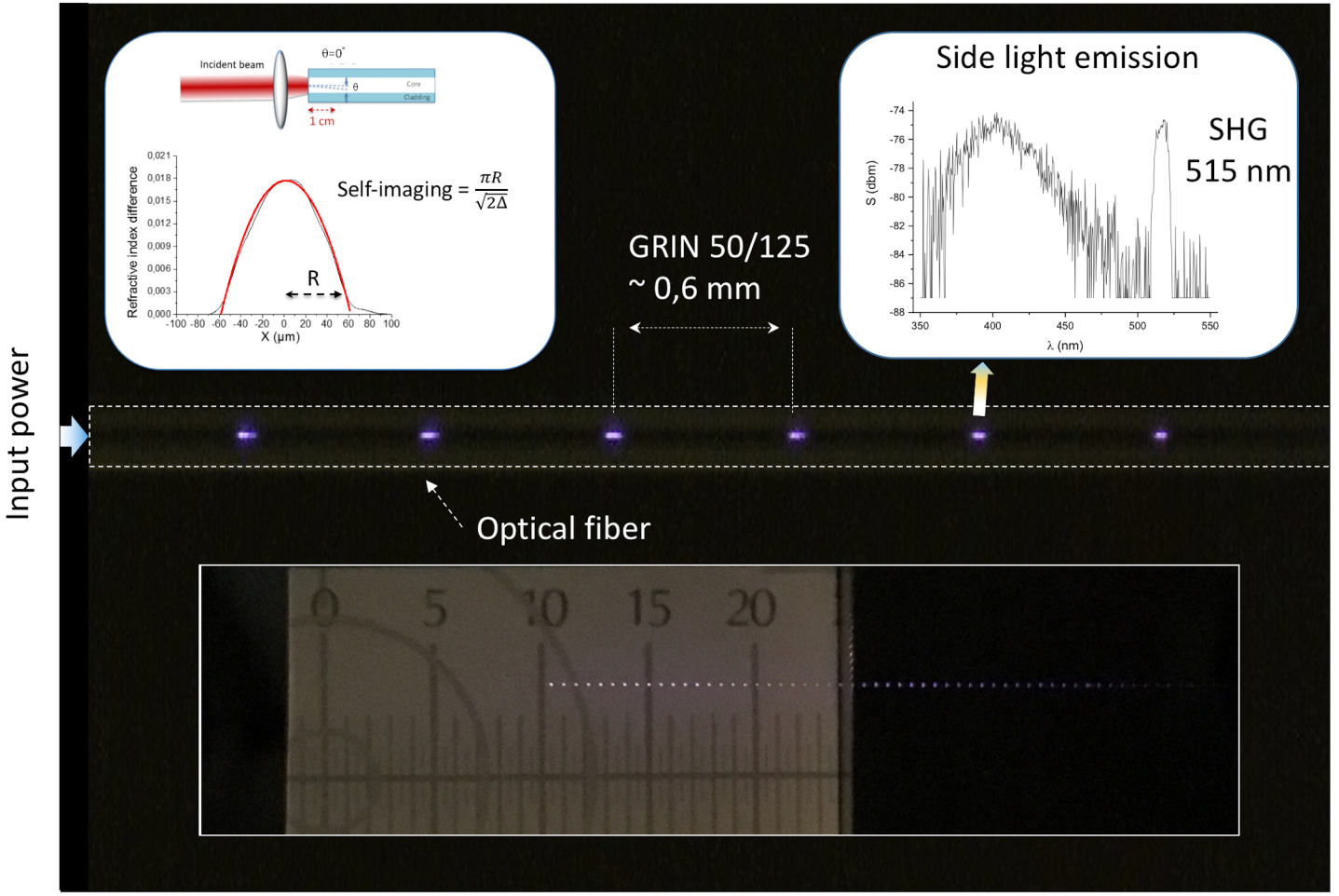
Incident beam
θ=0°
θ
Core
Cladding
1 cm
Refractive index difference
X (μm)
Self-imaging = $\frac{\pi R}{\sqrt{2\Delta}}$
R
Side light emission
SHG
515 nm
S (dbm)
λ (nm)
GRIN 50/125
~ 0,6 mm
Input power
Optical fiber

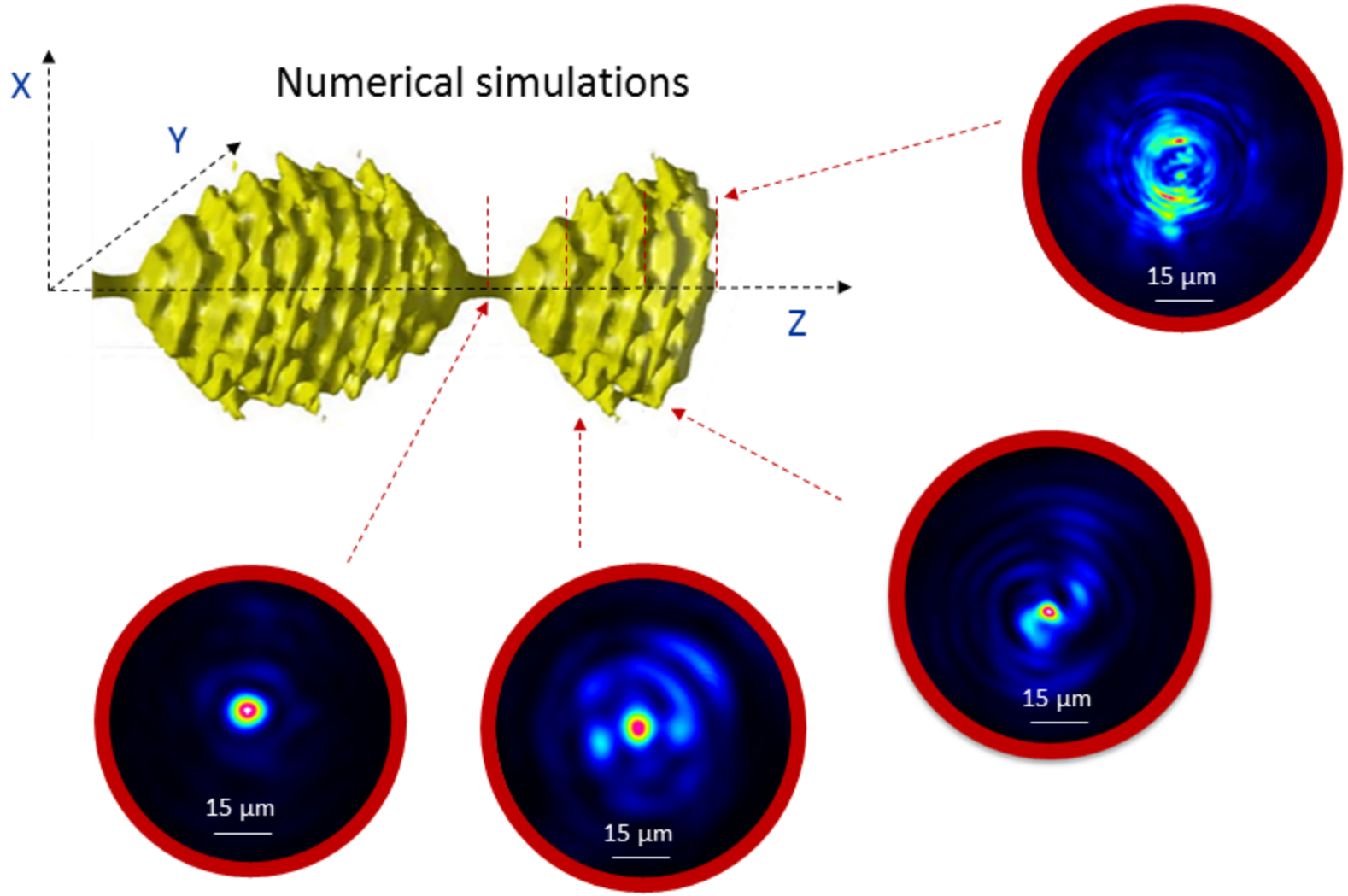
Numerical simulations
X
Y
Z
15 µm
15 µm
15 µm
15 µm
Experimental data

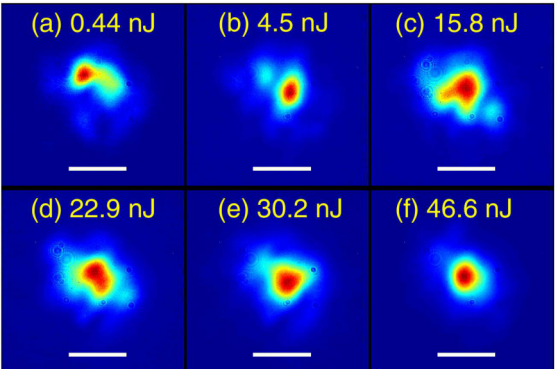
(a) 0.44 nJ
(b) 4.5 nJ
(c) 15.8 nJ
(d) 22.9 nJ
(e) 30.2 nJ
(f) 46.6 nJ

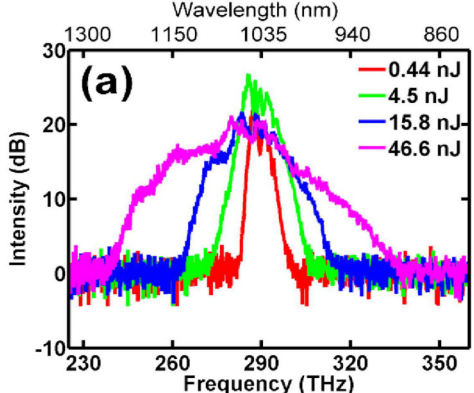
Wavelength (nm)
1300
1150
1035
940
860
(a)
0.44 nJ
4.5 nJ
15.8 nJ
46.6 nJ
Intensity (dB)
30
20
10
0
-10
230
260
290
320
350
Frequency (THz)

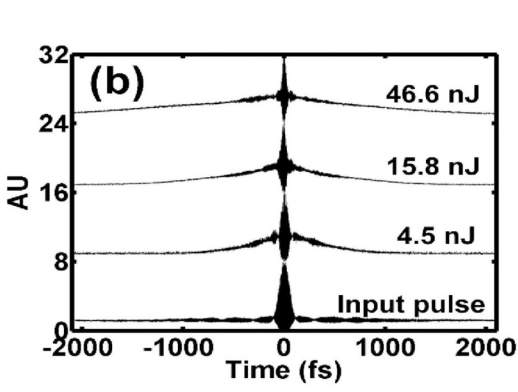
(b)
46.6 nJ
15.8 nJ
4.5 nJ
Input pulse
AU
32
24
16
8
0
-2000
-1000
0
1000
2000
Time (fs)

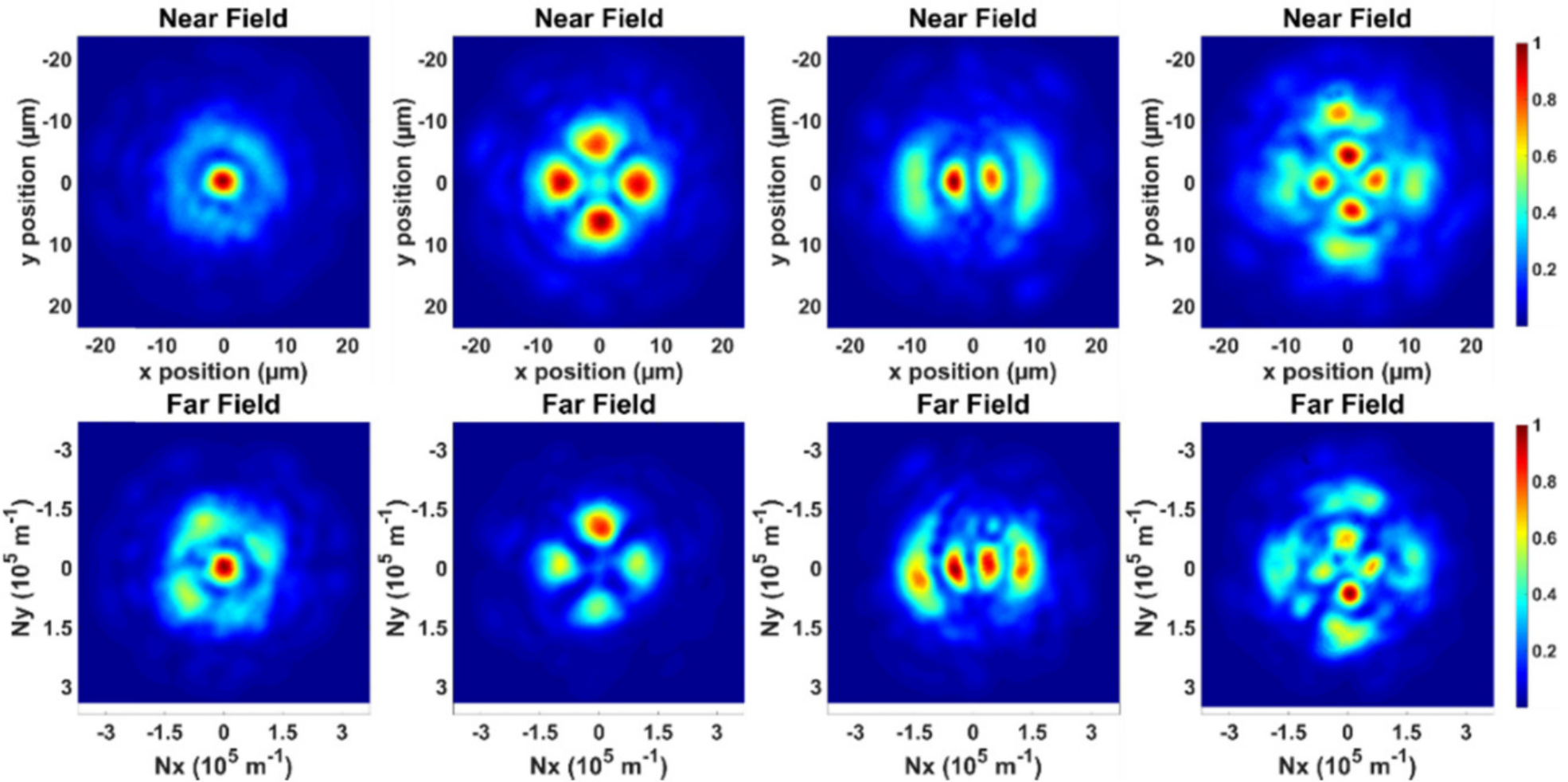
Near Field
Near Field
Near Field
Near Field
y position (μm)
x position (μm)
-20
-10
0
10
20
1
0.8
0.6
0.4
0.2
Far Field
Far Field
Far Field
Far Field
Ny (10^5 m^-1)
Nx (10^5 m^-1)
-3
-1.5
0
1.5
3

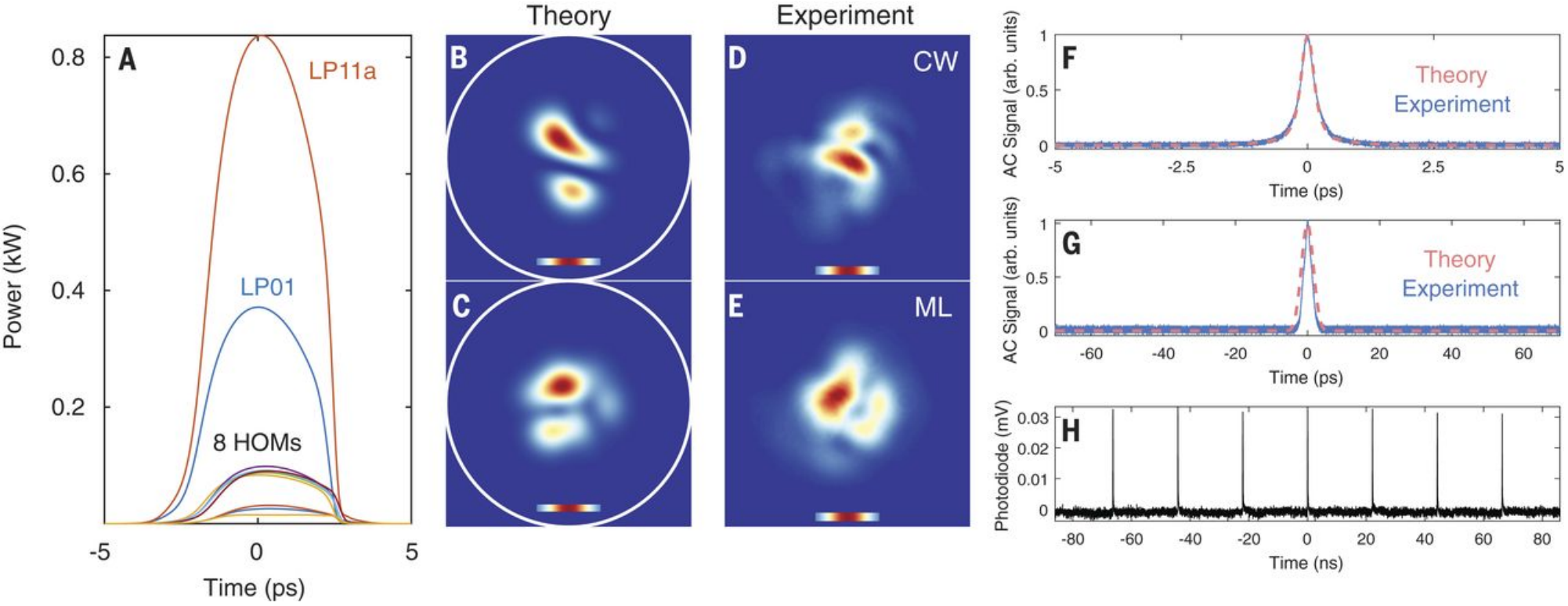
A
LP11a
LP01
8 HOMs
Power (kW)
Time (ps)
Theory
Experiment
B
C
D
CW
E
ML
F
Theory
Experiment
AC Signal (arb. units)
G
H
Photodiode (mV)
Time (ns)

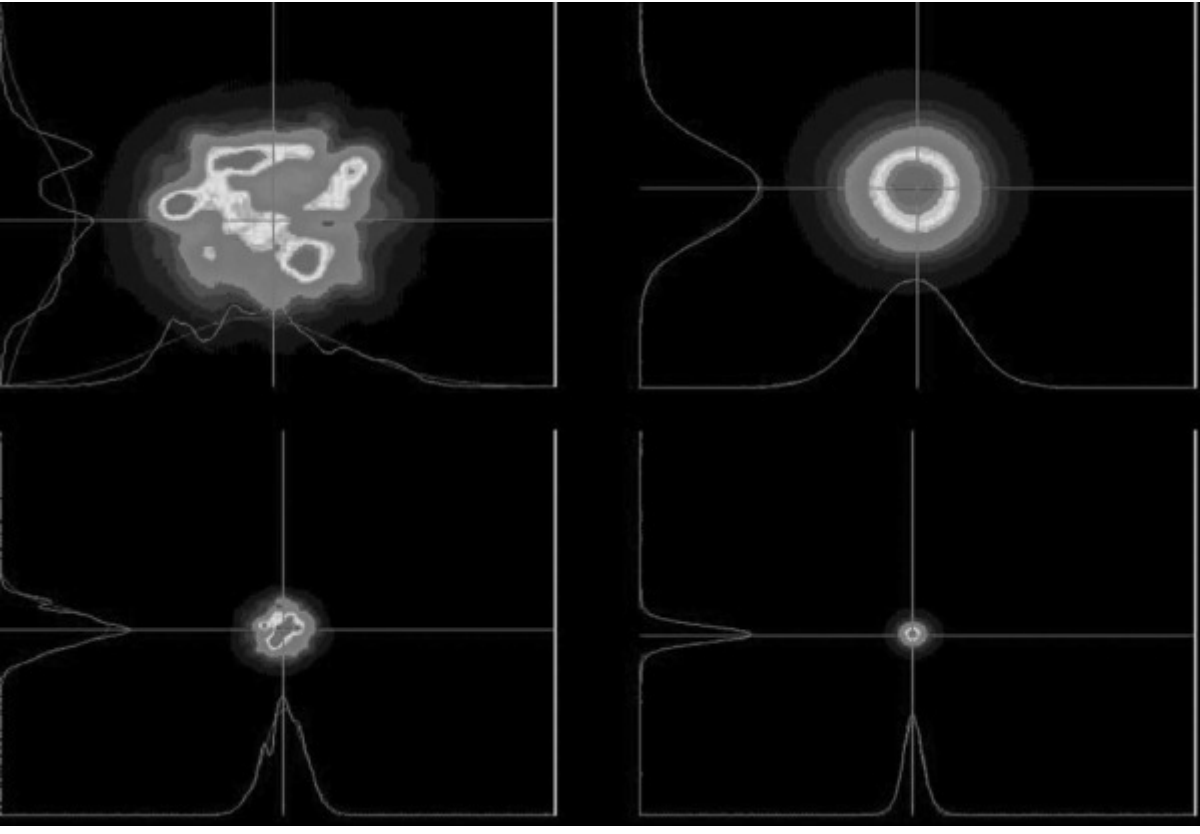

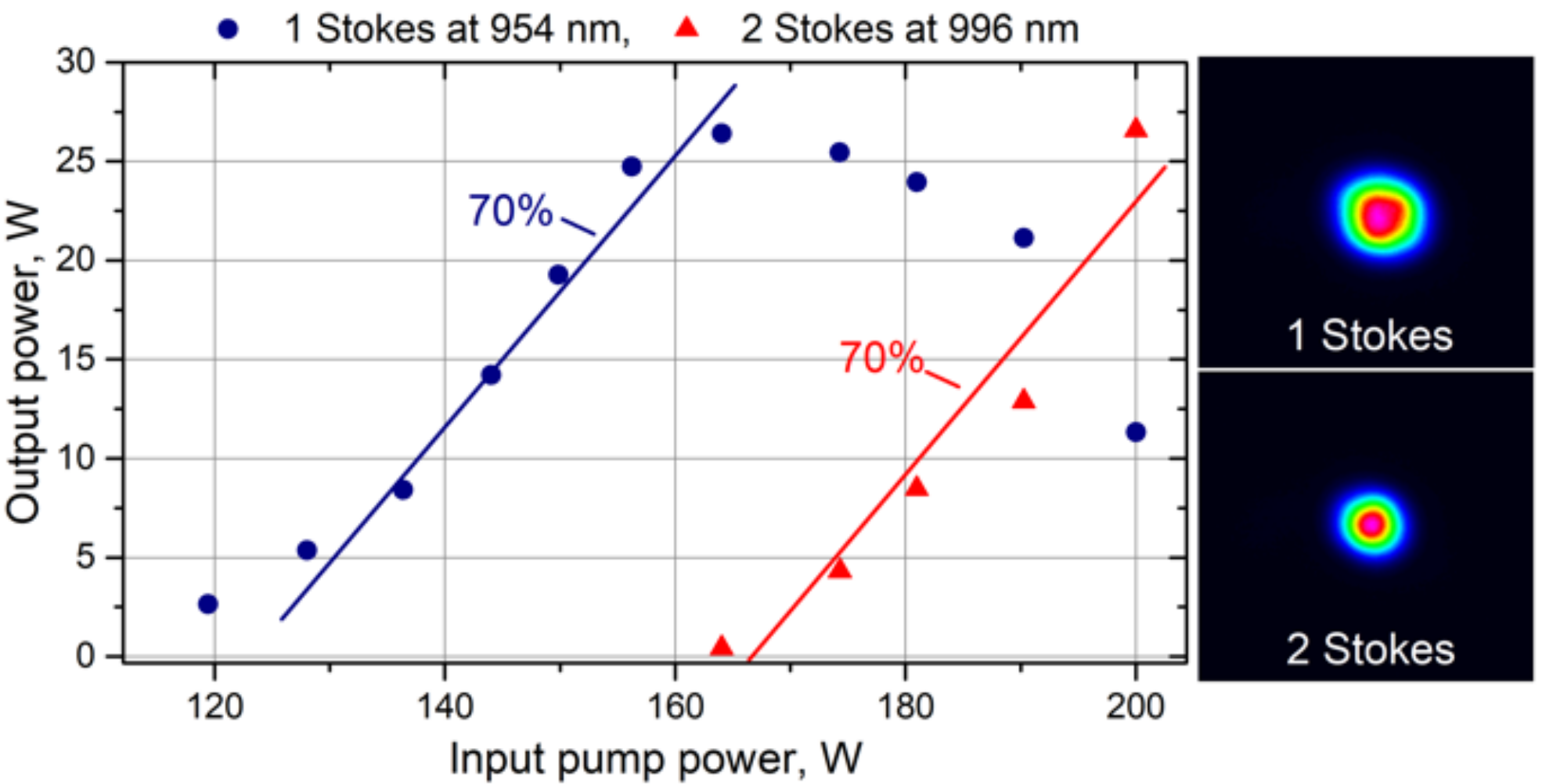
1 Stokes at 954 nm,
2 Stokes at 996 nm
Output power, W
Input pump power, W
70%
70%
1 Stokes
2 Stokes
0
5
10
15
20
25
30
120
140
160
180
200

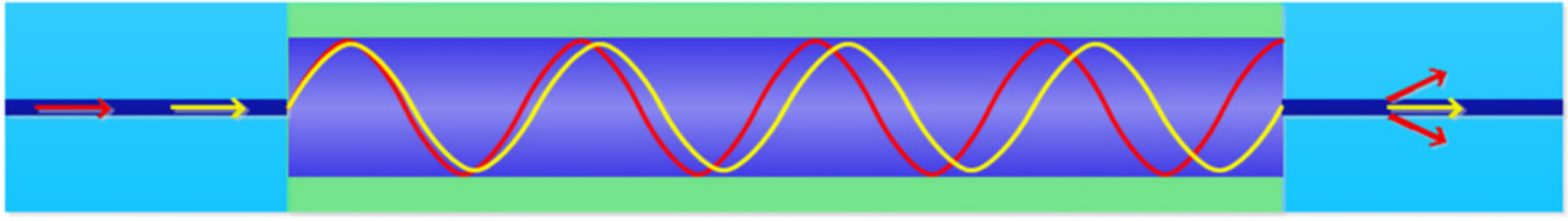

Low power signal

High power signal

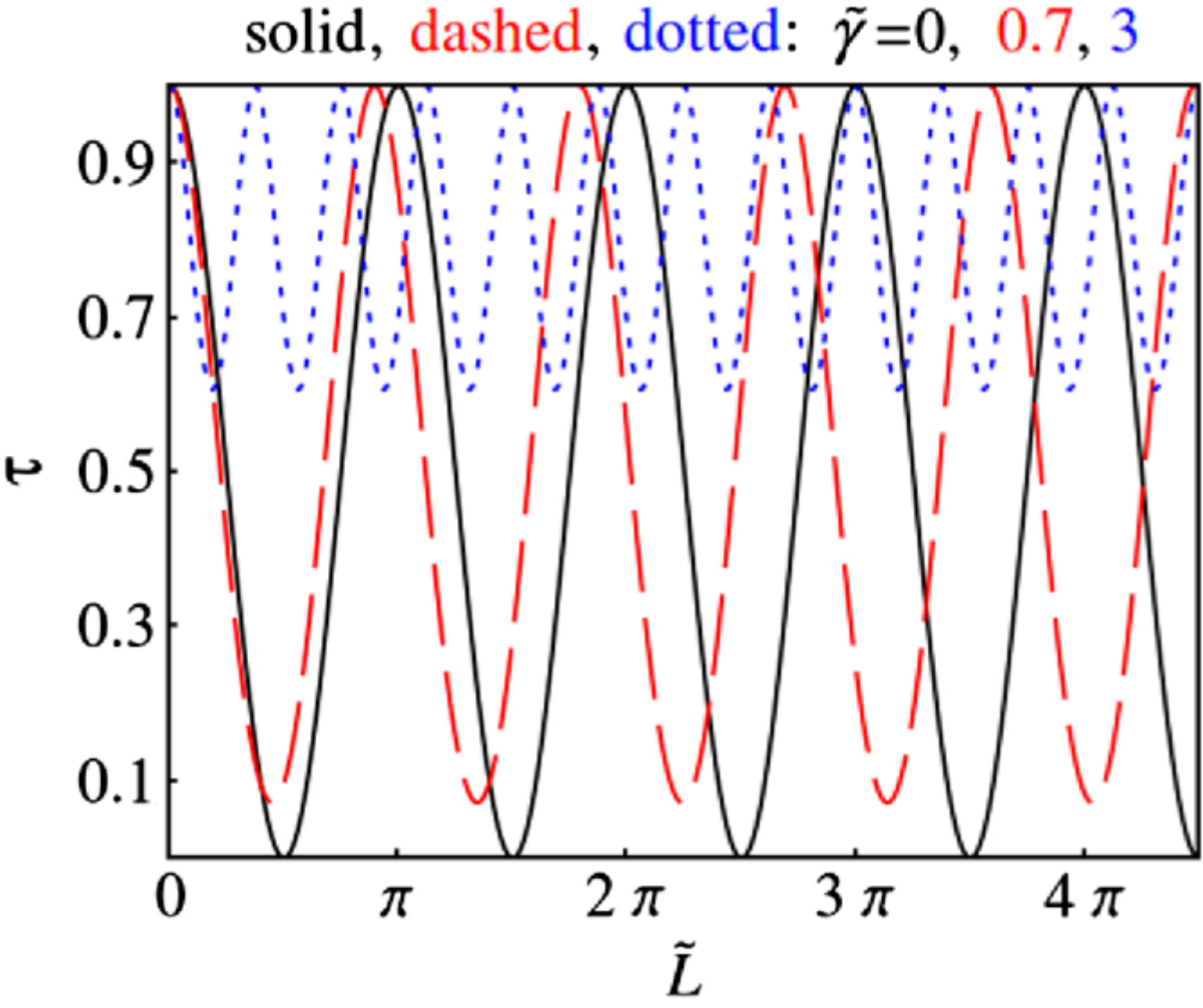
solid, dashed, dotted: $\tilde{\gamma}$=0, 0.7, 3
0.9
0.7
0.5
0.3
0.1
τ
0
π
2 π
3 π
4 π
$\tilde{L}$

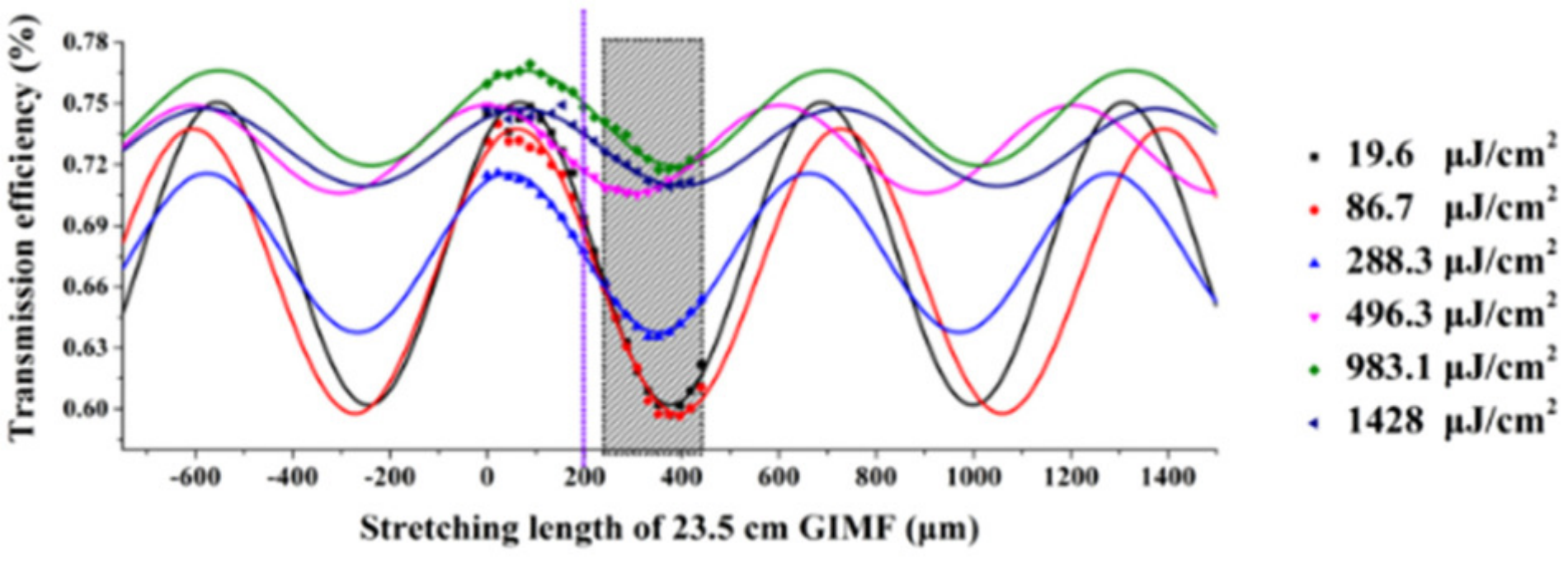
Transmission efficiency (%)
0.78
0.75
0.72
0.69
0.66
0.63
0.60
-600
-400
-200
0
200
400
600
800
1000
1200
1400
Stretching length of 23.5 cm GIMF (μm)
19.6 μJ/cm2
86.7 μJ/cm2
288.3 μJ/cm2
496.3 μJ/cm2
983.1 μJ/cm2
1428 μJ/cm2

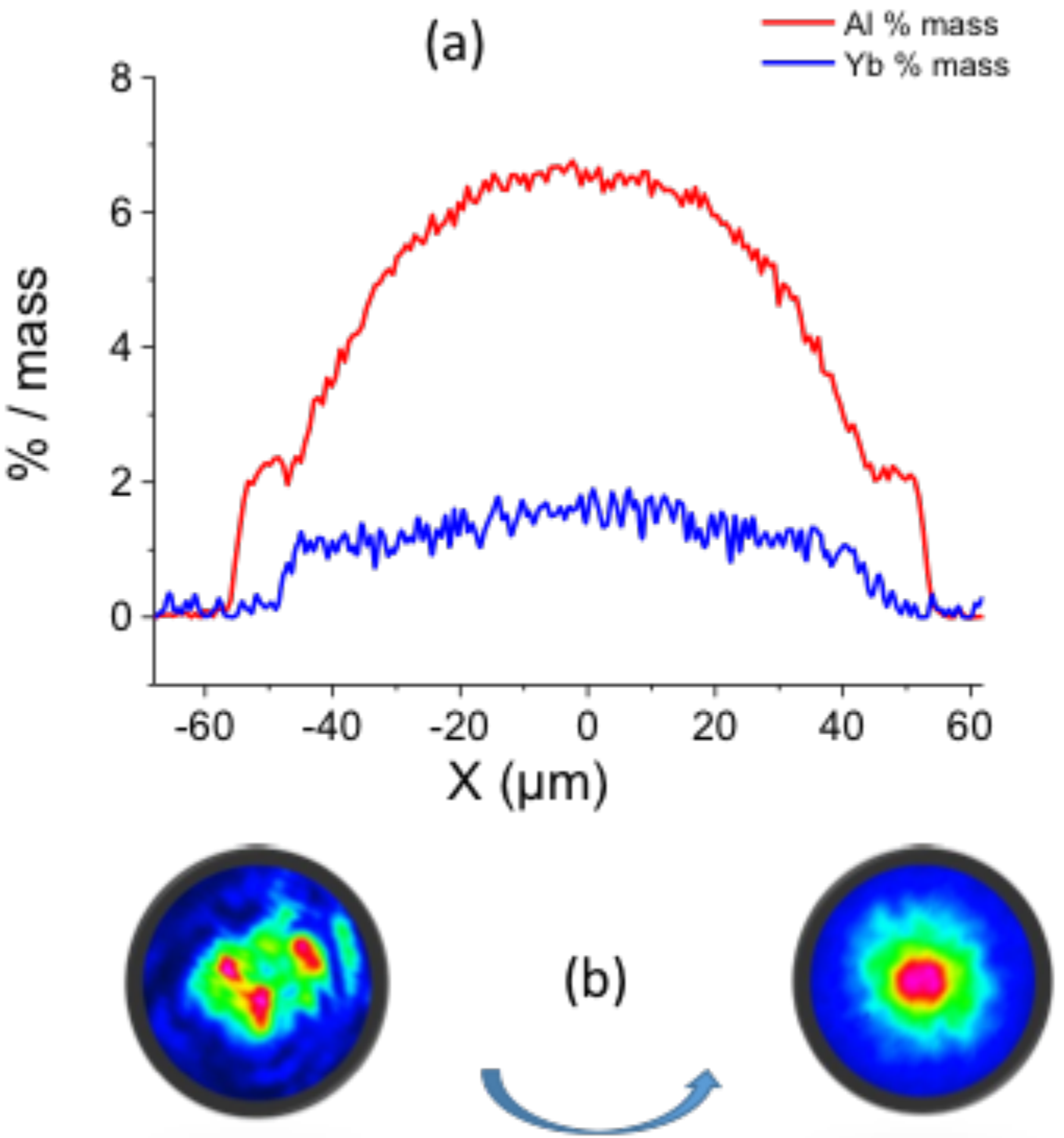
(a)
Al % mass
Yb % mass
% / mass
8
6
4
2
0
-60
-40
-20
0
20
40
60
X (µm)
(b)

(a)

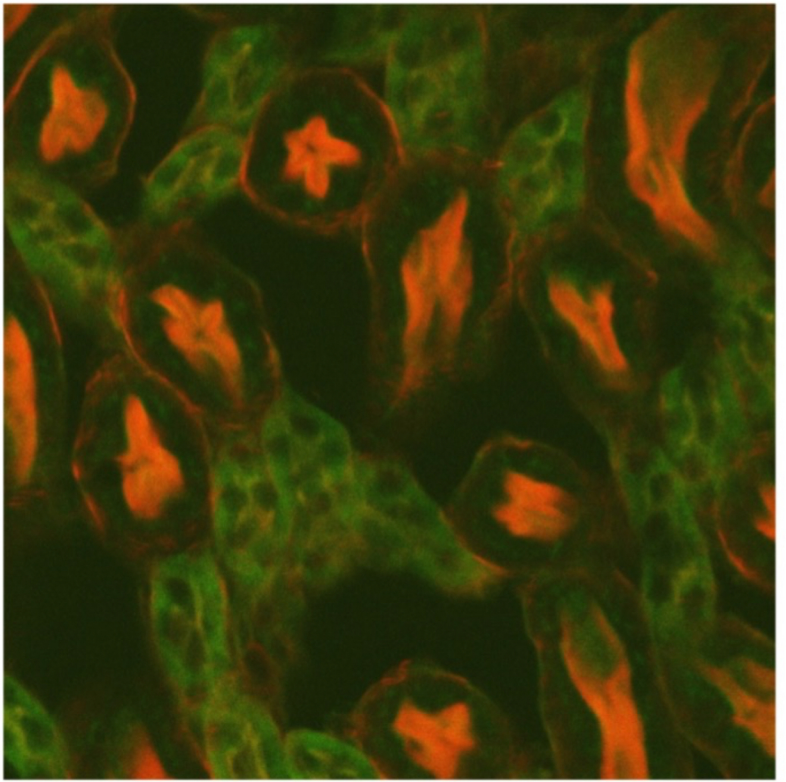

(b)

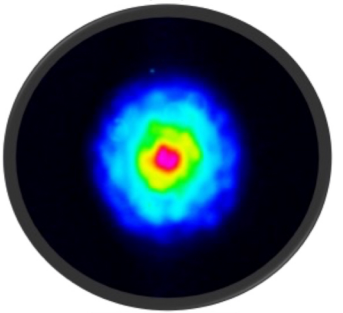

(C)

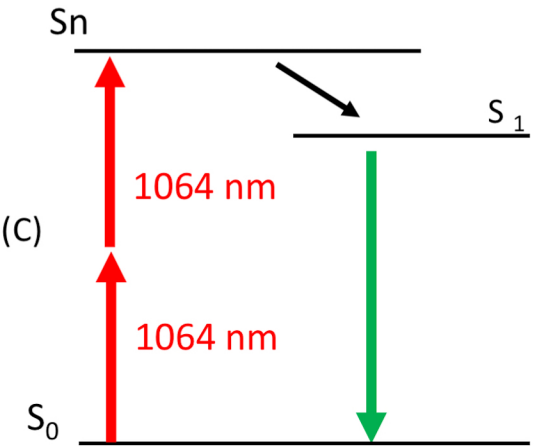

Two-photon excitation